5-1-2014

Analysis of Bolted Joints Under Medium and High Impact Loading

Deepak Somasundaram
University of Nevada, Las Vegas, somasund@unlv.nevada.edu

ANALYSIS OF BOLTED JOINTS UNDER MEDIUM AND HIGH IMPACT LOADING

by

Deepak Sankar Somasundaram

Bachelor of Engineering in Mechanical Engineering
Madras University, Chennai, India
May 2003

Master of Science in Mechanical Engineering
University of Nevada, Las Vegas
December 2008

A dissertation submitted in partial fulfillment
of the requirements for the

Doctor of Philosophy - Mechanical Engineering

Department of Mechanical Engineering
Howard R. Hughes College of Engineering
Graduate College

University of Nevada, Las Vegas
May 2014

UNLV
UNIVERSITY OF NEVADA LAS VEGAS

THE GRADUATE COLLEGE

We recommend the dissertation prepared under our supervision by

Deepak Sankar Somasundaram

entitled

Analysis of Bolted Joints under Medium and High Impact Loading

is approved in partial fulfillment of the requirements for the degree of

Doctor of Philosophy in Engineering - Mechanical Engineering

Department of Mechanical Engineering

Mohamed Trabia, Ph.D., Committee Co-Chair

Brendan O'Toole, Ph.D., Committee Co-Chair

Woosoon Yim, Ph.D., Committee Member

Zhiyong Wang, Ph.D., Committee Member

Yi-Tung Chen, Ph.D., Committee Member

Rama Venkat, Ph.D., Graduate College Representative

Kathryn Hausbeck Korgan, Ph.D., Interim Dean of the Graduate College

May 2014

ABSTRACT

Analysis of Bolted Joints under Medium and High Impact Loading

by

Deepak Sankar Somasundaram

Dr. Mohamed B. Trabia, Examination Committee Chair
Associate Dean for Research, Graduate Studies, and Computing
Professor of Mechanical Engineering
University of Nevada, Las Vegas

Dr. Brendan J. O'Toole, Examination Committee Chair
Professor of Mechanical Engineering
University of Nevada, Las Vegas

Understanding the transient behavior of structures with bolted joints when subjected to medium and high shock or impact loads can be challenging due to their nonlinear response, which is induced by the complex interactions between the bolts and the structure. While few researchers have considered shock transmission through bolted joints at low impact loading, there are little literature on shock transmission through bolted joints under high loading conditions. Low impact loading condition generally excites the lower order frequencies but under high impact loading higher order frequencies are excited. Typical factors that affect the response of a bolted joint include, preload (bolt tightening), intensity of the impact, and damping within the joint. The complexity in designing bolted joints under these conditions lies in the limitations of available methods to characterize their behavior.

The main objective of this work is to develop computational tools for predicting the shock transmission through bolted joints under medium and high impacts. Examples of these impacts are blast loading and projectile impact. The effect of tightening torque of the bolts on the response is also studied. The strain rate effect of the bolts due to high impact loading is also studied.

The study is done in two steps. The first step is a high impact study on a square flange system using a Two-stage gas gun. A steel plate is impacted using Lexan polycarbonate projectile at around 6 km/s. The impact surface is penetrated by the projectile on impact. The response acceleration is measured post joint. The second step would be to study medium impacts on a bolted connection using a circular fixture with a bolted lid to replicate a vessel. This structure is subjected to impact loading in a drop tower. The experiment is conducted at different pre-load torque for the bolts. The bolts are subjected to plastic deformation. The responses are measured using an accelerometer and a force sensor.

For these two cases, Finite Element Analysis (FEA) is performed. The bolts are modeled as solid elements. In both of these cases, strain rate effect is considered for both the structure and bolts. For high impact study using Two-stage gas gun, the impact region is modeled using Smooth Particle Hydrodynamic (SPH) technique and Lagrangian method is used for rest of the material.

The simulation and experimental results from both cases are compared using a combination of Fast Fourier Transforms (FFT) and Shock Response Spectrum (SRS).

ACKNOWLEDGEMENTS

My first task is to acknowledge all those people that have contributed to my work described in this dissertation. I would like to dedicate this work to my parents who have always been the zeal of inspiration to perform. I deeply express my sincere gratitude to my advisors Dr. Mohamed B. Trabia and Dr. Brendan J. O'Toole for trusting my abilities to work on this project. Their invaluable guidance, suggestions, thoughts throughout the entire course of this research work is priceless. They have also hugely influenced my professional & personal life in many ways.

I would like to thank Dr. Woosoon Yim, Dr. Yi-Tung Chen, Dr. Zhiyong Wang and Dr. Rama Venkat for their time in reviewing the prospectus, participation in defense and counseling of the dissertation as committee members. Their guidance throughout this dissertation review process has been invaluable. I would also like to express gratitude to those students and members of research staff that have assisted in completing this project. I would also like to thank Roy, Jagadeep, Nirup and Rana.

Finally, I would like to thank my wife Priya, for her support and motivation through my final days of completing my dissertation.

TABLE OF CONTENTS

LIST OF TABLES

LIST OF FIGURES

CHAPTER 1

RESEARCH OBJECTIVE

The objective of the research is to better understand how high levels of shock are transmitted through joints. High levels of shocks can be generated by hypervelocity impact. Generally hypervelocity impacts are defined as impact velocity on the order of or greater than the impacting material wave speed. In this section, high shock or impact refers to impact load acting on the structure, which can damage the structure or bolt assembly. Examples of these impacts range from blast to projectile impact.

Joints can be subjected to various degrees of shock loads depending on impact. Typical factors that affect the response of a bolted joint include, preload (bolt tightening), intensity of the impact, and damping within the joint. The complexity in designing bolted joints under these conditions lies in the limitations of available methods to characterize their behavior. It is important to construct a predictive model of structures with bolted joints undergoing high levels of shock. There are many parameters to choose and ignore when it comes to building a finite element (FE) model for simulation. Selecting and avoiding the correct parameters leads to reasonable simulations. The aim of this work is to develop a reasonable model for analyzing and predicting shock propagation across bolted.

The research mainly focuses on the effect of torque tightness on the joints. Experimental testing can act as a base for creating FEA model. The research investigates different modeling methods in predicting the shock response through joints.

To achieve the research objective, the task is subdivided into steps:

1. Design an experiment setup for dynamic testing of joints
2. Design data acquisition system
3. Validate different types of data acquisition system
4. Conduct series of dynamic experiments at different torque level
5. Identify a proper method to analyze the data
6. Analyze different software modeling techniques to solve this problem and isolate one suitable procedure
7. Model the experiments close to ideal situation using FEA and compare the results with experiments
8. Study the trend in acceleration with respect to different torque levels

CHAPTER 2

INTRODUCTION

Bolted joints are common type of fastener used in military vehicles and blast containment vessels. These equipment's consist of several parts which are jointed together with bolts through flanges. Mechanical joints have complex nonlinear behavior and it may be because of material, geometry and joints itself. Shock transfer through the joints has high degree of influence on the dynamics of the structure. Study of high shock transmission through bolted joint structures is of particular interest to the army. In this report, high impact or shock loading refers to impact load acting on the structure, which can damage or deform the structure or bolt assembly. In impact testing, an object of certain mass and velocity comes in contact with a stationary object at equilibrium which results in deceleration of the impact and transmission of force wave on the test specimen. Low shock loading is normally induced by impact hammer on the structure and doesn't create plastic deformation.

Few of the important transient shock loading can be initiated by projectile impact or blast. It's almost impossible to model or test the entire equipment because of the computation and experimental limitations. So it is important to understand the physics of shock transfer through bolted joints.

Finite Element method (FEM) is a common numerical method to solve problems in engineering. In FEM, the model is divided into smaller bodies called elements and these elements are interconnected through nodes. The elements have the material and

structural property defined. The solution to the problem is obtained by solving a set of differential equations. FEM uses piecewise polynomial solution to solve the differential equation. Finite element Analysis (FEA) is an implementation of FEM to solve a certain type of problems. The finite element method is a very useful tool for simulation of mechanical joints under impact loading. Even this method has limitations in simulating the dynamic response of the joints. The shock propagation in the bolted joints is a complex phenomenon ad involves short duration transient loading, large displacement, contact of the bolted joints and structure. To handle these complexities an explicit FE analysis tool, LS-DYNA is used.

This dissertation focuses on developing a tool to simulate the bolted joints when subjected to high impact loading. There are many parameters in FEA which controls the outcome of the simulations. Selecting the right parameter is critical step in modelling the experiments. Obtaining an exact solution from simulation when compared to the experiment would be very difficult. So the aim is to develop a satisfactory method for analyzing and designing the shock propagation in bolts connection.

In Chapter 2 of this thesis a literature review is presented which describes the work done in bolted joints. This review addresses different assessment method and tools available for bolted joints. It also describes the current methods that are available for developing a finite element model for shock propagation.

Chapter 3 describes the experimental setup and fixture design for impacts, when the structure is subjected to plastic deformation. The equipment used to subject the

structure to plastic deformation is also described. In Chapter 4 a FE model is constructed for simulating the experiment. The chapter describes different methods available for simulating the experiment. Selection of different parameters and the assumptions made for the simulation are also discussed. Chapter 5 shows the results from the experiment and FEA. The results are compared using different techniques. Results and methods are summarized in Chapter 5

In Chapter 6, an experimental fixture is designed in such a way that the bolts are subjected to plastic deformation. Chapter 7 discusses the finite element model and the material model used for defining the experiment. Chapter 8 discusses the results from FEA and experiment and results are compared.

Finally results of the dissertation are summarized and conclusion is presented in Chapter 9.

2.1 Literature review

The following is a brief overview of some of the research conducted in this area. There has been great number of work published with static and fatigue loads on bolted joints. Bahaari et al. [1] developed a methodology based on inelastic finite-element modeling to evaluate analytical stiffness and strength characteristics of steel bolted end-plate connections.

Ju et al. [2] used a three-dimensional (3D) elasto-plastic finite element method to study the structural behavior of the butt-type steel bolted joint and the results were compared with American Institute of Steel Construction (AISC) specification data. Maggi

et al. [3] did a parametric study on the behavior of bolted extended end plate connections using Finite Element (FE) modeling tools.

Mattern et al. [4] studied wave propagation in T shaped structures. The structure, discussed in this research is a steel construction of top-hat profiles and sheets, connected with spotwelds, which is impacted by a metal ball at the top.

The complex behavior of bolted joints plays an important role in the overall dynamics of the structure. This complex behavior can be effect of slip. Gaul and Lenz [5], focused on estimating the energy dissipation in bolted joints associated with microslip and macroslip regimes. Kess et al. [6] developed a finite element model to simulate energy dissipation through joints. Lobitz et al. [7] compared different modeling technique to predict the energy dissipation due to slip. Reid and Hiser [8] had done a detailed modeling of bolted joints with slippage to study the roadside structures. They studied discrete-spring based clamping model with rigid parts and stress based clamping model with deformable elements to determine joint slippage behavior. Force-deflection curves from simulation compared fairly well with the experiment results.

Kim et al. [9], investigated a modeling technique of the structure with bolted joints, they tested four kinds of finite element models; a solid bolt model, a coupled bolt model, a spider bolt model, and a no-bolt model. All the proposed took pretension effect and contact behavior between flanges to be joined into account. Among these models, the solid bolt model, which is modeled by using 3D solid elements and surface-to-surface contact elements between head/ nut and the flange interfaces, provides the best accurate responses compared with the experimental results

The slip mechanism also causes damping in the system. Gaul and Nitshe [10], studied the nonlinear transfer behavior of frictional interface and the damping mechanism in joints. Eskandaraian et al. [11], developed a finite element model to simulate the slip base bolted joint in a sign support beam. Wentzel and Olsson [12] created a FE model and incorporated coulomb friction to study the frictional and plastic dissipation in joints. And the results were compared with experiments.

Preload plays an important parameter in joints. It affects the dynamic response of the whole system. There has been number of work done on effects of preload on static loads. Park et al. [13] discussed preloading of core bolt of a vehicle rubber mount, which is subjected to impact. Here the bolt is preloaded by applying force directly on the bolt shank. The disadvantage of this method of applying preload is that, the preload force will not be constant throughout the explicit analysis. Schiffner [14] showed the simulation of pre-stressed screw joints in complex structures such as flywheel using truss and beam elements instead of 3-D volume elements.

Esmailzadeh et al. [15] analyzed the preloaded joints on decaying pressure. Damping through bolted joints was considered in modeling the system. A mass –spring-damper model for closure bolting system subjected to dynamic pulse loading were presented. It is observed that existence of damping reduces the maximum bolt deformation and stress. Duffey [16] developed a simple spring-mass model for closure bolting systems, including the effects of bolt pre-stress. An analytical solution was developed for the case of an initially peaked, exponentially decaying internal pressure pulse acting on the closure.

Duffey [17] presented bounding, closed-form solutions for selecting the bolt preload for a square, flat plate closure subjected to a pressure pulse load. The solutions considered the limiting case in which preload is primarily dependent on closure bending response as well as the limiting case in which preload depends on elastic bolt response.

Pilkey et al. [18] tried to develop a robust, practical procedure to identify damping matrices for structures modeled by linear viscous damping. Impact hammer was used for this purpose. Effect of bolt tightening on the frequency is also discussed. O'Toole [19] studied different finite element modeling techniques for applying preload on joints.

Kerekes [20] used a simple beam model of the screw with fatigue loading to show the damage vulnerability of pre-stressed screws on the flange plate. Hartwigsen et al. [21] used two structures with bolted lap joint to study the non-linear effects. They are beam with bolted joint in its center and a frame with bolted joint in one of its members. Songa, [22] developed an Adjusted Iwan Beam Element (AIBE), which can simulate the non-linear dynamic behavior of bolted joints in beam structures. The same element was used to replicate the effects of bolted joints on a vibrating frame; the attempt was to simulate the hysteretic behavior of bolted joints in the frame.

Feghhi [23] studied shock propagation in bolted structures and discussed several error analysis techniques to compare two time signals. Nakalswamy [24] showed different preload modeling procedure for dynamic finite element analysis and compared with experimental results. They used both cantilever beam and a hat section for the study. The fixtures were induced to low and high level impacts using hammer and gas

gun respectively. Semke et al. [25] studied the dynamic structural response of piping systems and effective analysis techniques were recommended to assess the influence of a bolted flange with an elastic gasket. The influence of an elastic gasket is minimal for dynamic loadings, as shown in both the experimental and numerical results presented. Impact hammer was used for the experiment. The dynamic effects of a bolted flange and gasket on a piping system are critical in their use and has been demonstrated that the finite element method can simulate the response of an overhanging beam with a varying mid span. Kwon et al. [26] studied FE analysis of bolted structures for static and dynamic loading. They developed three kinds of models for structures with bolted joints: detailed model, practical model and simple model. Based on the applications, one of these models can be selected for stress analysis.

There is little or no work done on joints when impacted at hypervelocity. Hypervelocity studies are generally done for testing materials which are used for armors, space vehicles and for bird impact testing on aircrafts. The mechanism of impact varies with impact velocity. Hopkins and Kolsky [27] defined five regimes of impact:

(I) Elastic impact: Where the stresses generated does not exceed the yield strength of the material. So the response of the material is only depended on elastic modulus and elastic wave velocity.

(II) Plastic impact: Where the velocity is higher than the elastic impact and stresses generated exceed the yield strength and undergoes plastic

deformation, but the density of the material does not change. But the response still depends on the material property.

(III) Hydrodynamic impact: As the velocity still further increases, the impacted material acts as a fluid. The material property changes with respect to changing density of the material

(IV) Impact at sonic velocity: As the impact velocity further raises and approaches or exceeds elastic wave speed, more energy is dissipated on the impact region and shock waves are generated. Normally shock waves travel faster than the elastic wave speed and it is function of impact speed, density of impactor and target material.

(V) Explosive impact: As the velocity further increases, all of the energy is dissipated in the impact region. The heat produced in the concentrated area in impact region is high enough to melt and vaporize the material.

There has been huge amount of research going on to understand the physics behind Impact at sonic velocity and Explosive impact for different materials. There are several limitations in understanding and modeling hypervelocity impact. Since the shock wave travels through the material faster than the elastic wave speed, it is very important to understand the physics of the impact first.

There is a certain difference in the way the material fails from a hypervelocity impact when compared to a regular impact. These high speed impacts produce inelastic collisions causing permanent deformations to both the bodies. Rolsten and Hunt [28]

showed that huge amount of heat and radiation is generated from the impact as the bodies collide.

To describe the physics of a hypervelocity impact, consider a simple two dimensional model of projectile and a target. When a projectile impacts the target, the particles on the front surface of the projectile are brought to rest instantaneously and a shock wave is formed. The shock wave brings each succeeding layer of particle to rest. The pressure in the shock compressed region is very high initially and is constant throughout the region at the time of impact. The particles on the edge of projectile are subjected to very high pressure gradient due to shock loading. This pressure gradient caused the particles to be accelerated radially outwards and a release wave is formed. This release wave relives the radial pressure of the projectile. Upon impact, two shock waves propagate away from the interface, one towards the end of the impactor and one towards the rear side of the plate. At the same instant, two additional waves are generated from the edges of the impactor towards the center. Rarefaction waves are generated from the back surface of the target and the impactor. Initial shock compression is a non-isentropic process and the release of the rarefaction waves is an isentropic process, the entropy of the material increases on impact and then brought back to ambient conditions adiabatically. Thus the additional energy is converted into localized heating at the impact region [29]. The rarefaction wave which are generated on the free surface act as a tensile wave. At any point when this tensile stress exceeds the tensile strength of the material, failure occurs. As a result of this, additional rarefaction waves are generated on the free surface of the material.

The radial pressure release causes shear stress to the developed on the edge of the projectile and radial acceleration of the particle causes tensile stress along the length of the projectile. When the stresses are above the strength of the material, the material starts to flow.

When the projectile impacts at the speed higher than the speed of elastic wave speed, shock waves is produced and the material act as fluid. The material property of the target plate doesn't remain constant throughout the experiment. Wilbeck [30] clearly showed that the pressure of the material is a function of the shock speed and particle speed on the material.

$$P_2 - P_1 = \rho_1 u_s u_p \quad (1)$$

Where, P_2 and P_1 are the pressures of the material in front of the shock region and behind the shock region and u_s and u_p are the shock speed and particle speed or impact velocity respectively. ρ_1 is the initial density of the material.

Difference between the pressures P_2 and P_1 is called the Hugoniot pressure (P_H). This pressure plays an important role in defining the material property when subjected to shock load. For low velocity impact, the shock velocity u_s , can be approximated to bulk wave velocity C_o .

$C_0 = \sqrt{\frac{K}{\rho}}$, where K is the bulk modulus of the material. (2)

Therefore,

$$P_H = \rho_1 C_0 u_p; \quad (3)$$

From the above equations 2 and 3, clearly shows that the physics of the model depends on the shock wave speed and it is not linear with respect to impact speed as shown in Figure 2.1. There is considerable difference in Hugonoit pressure when calculated from shock velocity to bulk speed velocity. Equation 3 may be ideal for low velocity impact, but at high speed impact, shock speed plays a major role.

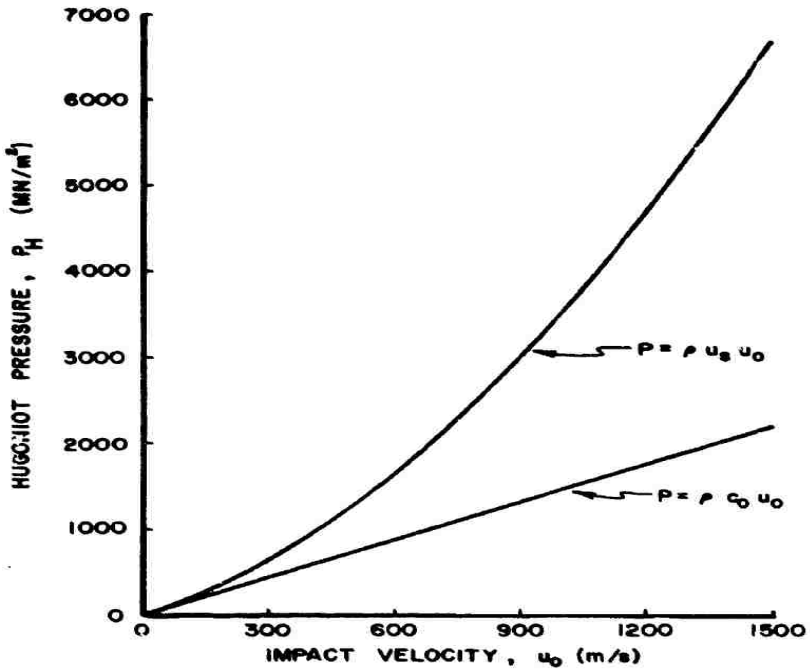

Figure 2.1. Relationship between Impact velocity and Hugoniot Pressure for Water [30]

CHAPTER 3

EXPERIMENTAL SETUP FOR BOLTED JOINT UNDER HIGH IMPACT

3.1 Introduction

In combat, military vehicles undergo a high impact/shock loading such as mine blast or projectile impact. These loads may yield or damage the structure and the bolts. There is only a limited amount of published literature describing the proper method for measuring or modeling the transient shock propagation across bolted connections for high impact loading.

The main objective of this research is to study the effects of bolted joints on shock propagation due to high impact.

This chapter provides a detailed experimental setup and procedure for conducting high impact loading on structure with bolted joint. A test fixture used for studying bolted joints subjected to high impact loading. This chapter also contains a description of ULNV two stage light gas gun facility and diagnostic equipment and other measurement techniques. Explanation of theory and design of two stage light gas gun is outside the scope of this project. However, the functioning of the gas gun has been explained. Figure 3.1 shows setup of two stage light gas gun at UNLV.

The gas gun was designed by Physics Application [31] to launch a polycarbonate Lexan projectile of 0.233gm mass at a speed of 4-7 Km/s using hydrogen or helium as a propellant. Such high speed impacts are generally termed as Hypervelocity Impacts [32].These kinds of equipment's have been proved to be a suitable for impact studies

because of their simplicity, velocity reproducibility. Two stage gas gun has been used to study the material properties at high strain rate.

For a typical shot, the time for preparation, setting up the target and instrumentations takes about 1 hour. With the target aligned and instrumentation set, the time for the shot takes only few minutes. After shot procedure like removing the target and cleaning the gun takes more than 1 hour.

3.2 UNLV Two-Stage Light Gas Gun and Diagnostic Equipment

3.2.1 Components in Two –Stage Gas Gun

This section describes different components that make up the gas gun. The section also describes the working of gas gun, procedure involved in firing the gun and the instrumentation used to measure velocity of the projectile and acceleration. The test fixture used for this experiment is also discussed.

The gun shown in figure 3.1, it consists of powder chamber, pump tube, launch tube, blast tank and target chamber. The 1.49 m long, 19mm diameter pump tube is initially filled with either hydrogen or helium gas. Lighter gases are generally used for obtaining higher projectile velocity. Velocity of the projectile is proportional to gas pressure at the base of the projectile. The velocity of the gas and therefore the velocity of the projectile are limited to the sound speed of the gas. The sound speed of the gas is

inversely proportional to molecular weight of the gas used. Thus using lighter gas like hydrogen and helium typically produces higher velocity [33, 34].

The 96 mm long, 21 mm diameter powder chamber holds the gun powder. The powder chamber is attached to the pump tube by threads. The pump tube in turn is attached to launch tube by a central breech assembly. The barrel of the central breech assembly tapers the diameter of the gun from 20 mm to 5 mm over the distance of 0.1905 m. The 1.016 m long launch tube guides the projectile and constrains the pump gas as the projectile accelerates.

3.2.1.1 Breech and Pump Tube

The powder chamber shown in Figure 3.2 contains burning gun powder during the firing of the gun. This drives a piston of 20mm diameter, 124mm long plastic piston down the pump tube. The ignition of the gun powder is achieved by firing of a primer at back of the cartridge. The cartridge, Figure 3.3, is also filled with gun powder. The discharge of capacitor is used to activate a solenoid which drives a firing pin into the primer. The capacitor, Figure 3.4 is normally charged by AC power supply shown in Figure 3.5. The gun powder in the cartridge burns rapidly when struck by firing pin, figure 3.6. This then ignites the gun powder in the powder chamber.

Figure 3.1: Two Stage Light Gas Gun at UNLV

Figure 3.2: Powder Chamber

Figure 3.3: Cartridge

Figure 3.4: Capacitor Box

Figure 3.5: AC Power Supply

Figure 3.6: Firing Pin and Solenoid

The ignition of the gun powder in the powder chamber drives the piston down the pump tube. The piston compresses the gas in the pump tube. For this research the pump tube is filled with helium gas to a pressure of 200 psi. Before filling up, the pump tube is completely evacuated using a vacuum pump. This is done to avoid any other gas present in the system. The gun powder used in powder chamber and cartridge are IMR 4064 and green dot smokeless powder respectively. For these experiments the cartridge was filled with 0.6.gm of green dot smokeless powder and powder chamber with 20gm of IMR 4064 powder.

The piston, as shown in Figure 3.7, is made of plastic. The shoulder at the powder chamber end of the piston prevents the movement of piston when the pump is evacuated and then pressurized before the shot. The O-ring on the piston restricts the flow of pump gas or gun powder around the piston. The piston mass is 26.72 gm for the all the experiments conducted. Figure 3.7 also shows the piston after the experiment.

Figure 3.7: Piston

3.2.1.2 Central Breech and Launch Tube

The central breech between the pump tube and launch tube is show in the Figure, 3.8. The central breech provides a means of stopping the piston and aids in maintaining high pressure at the base of projectile. The central breech must be able to withstand the high pressure developed during the compression of pump gas by the piston. The strength of the coupling section is one of the limiting factors of the gas gun performance [35].

Figure 3.8: Central Breech

A petal, as shown in Figure 3.9, prevents the acceleration of the projectile until the pump gas pressure reaches a specified value. The valve is a 1.57mm thick, 57mm diameter 304 stainless steel disk which is scored with a cross. These groves gives controlled burst geometry and burst pressure for the valves. The pressure built up causes the valve to rupture. Figure 3.8, also shows the petal valve after the experiment. Since this pressure is dynamic and not static, it's difficult to find actual pressure for the opening of the valve. The petal valve is placed on O-rings to avoid the leakage of gases from the central breech assembly.

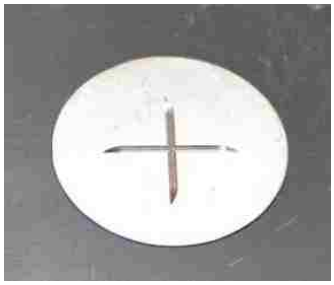

Before

After

Figure 3.9: Petal Valve

The projectile as show in figure 3.10 is located in the launch tube. The projectile is a cylinder with 5.5mm diameter and 8.6mm long. It weight around 0.25 gm. It is made up of polycarbonate. Polycarbonate projectiles are generally used since it acts as a lubricating agent as it moves along the launch tube. Usage of metallic projectile is very limited, since it damages the inner surface of the launch tube. But metallic projectiles can be used with polycarbonate sabot. The projectile is roughly placed 4 cm inside the

launch tube. The 5.5 mm barrel of the launch tube has a smooth bore, as shown in Figure 3.11.

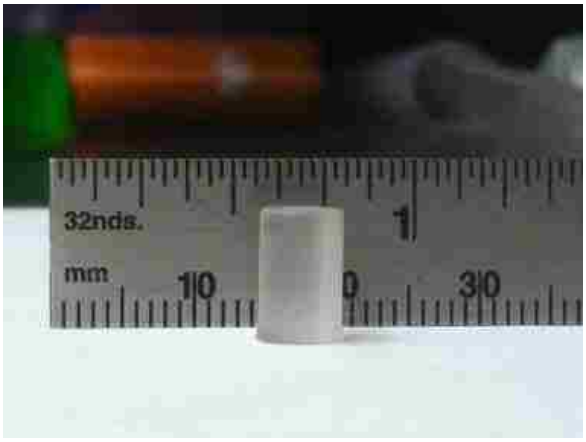

Figure 3.10: Polycarbonate (Lexan) Projectile

Figure 3.11: Launch Tube

3.2.1.3 Blast Tank and Target Chamber

The blast tank, as shown in Figure 3.12 approximately 0.228m diameter and 0.812m long provides the volume for the expansion of the propelling gas.

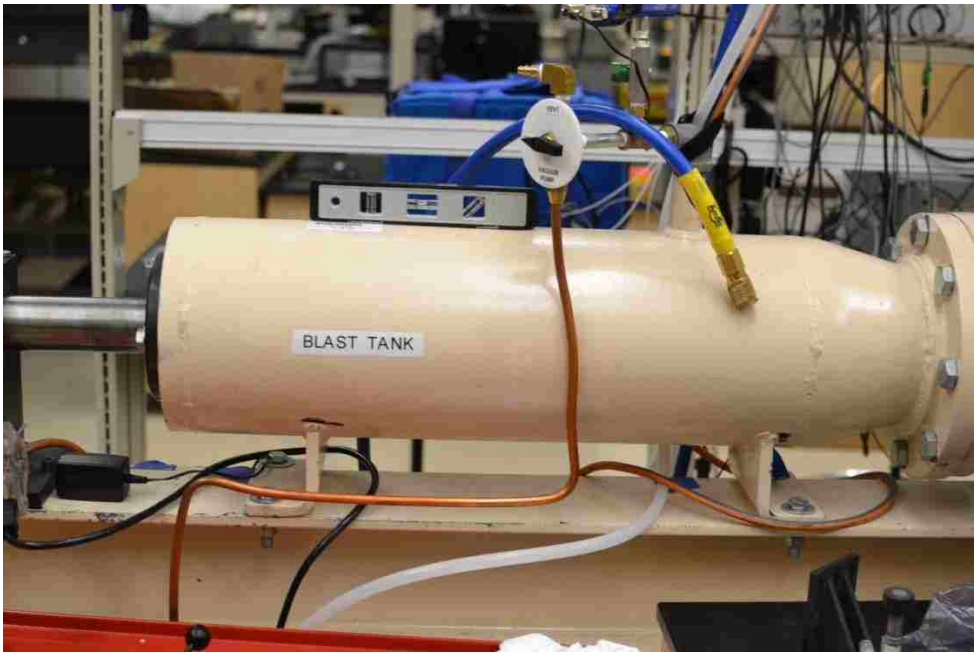

Figure 3.12: Blast Tank

Blast tank also has an evacuation valve to let the out the gasses after the experiment. Immediately on the downrange of the blast tank is the instrumentation tube, as show in Figure 3.13. The instrumentation tube or drift tube is 0.152m in diameter and 0.609m long. The drift tube allows us to measure the velocity of the projectile. It has two see through glass ports. The velocity measurement instrument is described in the next section.

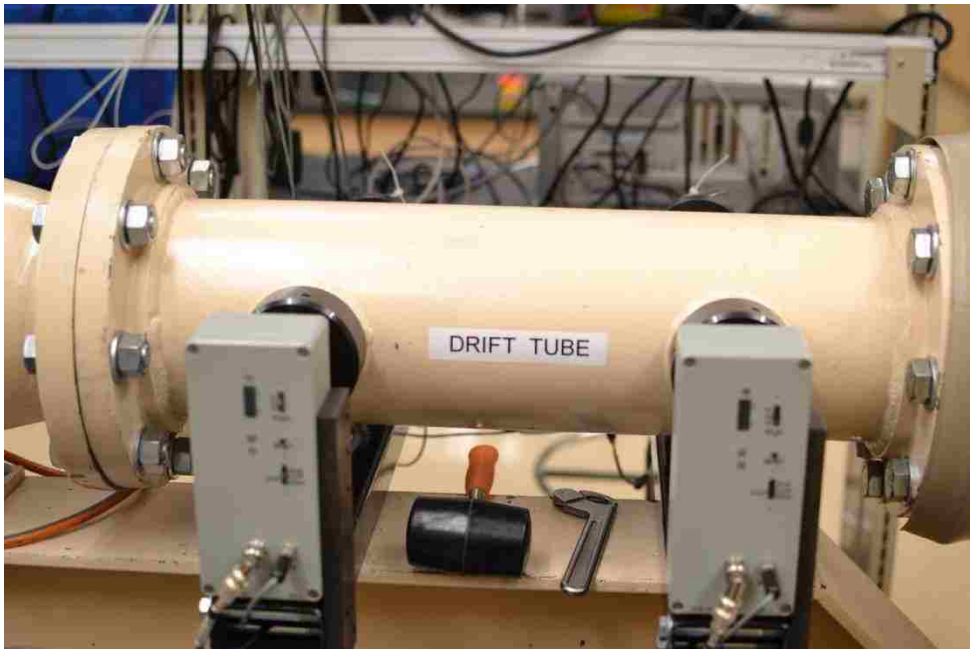

Figure 3.13: Drift Tube and Ports for Velocity Measurement

The target chamber, as show in figure 3.14, is the final stage of the gas gun. It is 0.6096m in diameter and 0.3048m deep. The target tank provides space for mounting the bolted joint fixture and carry instrumentation. Ports in the target tank as shown in Figure 3.15 provide access for various instrumentations. All flanges, ports and joints in the tank assembly are assembled together with O-rings. This is done to isolate the interior volume from the atmosphere.

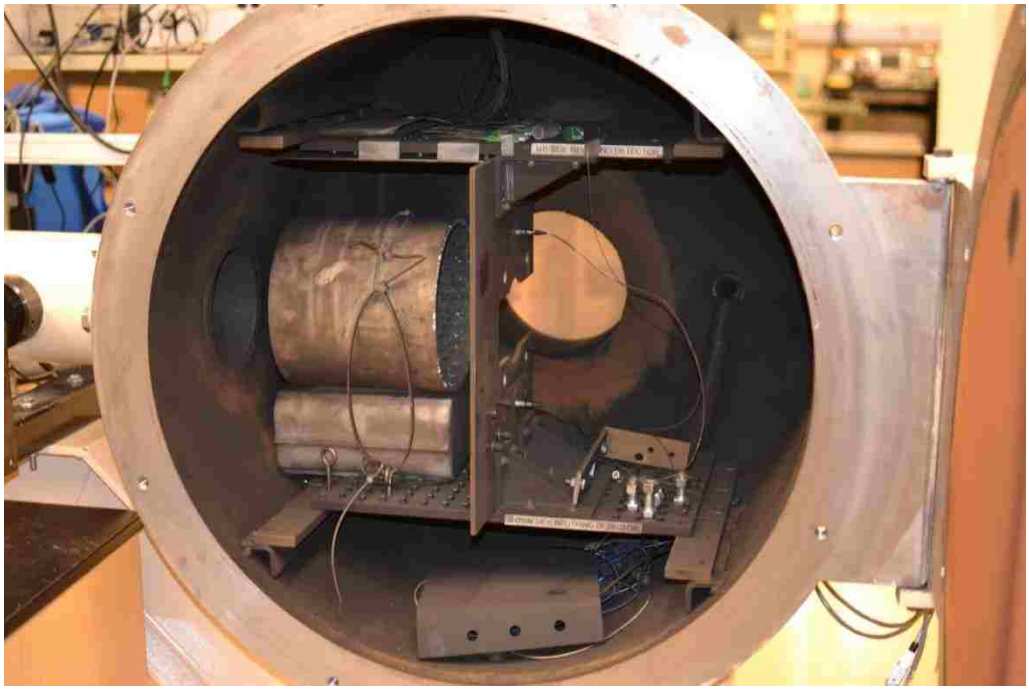

Figure 3.14: Target Chamber

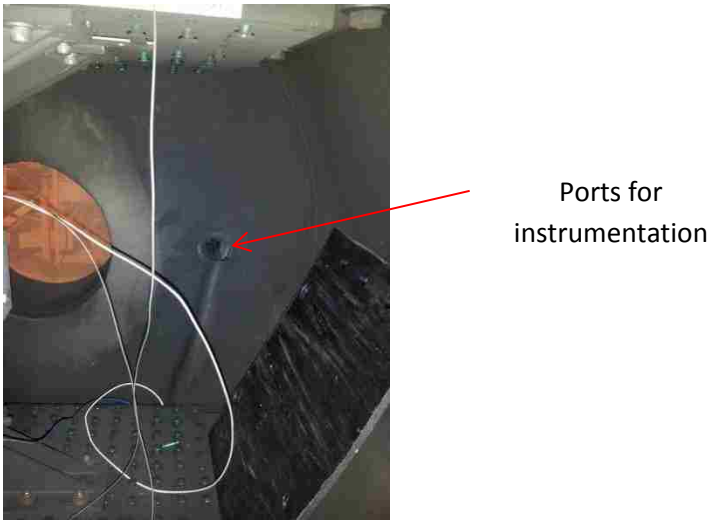

Figure 3.15: Ports inside Target Chamber

Pressure in the launch tube, blast tube and target chamber are reduced to around 666 Pa absolute pressure (99.4 % vacuum, 5 Torr) before the experiment. This is

done to avoid the friction between the projectile and air, which might disintegrate the projectile and reduce the speed of the projectile. Care is also taken to shield the diagnostic equipment from the debris produced by the projectile impact on the target.

The gas gun and the target tank assemblies are mounted on a single beam, which in turn is supported by 3 legs. The 3 legs are grounded to the floor. The gun assembly is supported with adjustable mounts that allow the pump tube to be aligned. Figure 3.16 shows the support for the gas gun.

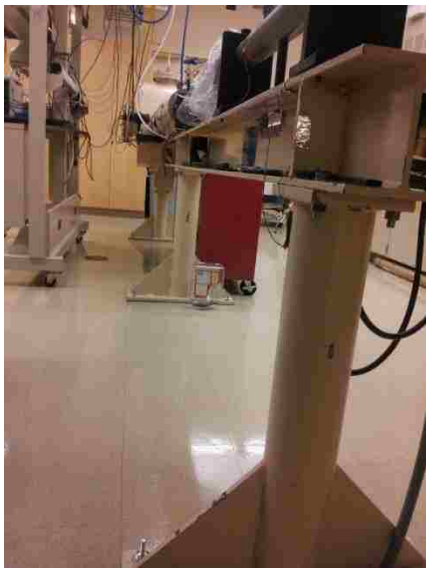

Figure 3.16: Support for the Gas Gun

3.2.2 Projectile Velocity Measurement

The projectile velocity is measured using two station laser intervalometer system. The unit has two laser sources at 670 nm wavelength one each at start and stop

port. Each laser beam is passed through one port to a receiving station. The receiving station has a narrow band pass filter centered at 670nm wavelength. This is to ensure that the array does not detect external light. The laser illuminates a linear array of 32 photodiodes in the receiving station. The passage of projectile is sensed by the array with reduction on light level at photodiodes. The receiving station then triggers the timer unit with 1.5V signal, show in figure 3.17. The "start" receiving station triggers when the projectile reaches the "start" port and another signal is send from the "stop" station when the projectile reaches the stop port.

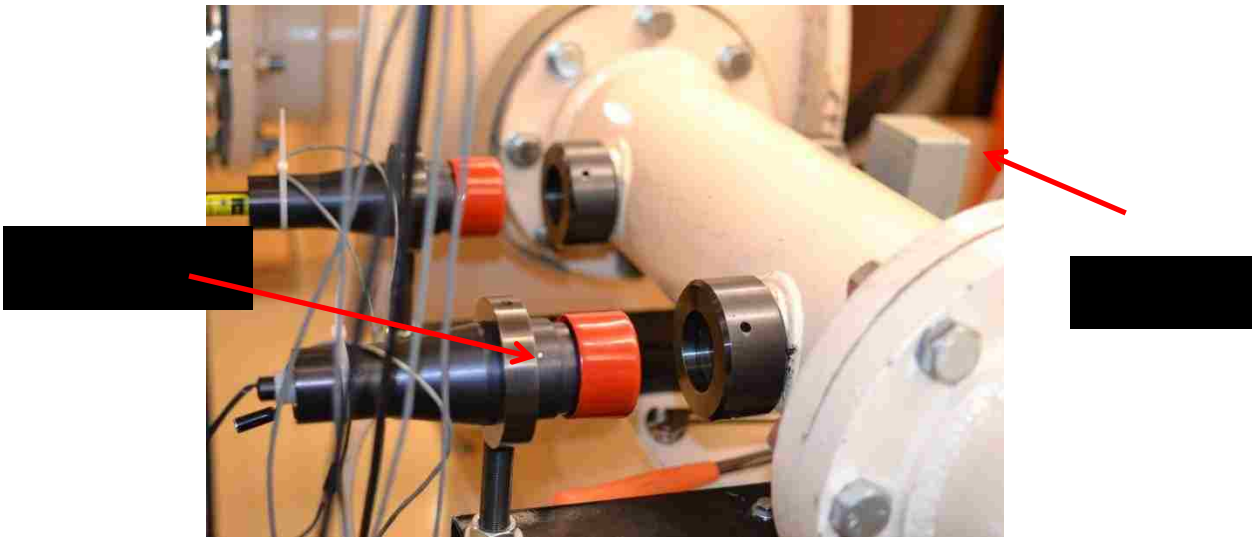

Figure 3.17: Laser Intervalometer System

The timer unit, as show in Figure 3.17, is a six-digit counter with an in build timer, is enabled by a signal from "start" laser. The counter continues to increment until it receives the "stop" signal from the "stop" receiving station. Knowing the distance between the two stations and the time for travelling the distance, speed of the

projectile can be calculated. Typically the distance between the two receiving station is 0.3048m.

Figure 3.18: Timer Unit

3.2.3 Gas Handling System

The gas gun is supplied with gas handling control panel, show in Figure 3.19. The control panel is used for evacuating, filling and venting the pump tube. The control panel is assembled with manually operated valves, regulators and pressure and vacuum gauges. The control panel has two pressure gauges which indicate the pressure on the gas cylinder and pump tube pressure. The vacuum pressure gauge indicates the vacuum pressure on the downstream side of the projectile and the pump tube. The gas cylinder which holds helium or hydrogen is connected to the control panel through high pressure rated hoses, which in turn is connected to the pump tube using hoses. A manually

operated valve is used for selecting either hydrogen or helium gas to be filled in pump tube. A small vacuum pump is connected to the system though brass fittings. The vacuum pump is used to evacuate the downstream side of the projectile. A vent valve allows to the gas in pump tube to be evacuated after the experiment or during emergency.

Figure 3.19: Gas Handling System

3.3 Test Fixture

For the study of bolted joints, a fixture is developed as shown in Figure 3.20. The fixture has three components: target, target holder and bolts. The target and target holder are held together by four grade 5 ½" bolts. The target and target holder are made up of A36 mild steel. Figure 3.21a and 3.21b shows the dimensions of the target

plate and target holder respectively. The fixture is assembled is manner that the bolts take tensile load.

The target plate is fixed to two ¼" thick optics bread boards (top and bottom) through 4 angle brackets. The optics bread boards are in turn supported by c–sections that are welded to the target chamber. The angle bracket and optics bread board assemble are show in Figure 3.22. The target holder and target are set at 14" inside target chamber.

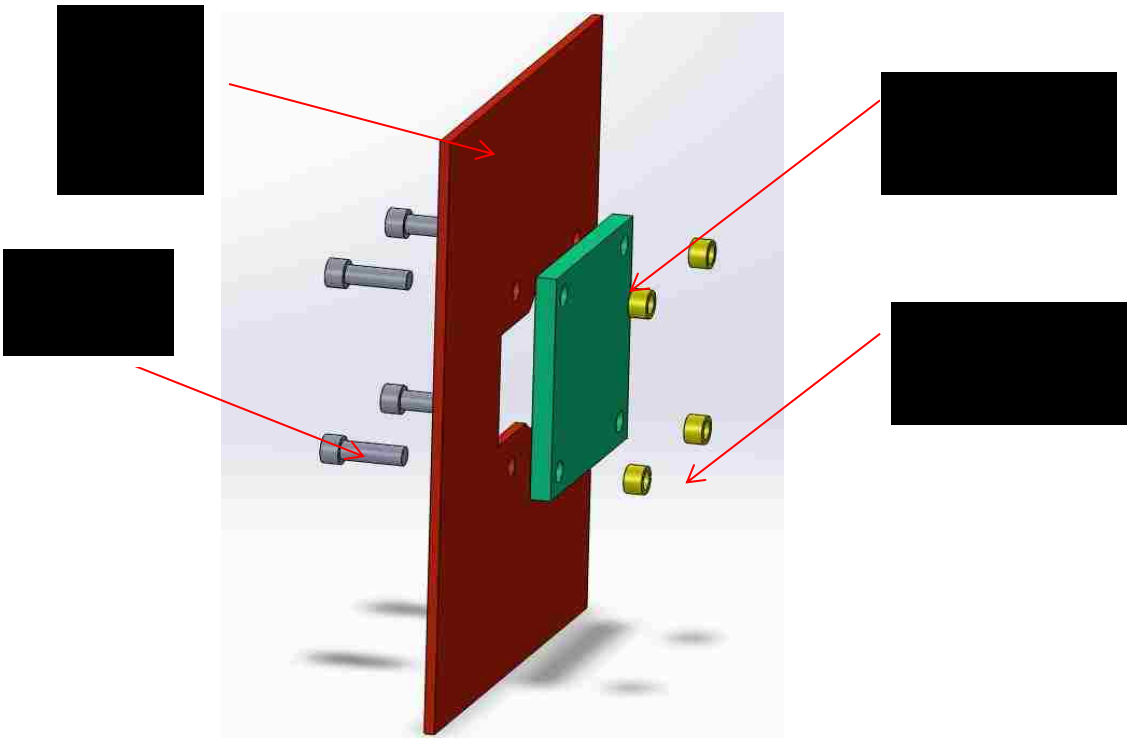

Figure 3.20: Exploded View of Fixture

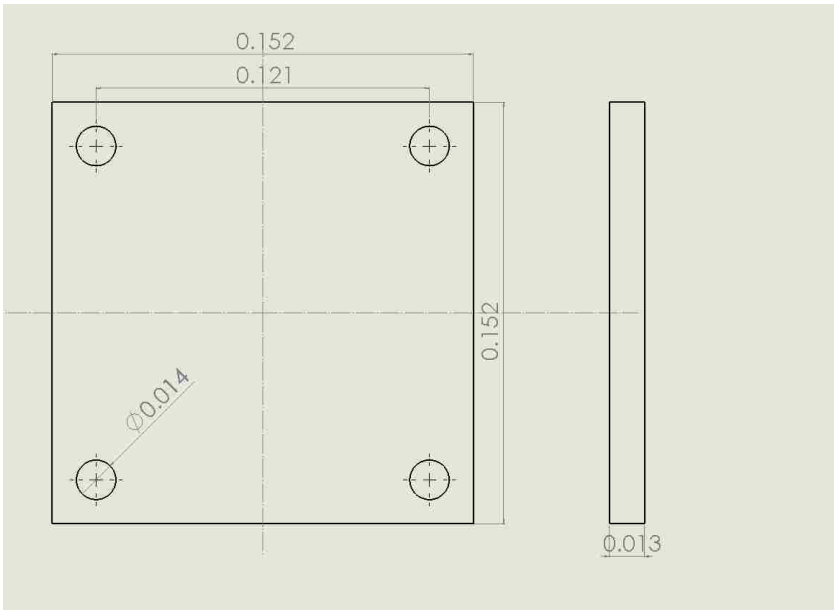

Figure 3.21a: Target Plate (Dimensions in m)

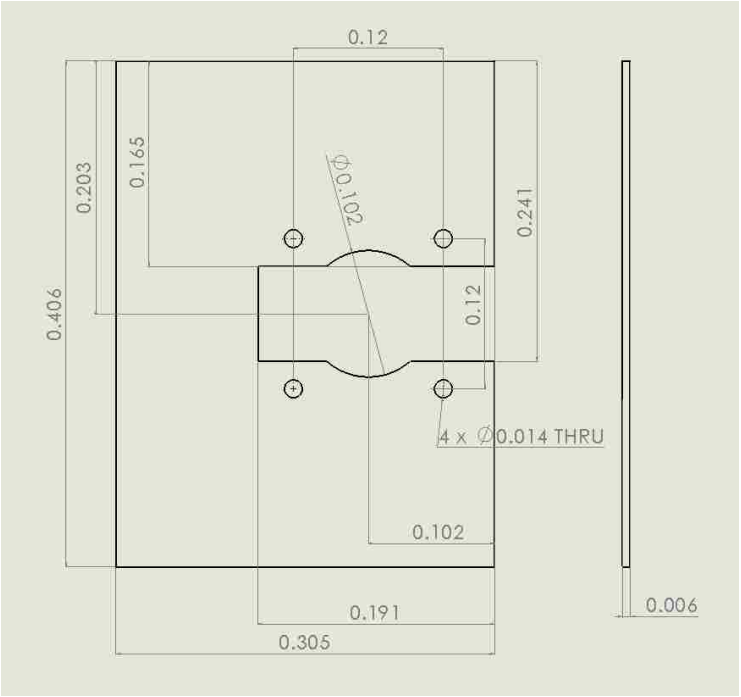

Figure 3.21b: Target Holder (Dimensions in m)

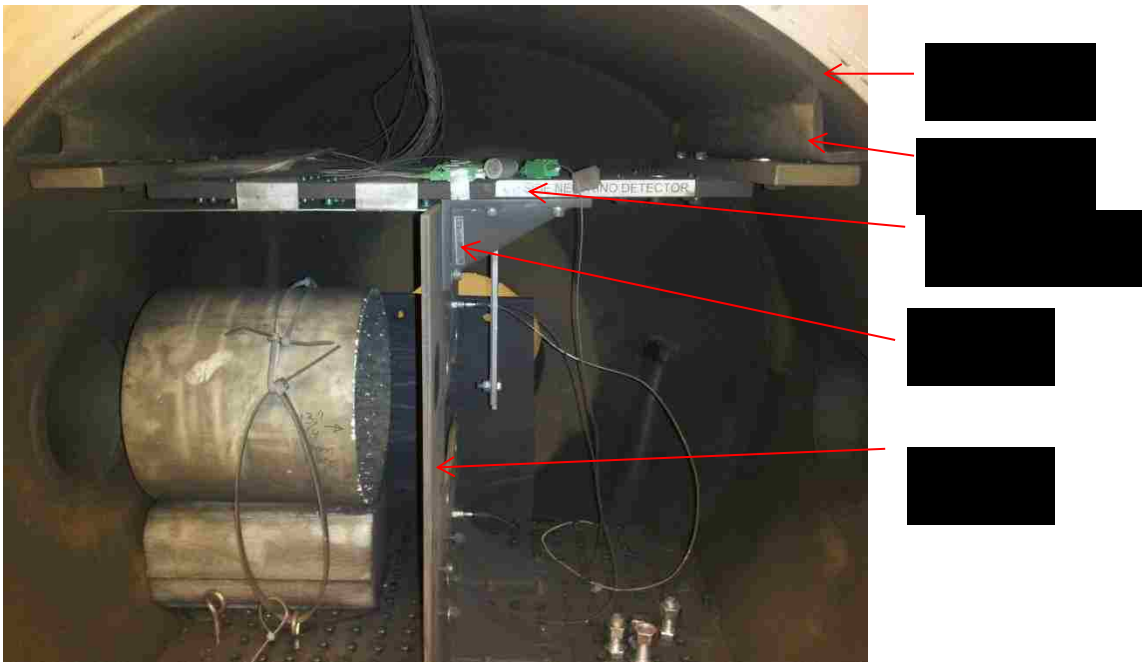

Figure 3.22: Target Holder Support System

3.4 Accelerometer

The accelerometer, Dytran 3200b, is used to measure the acceleration target holder. Figure 3.23 shows the accelerometer used in the experiment. Pertinent information for the accelerometer is shown in Table 3.1.

Figure 3.23: Dytran 3200B Accelerometer

Table 3.1: Dytran 3200B Accelerometer Information [36]

Performance	**Units (SI)**
Sensitivity (± 10%)	0.05 (mv/G)
Measurement Range	± 70,000 G
Resonant Frequency	>90 kHz
Frequency Range (± 10%)	0.35 to 10,000 Hz
Physical	
Sensing Element	Ceramic
Sensing Geometry	Shear
Size (Hex X Height)	9.5 X 16.25 mm
Weight	6gm
Mounting	¼" – 28 mounting stud
Electrical Connector	10 – 32 micro-coaxial

The accelerometer is connected to a data acquisition system through a signal conditioner. This particular accelerometer uses a 10-32 micro–coaxial cable as a connector. A signal conditioner is a device that converts one type of electronic signal into another type of signal. Its primary use is to convert a signal that may be difficult to read by conventional instrumentation into a more easily read format. In performing this conversion a number of functions may take place. For example, when a signal is amplified, the overall magnitude of the signal is increased. Converting a 0-10mV signal

to a 0 -10V signal is an example of amplification. 4103C current source power unit, manufactured from Dytran Instruments, was used as the signal conditioner shown in Figure 3.24. The input to the signal conditioner is the accelerometers and the output from this instrument is received as input by the data acquisition system. Specification of the signal conditioner is shown in the Table 3.2

Figure 3.24: Dytran 4103C Signal Conditioner

Table 3.2: Dytran 4103C Signal Conditioner Information [37]

Power Source	9 V (two in number)
Battery Life	40 hours
Size (H x W x D)	2.5 x 5.2 x 3.3 inches
Weight	12 ounces

3.5 Data Acquisition System

Data acquisition systems, as the name implies, are products and/or processes used to collect information to document or analyze some phenomenon. As technology has progressed, this type of process has been simplified and made more accurate, versatile, and reliable through electronic equipment. Equipment ranges from simple recorders to sophisticated computer systems. Data acquisition products serve as a focal point in a system, tying together a wide variety of products, such as sensors that indicate strain, flow, level, or pressure.

The accelerometer is connected to the Dytran 4103C signal conditioner and the output of the conditioner is captured using the DL 750 scopecorder oscilloscope as shown in Figure 3.25. An oscilloscope is a type of electronic test equipment that allows signal voltages to be viewed, usually as a two-dimensional graph of one or more electrical potential differences (vertical axis) plotted as a function of time or of some other voltage (horizontal axis). Sampling rate of 10ms/s was used in all the test cases for data acquisition.

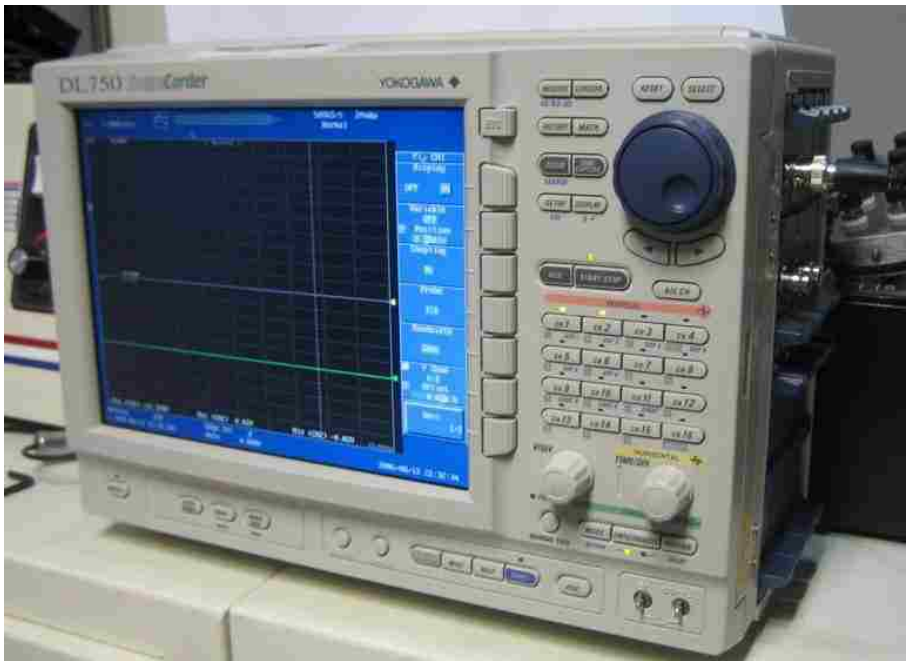

Figure 3.25: DL 750 Scopeorder Oscilloscopes

Figure 3.26 shows the accelerometer location, which is at 0.123m from the center of the test fixture. This location was selected to ensure the accelerometer is not overloaded and to avoid any physical damage. The accelerometer is threaded to the target holder plate in a ¼" – 28 threaded hole as shown in Figure 3.27.

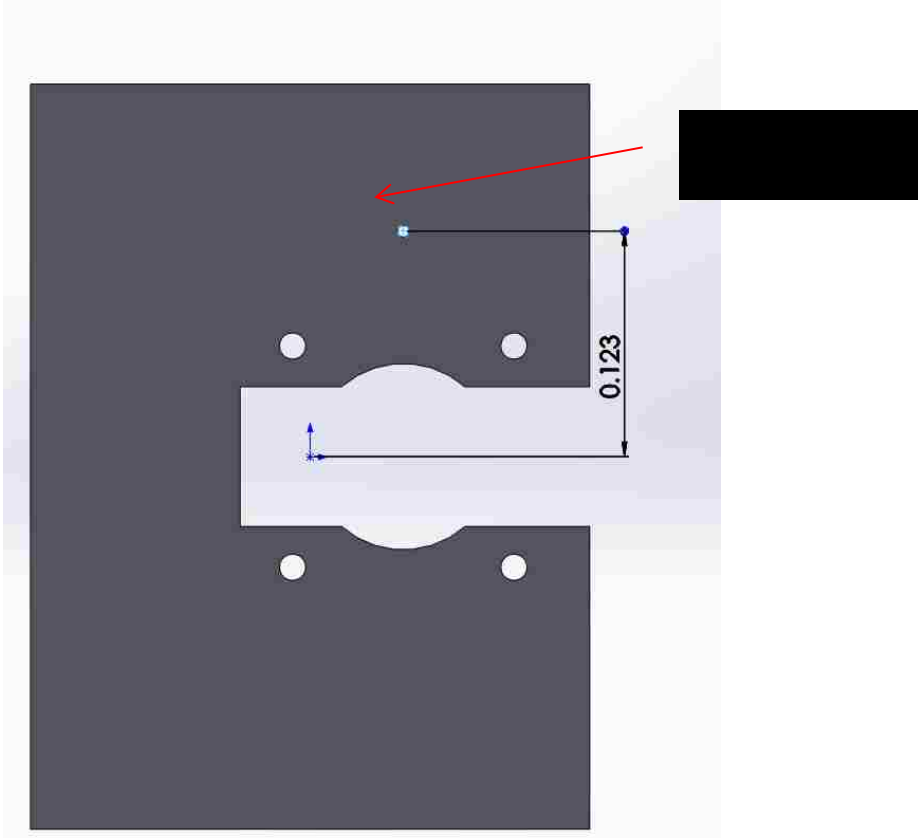

Figure 3.26: Accelerometer Location (Dimensions in meter)

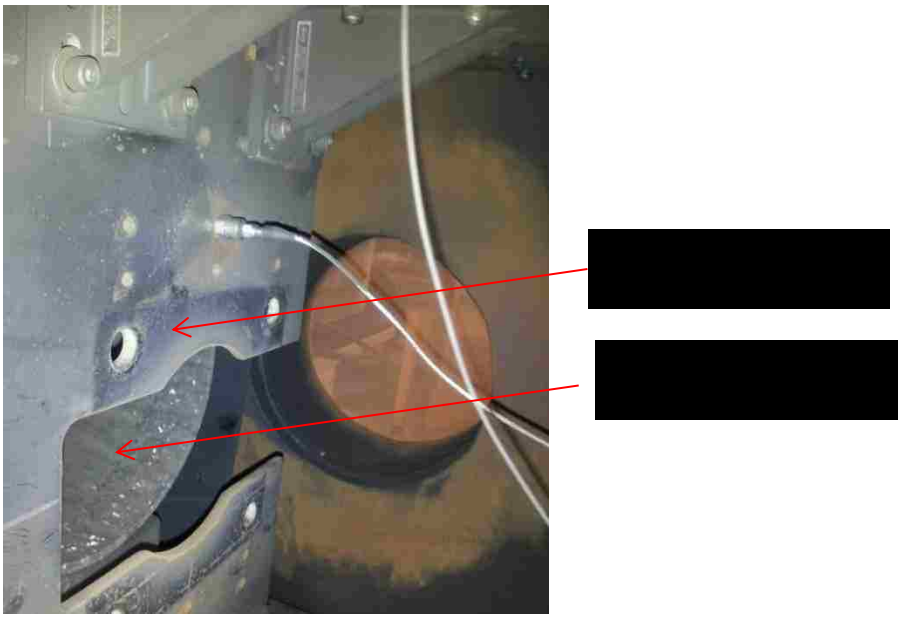

Figure3.27: Accelerometer attached to the Target Holder

The oscilloscope is trigged from the “stop” signal using Stanford Research Systems, Model DG535, 4 channel digital delay/pulse generator as shown in Figure 3.28. Time delay of 85 µs is applied to the signal generator.

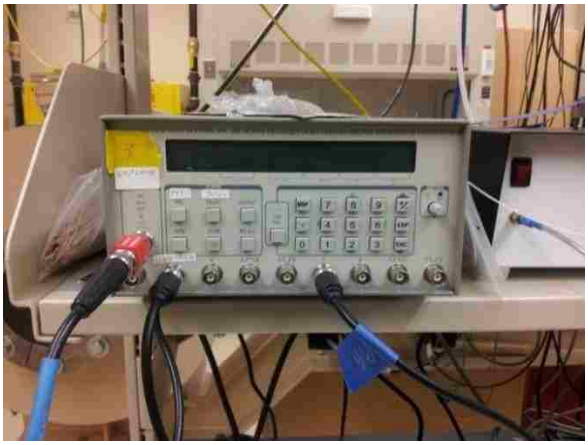

Figure 3.28: Stanford Research Systems Model DG 535 Digital Delay/Pulse Generator

Experimental setup for high impact testing is shown in Figure 3.29. Figure 3.30 shows a typical damage of target plate from projectile impact.

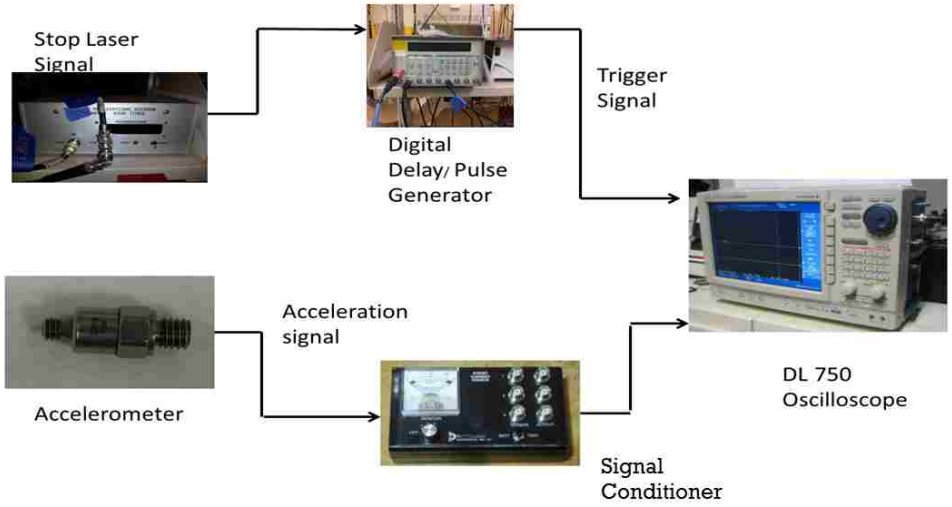

Figure 3.29: Experimental Setup

Front Side

Back Side

Figure 3.30: Typical ½" A36 Plate Damage

3.6 Typical Experimental Results

Damage of the target plate is measured by three parameters: Depth of penetration, diameter of the hole and bulge on the back side of the plate. Measurement techniques are explained in Appendix A. Appendix A also explains the repeatability of the experiment. Table 3.3 shows a typical damage on the plate with a projectile velocity of 4540 m/s.

Table 3.3 Damage Area for a Typical Experiment with Projectile Velocity of 4540 m/s

	Bulge (mm)	Penetration (mm)	Diameter (mm)
Experiment	2.10	6.20	16.30

Figure 3.31 shows a typical acceleration profile in time domain from an experiment. The acceleration signal is measured for 8 ms at a sampling rate of 10^7 samples per second. The acceleration results were filtered using a band-pass

Butterworth filter from 3000 Hz to 10,000 Hz. The acceleration signals are high-pass filtered at 3000 Hz to remove the DC shift created by the accelerometer. The low-pass filter is at 10,000Hz, since the accelerometer has a range from 0.35 to 10,000 Hz. The results are show in Figure 3.32. Validation of the accelerometer for these high accelerations is done using Planar Doppler Velocimetry (PDV) developed by NSTec and show in Appendix B. Appendix C explains the reasons for filtering at 3000 Hz.

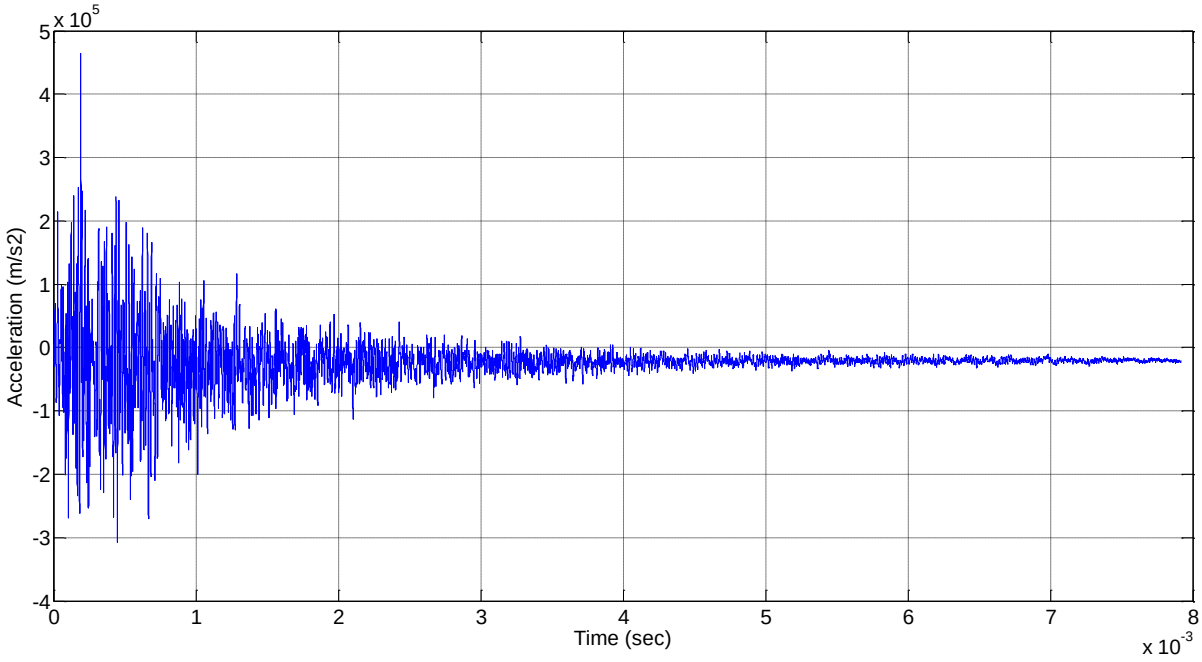

Figure 3.31: Typical Unfiltered Acceleration Data

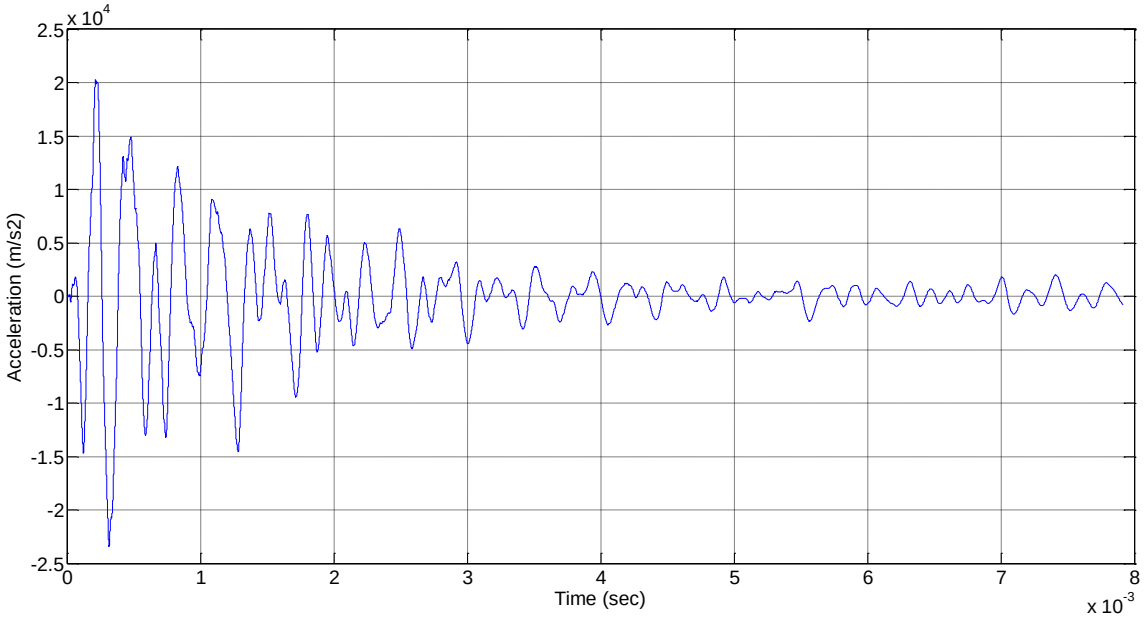

Figure 3.32: Typical Filtered Acceleration Data

CHAPTER 4

FINITE ELEMENT ANALYSIS OF HIGH IMPACT EXPERIMENT

4.1 Objective

Finite Element Analysis (FEA) was performed to simulate the experiments and study the behavior of joints under hypervelocity impacts. The objective of this study is to reduce the need for experimental testing by developing procedures that allow the use of FEA to simulate impact.

4.2 Hardware and Software

All the computation analysis was done on 64 GB, 48 cores Linux server located at UNLV. ANSYS workbench and LS-Prepost was used as a preprocessor to create and mesh the 3D model of fixture. LS.DYNA v975 [38] was used to simulate the structure response. The following unit system was used for all computational modeling:

- Force: Newton (N)
- Length: Meter (m)
- Mass: Kilogram (kg)
- Time: Seconds (sec)

4.3 Element

For low impact analysis, Lagrangian finite element method approach is used. Lagrangian approach generally uses nodes and elements. A typical type of element is show in Figure 4.1. The geometry, node locations, and the coordinate system for an element are also shown.

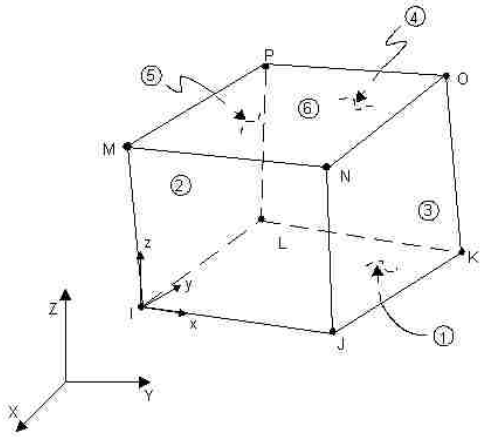

Figure 4.1: Typical Lagrangian Solid element [39].

These elements have nine degrees of freedom at each node: translations, accelerations and velocities in the nodal x, y and z directions and rotations about the x, y and z axes.

Simulation of penetration of projectiles into target material requires a numerical technique that allows the penetration of one body by another, which results in high deformation of material. This type of problems is typically difficult to simulate. For penetration problems, using Lagrangian approach, the mesh undergoes huge deformation, which causes mesh instability issues. Normally Lagrangian method requires some kind of augmentation to minimize large mesh distortions. One of the most common methods used to avoid mesh distortion is material erosion technique. This technique removes the distorted elements from the simulation based upon user defined failure criteria such as defining the failure strain of the material. However, there are no general guidelines for defining these criteria. The other most common numerical technique for simulating large deformation problem is Eulerian approach. The main

problem with this approach is mixing of materials when the projectile and target deform. The problem gets too fuzzy and results in numerical instability.

A more recent numerical approach for large deformation problem is Smooth Particle Hydrodynamics (SPH), which is a new class of numerical method that was developed particularly for large deformation problems. SPH is a meshless Lagrangian method that doesn't not require a numerical grid or element to calculate spatial derivative, which enables SPH method to avoid mesh tangling and distortion. In SPH, a set of particles represent the solid geometry. Each particle represents an interpolation point for which all properties are known. Nodal forces, energy and pressure are computed between each particle with regular interpolation function known as smoothing length. Hayhurst and Clegg [40] performed a number of hypervelocity impact simulations on Aluminum plates using SPH technique. Schewer [41] compared Lagrangian, Eulerian and SPH method. The analysis was compared with experimental data. They concluded that for high impact and high deformation analysis, SPH has more advantages when compared to other method. Farauad et al. [42] showed SPH method has few limitations like mesh stabilization, global energy, incorrect plastic estimation, maximum pressure overestimation pressure fluctuation with nearby particles and heavy computational time. Jackson et al. [43], studied the mesh refinement issue with SPH particle. The FE simulation was compared with experimental data on fuselage section of an aircraft. Coarser mesh yielded better result when compared with finer mesh. They concluded that by simply refining the mesh density doesn't yield better results. And the mesh sizing is dependent on problem formulation.

It was decided to develop and run SPH models. Since, SPH models are computationally expensive, it was decided to model only the damage area of the target and entire projectile as SPH and rest of the target and target holder as Lagrangian.

4.4 Model Development and Meshing:

Similar to the experimental setup, the FEA model has four basic components: projectile, target, target holder and bolts. Finite Element Lagrangian model was created in solid works as shown in Figure 4.2. Bolt and nut were modeled as a single part. The damage area from the experiments was approximately 20mm in diameter. It was therefore decided to have SPH elements in a cylinder of 40mm diameter in the center of the target plate to simulate damage area.

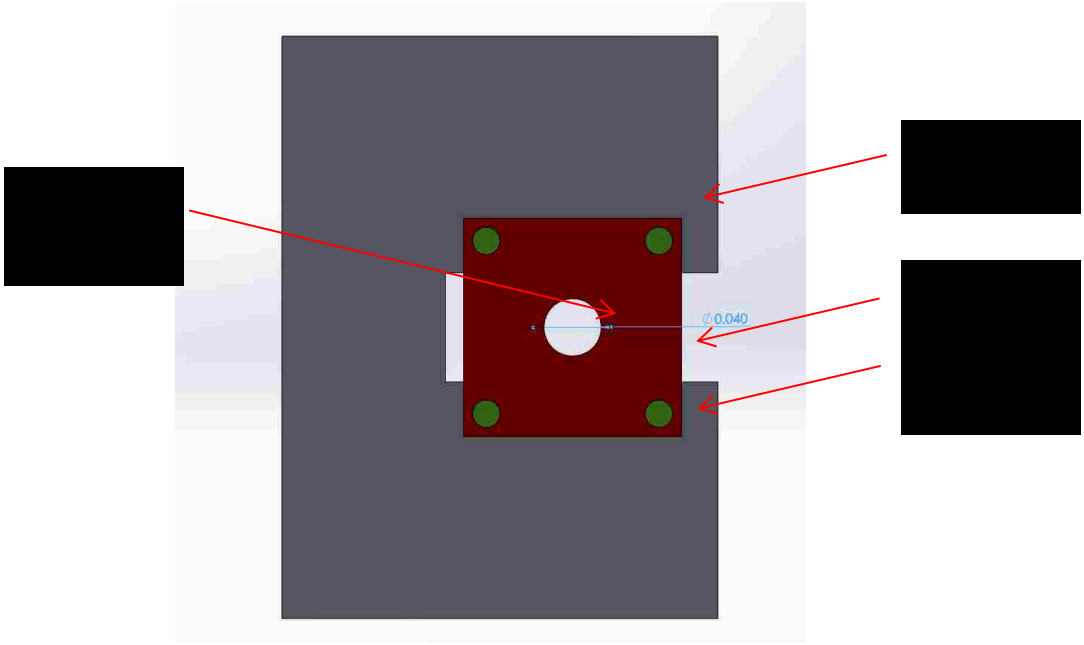

Figure 4.2: Solid Works Model

The solid works model was imported into ANSYS WorkBench for meshing. Target, Target holder and the bolts were meshed using Multizone option available in ANSYS Workbench. Table 4.1 shows element sizing and number of elements for each component. The target and target holder has 2 and 7 elements along the thickness directions.

Table 4.1: Lagrangian Element Size and Number of Elements

Part	**Element Size (10^{-3} m)**	**No. of elements**
Target	2	37,324
Target Holder	4	14,232
Bolts (4)	1.5	10,186

Figure 4.3 shows the meshed model of the entire fixture and Figure 4.4 shows the meshed model of ½" bolt.

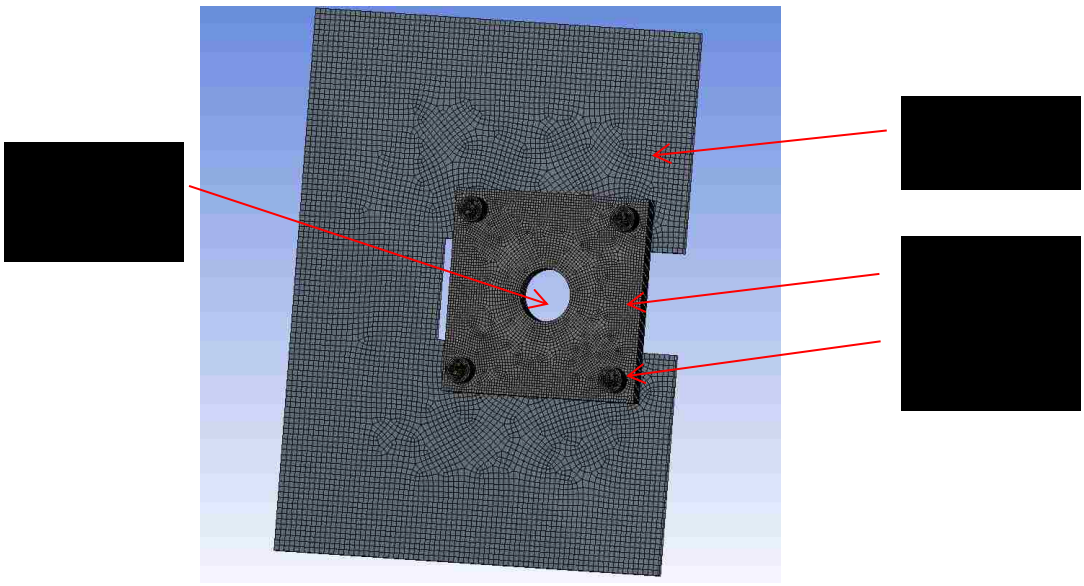

Figure 4.3: Meshed Geometry of the Fixture

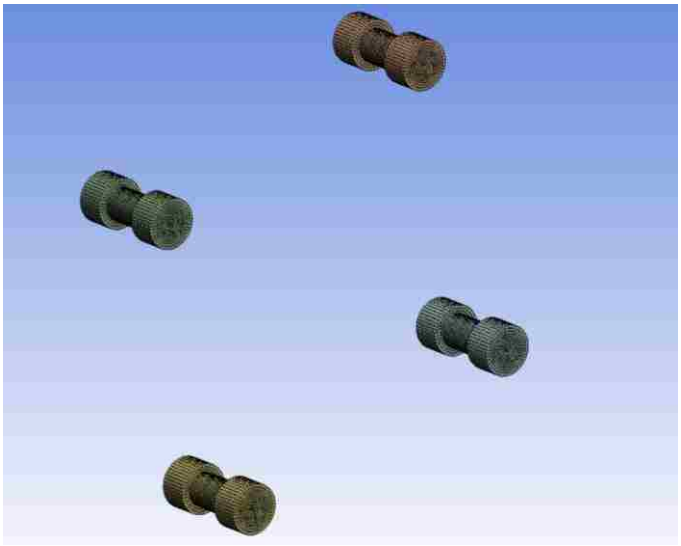

Figure 4.4: Meshed Model of ½" Bolts

An input file (.k) of the whole setup was created from ANSYS WorkBench. The input file was imported to LS-Prepost for the creation of SPH elements. Cylinder method in SPH generation option of LS-Prepost was used in creating the elements. This method requires the x, y and z coordinates with diameter and length of the cylinder, in our case it is both target and projectile. Density of the material and number of elements in x, y and z parameters are also required for the creating SPH elements.

Mesh dependency study for these experiments are outside the scope of the project. Different mesh densities were compared with the experimental data and it was found that 0.5mm spacing for both projectile and target produced better results.

Figure 4.5a and Figure 4.5b, shows the entire finite element model along with SPH element. The projectile and target has 1649 and 125,600 SPH particles which are equally spaced.

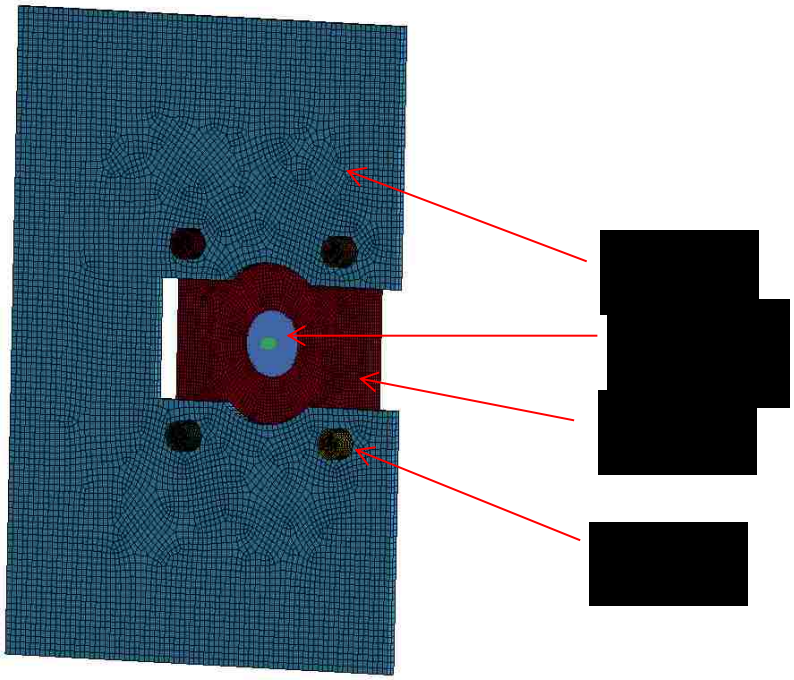

Figure 4.5a: Finite Element Model with SPH Elements

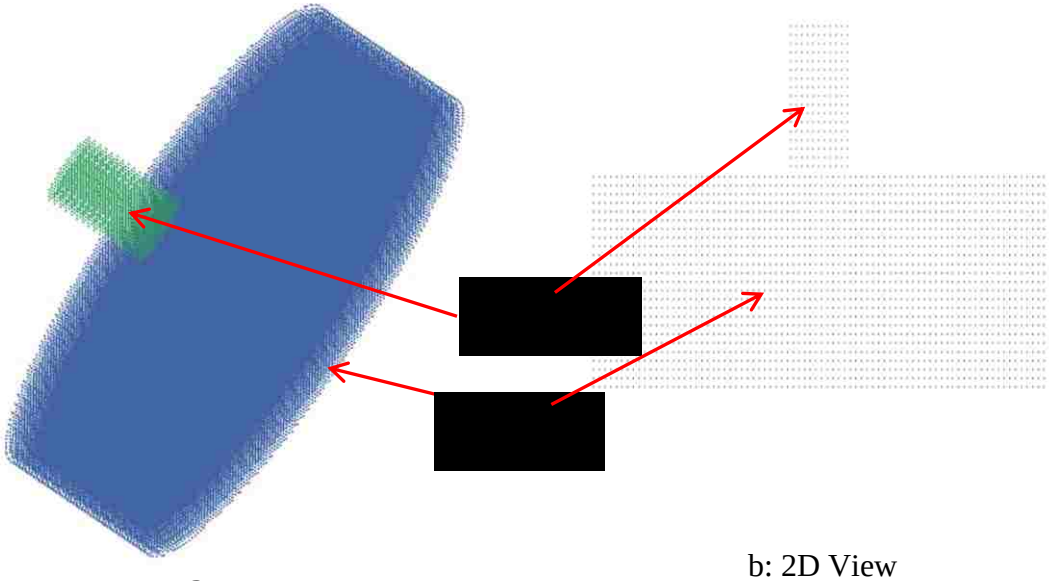

a: 3D View

b: 2D View

Figure 4.5 b: Target and Projectile Modeled as SPH Particles

4.5 LS-DYNA Input Cards

An input file was created in LS-DYNA after modeling the whole setup. In LS-DYNA all the information about the model was written in the form of cards in the input file. Cards are the commands, which contain information about various aspects of the model such as node and element definitions, materials, loads, boundary conditions etc. The following cards are used in the current model.

1. Control cards
2. Database cards
3. Material cards
4. Cards defining the parts and sections
5. Cards defining the nodes, elements
6. Contact cards
7. Cards defining the boundary conditions
8. Cards defining initial velocity and preload for the bolt
9. Cards defining box
10. Cards defining output

Descriptions of these cards are given below.

4.5.1 Control Card

CONTROL_SOLID and CONTROL_SPH provide control for respective elements. Default control parameters were used for solid elements. For SPH particles, “memory” parameter of 500 is used for all the simulations. It defines the memory allocation of

arrays during the initialization phase. Any finite element simulation with SPH particle is computationally expensive and also the projectile impact on the target material happens at a very short duration of time which is in the order of few microseconds, the SPH particles are killed after 80 microseconds. After this time period, interaction between SPH particles are not considered, but the mass of the particles are considered for the entire duration. Here is the example of the LS-DYNA card used.

```
*CONTROL_SPH
$$    NCBS     BOXID        DT      IDIM    MEMORY      FORM     START      MAXV
$#    ncbs     boxid        dt      idim    memory      form     start      maxv
         1         0    08E-05         3      0500         1     0.000     0.000
$$    CONT     DERIV       INI     ISHOW     IEROD     ICONT     IAVIS
$#    cont     deriv                iact
         0         0         0         1
```

4.5.2 Material Models

Constitutive relationships that account for large strains, high strain rates and temperature softening are essential for describing the behavior of materials that are subjected to high impact loading. As highlighted by Zukas [44], erroneous results can occur from use of inappropriate property data and constitutive relations.

LS-DYNA offers few material models which can define the constitutive behavior of metals. These include strain, strain rate and temperature effect on the stress state of the metals. Johnson and Cook [45] and Zerilli and Amstrong [46] are the few models available. Many researchers have shown the effectiveness of the Johnson and Cook model for high strain rate and high deformation problems.

In LS-DYNA, MAT 15 card is used for the defining the Johnson and Cook parameters. The Johnson and Cook constitutive relation defines the flow stress as a function of strain rate, equivalent plastic strain and temperature. The dynamic flow stress is expressed as:

$$\sigma_y = \left(A + B\,\epsilon^{pn}\right)(1 + C\ln(\dot{\epsilon}))\,(1 - T^{*m}) \quad (4)$$

where, σ_y is the flow stress A is the yield stress under quasi-static conditions, B and n are strain hardening parameters, m controls the temperature dependence and C the strain rate dependence.

ϵ^p is the equivalent plastic strain.

$\dot{\epsilon}$ is the effective plastic strain given by $\frac{\epsilon^p}{EPSO}$; where EPSO is the reference strain rate

T* is the homologous temperature and is defined as

$T^* = \frac{T - T_r}{T_m - T_r}$; where T is the absolute temperature and suffixes r and m indicate room and melting temperature.

The computational damage parameter "D" for Johnson and Cook is based on damage buildup and is given by

$$D = \sum \frac{\Delta\epsilon^p}{\epsilon_f} \quad (5)$$

Where D is the damage to material element, $\in^{p}$ is the increment of accumulated plastic strain, $\in_{f}$ is the accumulated plastic strain to failure from stress trixiality, temperature and strain rate and is given by

$$\varepsilon^{f} = [D_1 + D_2 \exp D_3 \sigma^*] [1 + D_4 \ln \varepsilon^*] [1 + D_5 T^*] \quad (6)$$

where, D_1, D_2, D_3, D_4 and D_5 are material parameters found experimentally.

σ* is the ratio of pressure to effective stress.

ϵ^* is the effective plastic strain given by $\frac{\epsilon^p}{\text{EPSO}}$; where EPSO is the reference strain rate.

Failure occurs when the facture parameter "D" reaches the value of 1. The values of Johnson and Cook parameter for Lexan projectile and A36 steel target are given in Table 4.2

Table 4.2: Johnson and Cook Material Properties

Parameter	**Lexan Projectile [47]**	**A36 Target[48]**
A	75.8 MPa	286.1MPa
B	68.9 MPa	500.1 MPa
C	0	0.022
M	1.85	0.917
N	1.004	0.2282
T_m	433 ^{o}K	1811 ^{o}K
γ	0.344	0.26
D_1	0	0.403
D_2	0	1.107
D_3	0	-1.899
D_4	0	0.00961
D_5	0	0.3

As discussed earlier, when the rarefaction wave from the free surface at any point exceeds the tensile strength of the material, failure or spalling occurs. A typical example of spall failure is shown in Figure 4.6. In LS-DYNA spall failure criteria is given by pressure cut-off (P_{min}) value in Johnson-Cook material card.

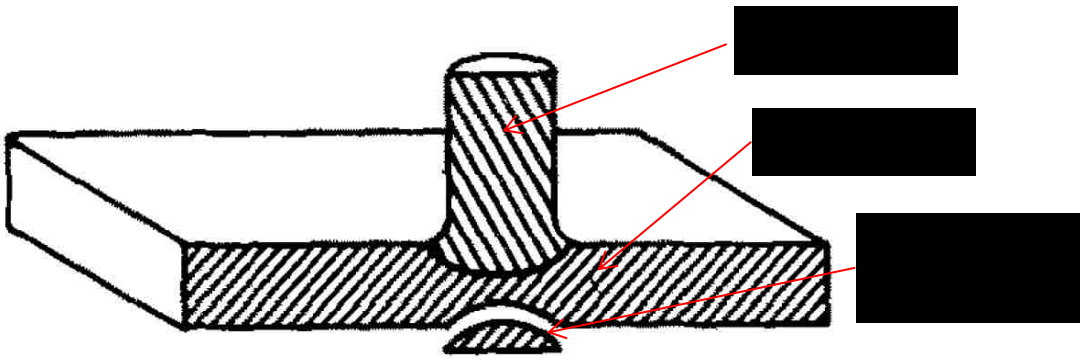

Figure 4.6: Typical Spall Failure [49]

For projectile (Lexan) the pressure cut off value is assigned as 160 MPa [50]. There is not much literature available for spall strength on A36 steel so it was assumed as 300 MPa and this value is comparable to other medium strength steel.

During hypervelocity impact, pressures are generated that can exceed the strengths of impacting materials by orders of magnitude [51], thus the materials are effectively behaving hydro-dynamically. In order to describe hydrodynamic response of a material under shock loading constitutive modeling is required.

Shock waves can be characterized as discontinuity in the properties of the medium. Across the shock there is a sudden change in pressure, temperature, internal energy and density. Therefore for analyzing the shock wave propagation, regions immediately ahead and behind the shock waves should be considered. The conservation laws across a shock front were originally defined by Rankine and Hugoniot for fluids, and are defined as:

Conservation of mass:

$$\rho_0 U_s = \rho_1 (U_s - U_p) \quad (7)$$

Conservation of momentum

$$(p_1 - p_0) = \rho_0 U_s U_p \quad (8)$$

Conservation of energy

$$E_1 - E_0 = \frac{1}{2} (p_0 + p_1)(V_1 - V_0) \quad (9)$$

where, V = 1/density

U_s and U_p are the shock and particle velocity respectively

P_0 and P_1 are the pressures behind and ahead of the shock

ρ_0 and $\rho_1$are the mass densities behind and ahead of the shock

E_0 and E_1 are the internal energies per unit mass behind and ahead of the shock

To solve the conservation equations, the equation of state (EOS) is required, which is commonly expressed in the Mie-Grüneisen form [51]:

$$P = P_r(V) + \frac{\Gamma(v)}{v} [E - E_r(\gamma)] \quad (10)$$

Where Γ is the Gruneisen parameter gamma: $\Gamma(v) = v \left(\frac{\partial p}{\partial E}\right)_v$

The functions $P_r(v)$ and $E_r(V)$ refers to the internal pressure and energy of the compressed material in terms of volume and are generally known parameter in Hugoniot shock curve. Using the above data, the internal energy and pressure can be

calculated at any point by using the reference Hugoniot shock curve and Gruneisen parameter gamma. In LS-DYNA, Equation (7) is typically expressed in form [38]:

$$P = \frac{\rho C^2 \mu \left[1+\left(1-\frac{\gamma}{2}\right)\mu-\frac{a}{2}\mu^2\right]}{\left[1-(S_1-1)\mu- S_2 \frac{\mu^2}{\mu+1}- S_3 \frac{\mu^3}{(\mu+1)^2}\right]^2} + (\Gamma + a\mu)E \qquad (11)$$

where, P is the pressure

C is the intercept of the shock and particle velocity curve

S_1 , S_2 and S_3 are coefficient of slope of shock and particle velocity curve.

Γ is the Gruneisen coefficient.

a is the volume correction factor

ρ is the density

$\mu = (\rho/ \rho_0) -1$

Mie – Gruneisen equation of state parameters for projectile (Lexan) and target (A36) are given in Table 4.3. Examples of cards defining the material property and equation of state are shown below.

Table 4.3: Mie – Gruneisen Equation of State

Parameters	Projectile (Lexan) [50]	Target (A36 steel) [66]
ρ (kg/m^3)	1190	7890
C (m/s)	1933	4659
S_1	1.42	1.49
Γ'	0.61	2.17

```
*EOS_GRUNEISEN
$#   eosid         c        s1        s2        s3     gamao         a        e0
         1 1933.0000  1.420000     0.000     0.000  0.610000     0.000     0.000
$#      v0
  1.000000
*MAT_JOHNSON_COOK
$#     mid        ro         g         e        pr       dtf        vp    rateop
         1 1190.0000 7.8600E+8 2.5400E+9  0.340000     0.000     0.000     0.000
$#       a         b         n         c         m        tm        tr      epso
 7.5400E+7 6.8900E+7  1.004000     0.000  1.850000 533.00000 298.00000  1.000000
$#      cp        pc     spall        it        d1        d2        d3        d4
     0.000 -1.600E+8  2.000000     0.000     0.000     0.000     0.000     0.000
$#      d5      c2/p      erod     efmin
     0.000     0.000         0     0.000
```

4.5.3 Cards Defining the Parts and Sections

In LS-DYNA, for SPH particles smoothing length parameter is used to determine the region of influence of the neighboring particles. The smoothing length which is depended on space and time variable is constant for each part initially. It is calculated by as the maximum value of all the minimum distance for each particle. This variable can be scaled by user defined variable, Hmin and Hmax in SECTION_SPH card. For all the simulations in this report, Hmin and Hmax value of 0.2 and 6 is assigned respectively. Here is the example of LS-DYNA cards used in this method.

```
*SECTION_SPH
$HMNAME PROPS       3sph
$#    secid      cslh      hmin      hmax    sphini     death     start
         7  1.200000  0.200000  6.000000     0.000     8E-05     0.000
```

4.5.4 Contact Card

Surface to surface contact is defined between bolts and target, target surface and target holder and bolt and target holder. Tied nodes to surface is defined between target SPH elements and target Lagranian elements.

4.5.5 Boundary Condition

In the experiment, the target holder is held in position by four angle brackets. We can safely assume that the angle brackets and the chamber are rigid and do not interfere with the response of the structure. To include the rigidness of the bracket, the area under the bracket on the target holder is fixed in all directions, as shown in Figure 4.7. In LS-DYNA BOUNDARY_SPC_NODE card is used for this purpose.

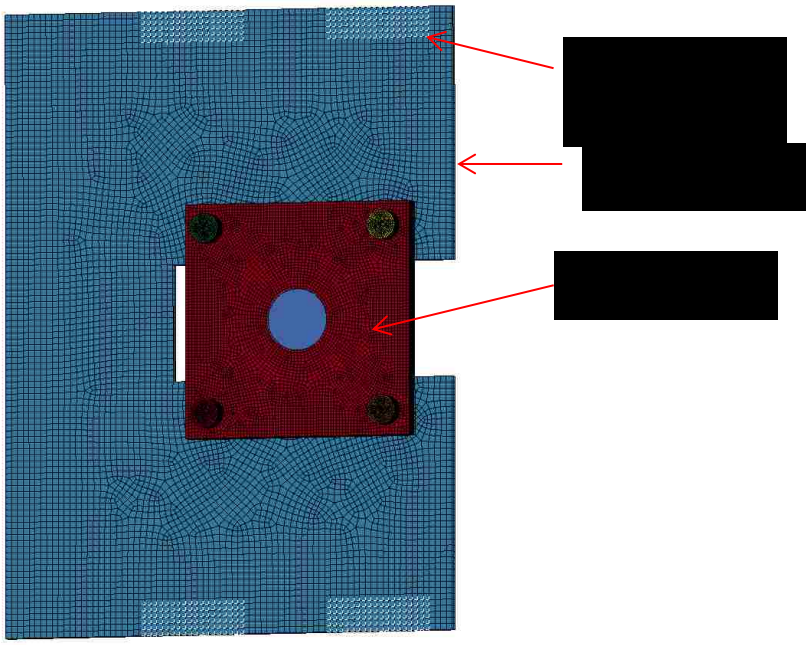

Figure 4.7: Fixed Boundary Condition

This card has the option of constraining a specified node or a set of nodes along the six degrees of freedom (three translational along the three coordinate axes x, y and z, and three rotational about these axes). Below is a sample of this card defined in the LS-DYNA input file,

```
*BOUNDARY_SPC_SET
$     1NSID       2CID      3DOFX      4DOFY      5DOFZ     6DOFRX     7DOFRY     8DOFRZ
$#     nsid        cid       dofx       dofy       dofz      dofrx      dofry      dofrz
```

4.5.6 Cards Defining Preload for the Bolt

In LS-DYNA bolt preload can be modeled in several ways. Few of the techniques are listed below. These techniques can be used in other applications to preload or pre-stress the structures.

- Applying force on the bolt and nut
- Applying force on the bolt shank
- Modeling interference fit between nut and plate
- Applying thermal gradient on the bolt shank
- Using INITIAL_STRESS_SOLID card in LS-DYNA
- Using INITIAL_STRESS_SECTION card in LS-DYNA

Pre-load is defined using INITIAL_STRESS_SECTION card throughout this research. INITIAL_STRESS_SECTION card method of modeling the preload in a bolt assembly is an easy and straightforward method that can be used in many applications to define preloads. This method uses these LS-DYNA keyword cards:

- DATABASE_CROSS_SECTION_PLANE: defines the cross-section of the part where the preload need to be applied.
- INITIAL_STRESS_SECTION: assigns the stress (preload) to the part and the stresses are defined using DEFINE_CURVE card.

Figure 4.8 shows a bolt assembly subjected to preload. The N, L and M vector defines the cross section of the part.

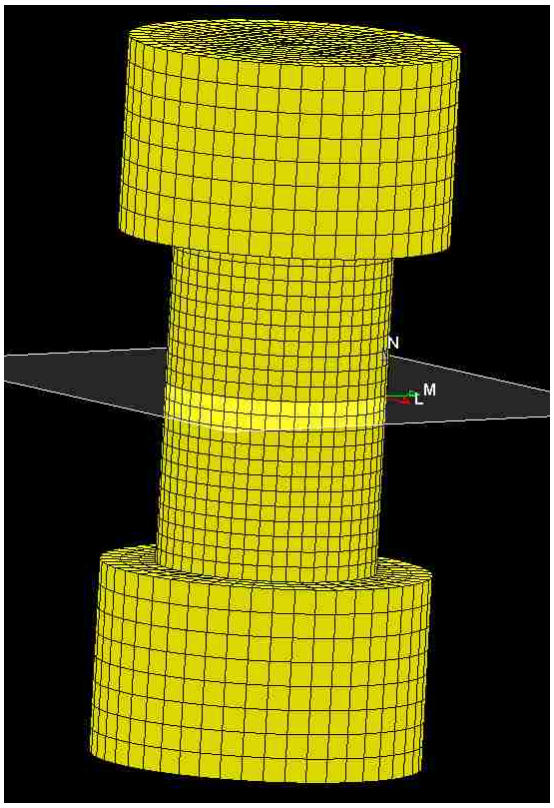

Figure 4.8 Bolt with Vectors Defining Pre-Stress

All the four bolts were equally stressed using the DEFINE_CURVE card. The stresses on the bolts are ramped linearly from 0 to the desired value in 10 microseconds and are held constant throughout the simulation. A sample of LS-DYNA card is shown below.

```
*DATABASE_CROSS_SECTION_PLANE_ID
$#     csid                                                                 title
         3
$#     psid       xct       yct       zct       xch       ych       zch    radius
         3 -0.061154  0.066621  0.004041 -0.061154  0.066621  1.004040     0.000
$#     xhev      yhev      zhev      lenl      lenm       id     itype
     0.000     0.000     0.000     0.000     0.000        0         0
*SET_PART
$       SID       DA1       DA2       DA3       DA4
         3       0.0       0.0       0.0       0.0
$      PID1      PID2      PID3      PID4      PID5      PID6      PID7      PID8
         3
*INITIAL_STRESS_SECTION
$     ISSID     SECID      LCID      PSID
      1,          3,        7,         3
*DEFINE_CURVE
7
0,0
1.00E-06,3.46E+07
```

4.5.7 Cards Defining Initial Velocity

Velocity of the projectile in LS-DYNA is defined using INITIAL_VELOCITY_GENERATION card. Since the preload is applied for initial 10 microseconds of the simulation, the velocity to the projectile is introduced after 10 microseconds using INITIAL_VELOCITY_GENERATION_START_TIME. Below is a sample of this card used in LS-DYNA.

```
*INITIAL_VELOCITY_GENERATION
$,S,0,X,Y,Z
29,3,0,0,0,5240
0,0,0,0,0,0,1,0
*INITIAL_VELOCITY_GENERATION_START_TIME
10e-6
```

4.6 Simulation Results

Acceleration is measured in a node that corresponds to the accelerometer location as show in Figure 4.9. The acceleration is sampled at 50Ms/sec. Figure 4.10, 4.11, 4.12, shows damage of the projectile and target at 5µs, 10µs and 70µs respectively

after impact for an impact velocity of 4540m/s. From figure 4.12, it can be clearly seen that by 70μs, the projectile is completely disintegrated. Figure 4.13 shows the velocity contour of the target and target holder at different time interval. The SPH particles are disabled in these figures. The average shock speed along the thickness of the target is around 10583 m/s. The shock speed is calculated knowing the arrival time of the wave on top surface and bottom surface of the target and the distance between them. This speed is 2.27 times the elastic wave speed of A36 steel plate.

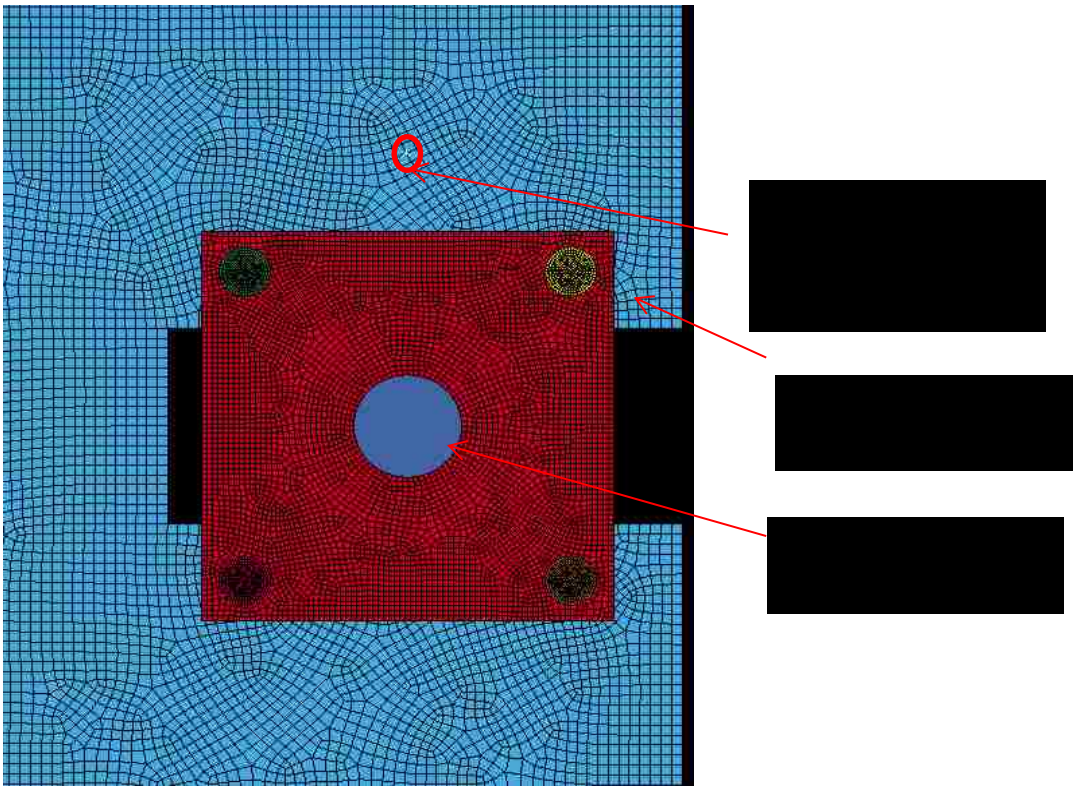

Figure 4.9: Experiment Fixture with Accelerometer Location

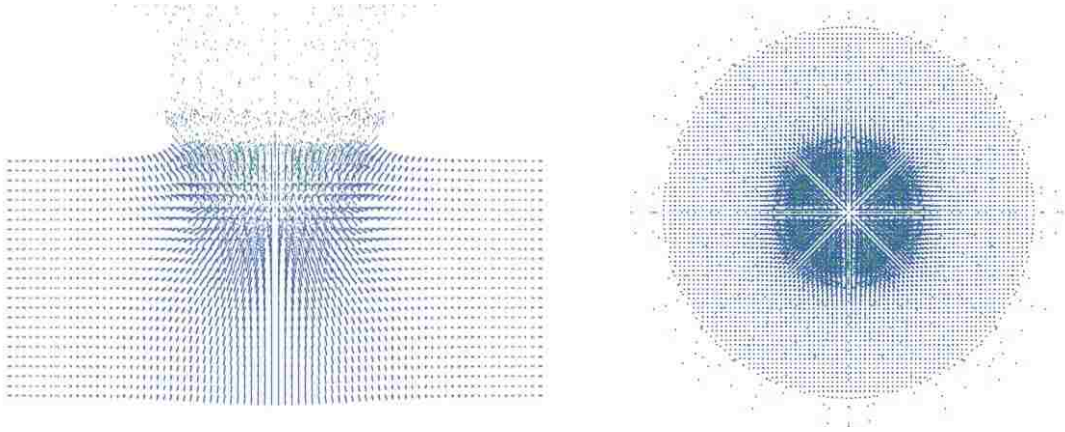

Front View

Top View

Figure 4.10: Projectile and Target Damage at 5µs

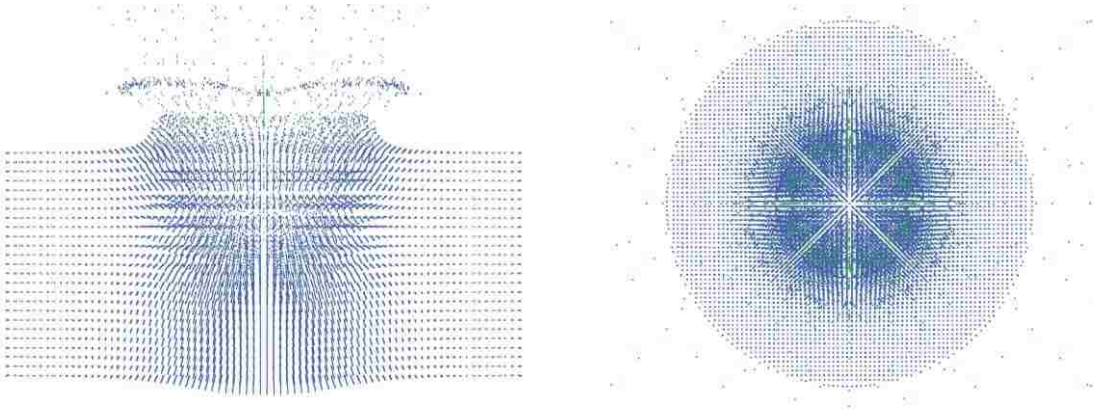

Front View

Top View

Figure 4.11: Projectile and Target Damage at 10µs

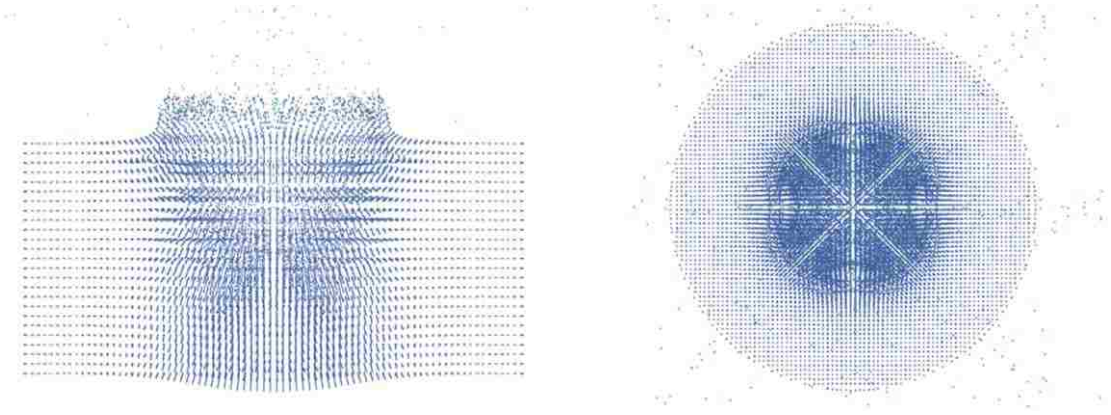

Front View Top View

Figure 4.12: Projectile and Target Damage at 70µs

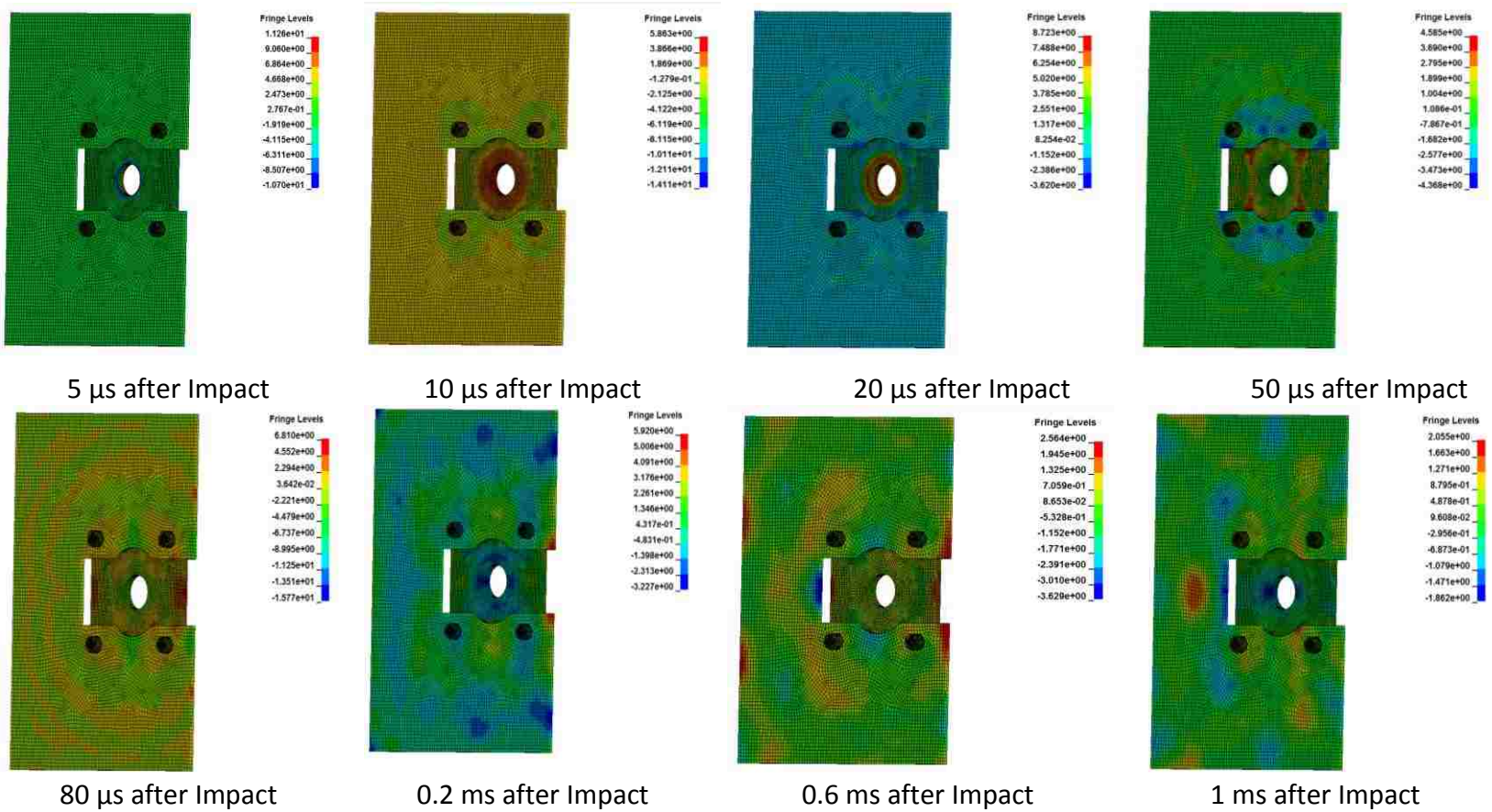

Figure 4.13: Velocity Contour from FEA

With projectile impact at a velocity of 4540m/s, Table 4.4 shows a damage area for FEA.

Table 4.4 Damage Area for a Typical FEA with Projectile Velocity of 4540 m/s

	Bulge (mm)	Penetration (mm)	Diameter (mm)
FEA	2.1	6.2	16.59

This response has been obtained by solving the finite element model in duration for 1ms. The results had been filtered between 2000Hz and 10000Hz, shown in Figure 4.15. To remove any DC shift in accelerometer, the results were high-pass filtered at 2000Hz and the low pass filtered at 10,000Hz, since the accelerometer range was 1 to 10,000Hz.

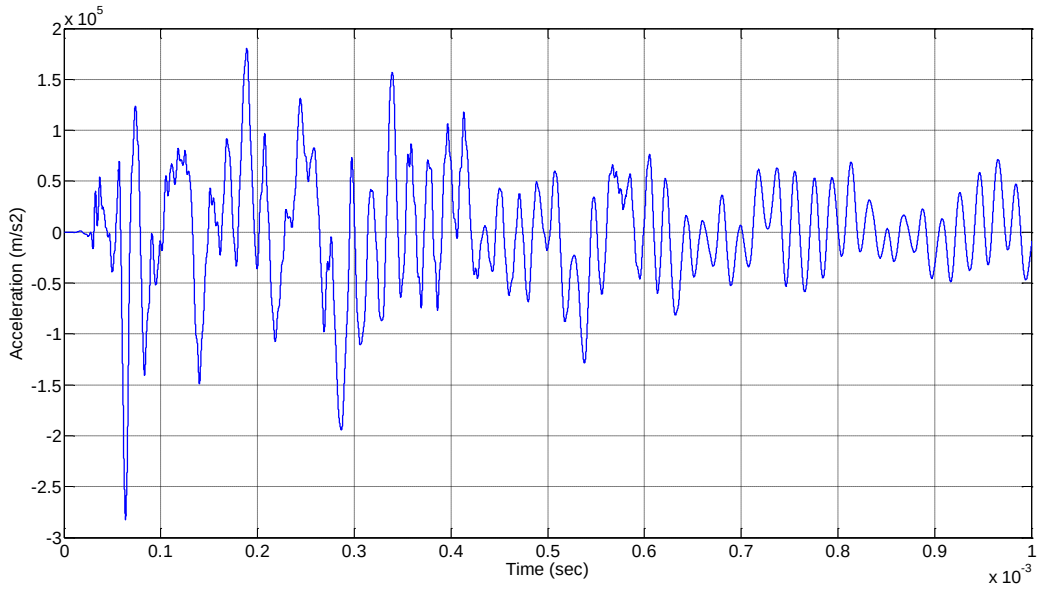

Figure 4.14: Unfiltered Acceleration Data from FEA

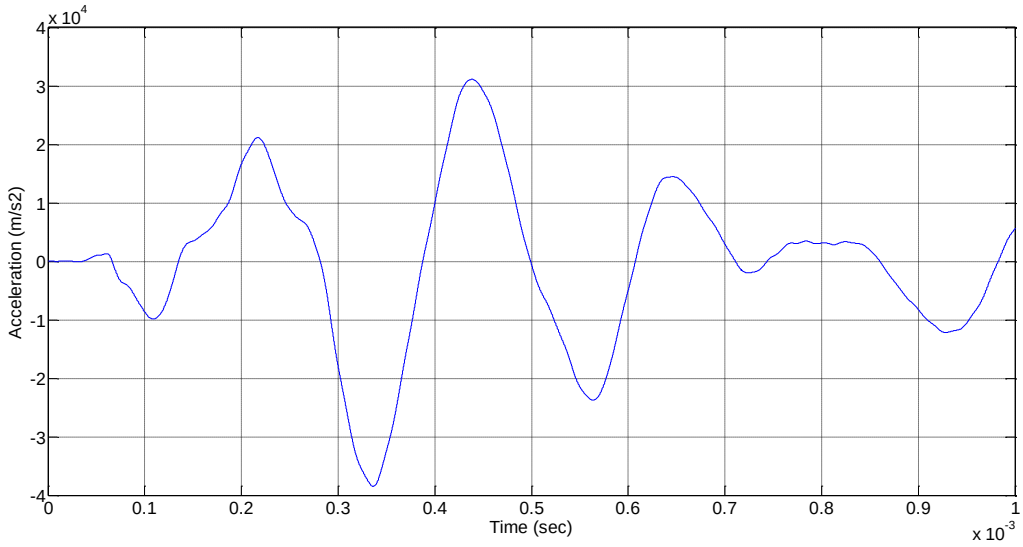

Figure 4.15: Filtered Acceleration Data from FEA

CHAPTER 5

RESULTS COMPARISON

5.1 Preload on the bolt

One of the most common reasons of bolted joint failure can be attributed to the lack of sufficient preload or clamp load on the bolts. It has been widely proved showing the importance of preload on bolts carrying load. Preload is applied by tightening of the bolts, higher the tightness, higher the preload. Preload is generally a fraction of bolt's proof strength. When the bolts are tightened, it is stretched and the parts being fastened are compressed. Bolted joints can be loaded with tensile force, shear force or combination of both. When the bolted joint structures are subjected to tensile load, the preload prevents the separation of joint faces. The maximum tensile load the joints can take is defined by preload applied on the bolts. The maximum strength of the joint is limited by the strength of the bolt. Anyhow, the higher the preload force the better the joint, because it will prevent the assembled parts from separation. This is an important criterion in most applications. As the strength of the bolted joints is mainly dependent on the preload force, the preload has a significant effect on the response of the bolted joint to dynamic or shock loads. A typical bolted joints with force is shown in Figure 5.1

The bolt, clamping material and the joint can be modeled as a spring-like assembly. The clamping force is what holds the parts together and is given by

Clamping force: $F_c = F_p - F_t$ (12)

where

- F_c is the clamping force
- F_p is the preload force
- F_t is the tension force or external load

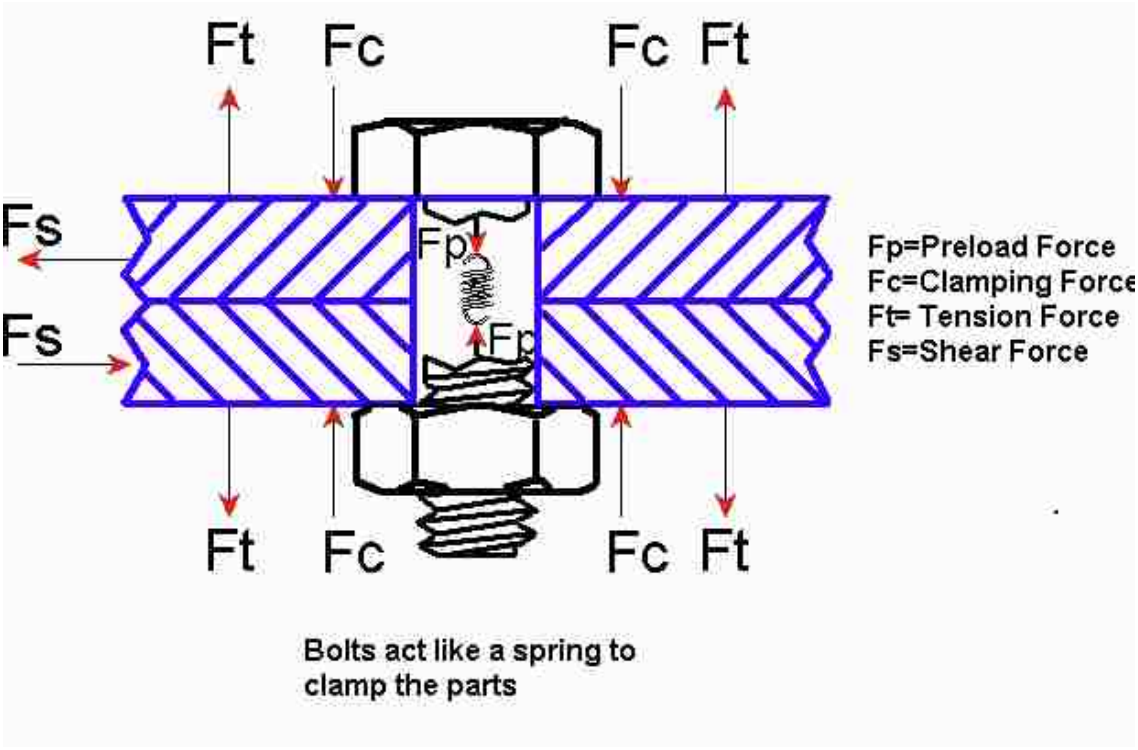

Figure 5.1: Force Diagram for a Typical Bolted Joint [24]

Bolt preload is an important factor that affects the strength and response of the structure. To understand the effects of bolt preload on the dynamic response of structure, it was decided to conduct experiments at three different preload levels. Bolt preload is measure in terms of proof load, which is maximum tensile force which does not produce any permanent deformation. The initial tensile force is calculated by the equation given below [53]

$$F_i = K A_t S_p \quad (13)$$

where,

- F_i is the initial tensile force on the bolt
- K is the constant ranging from 0.75 to .99
- A_t is the tensile stress area
- S_p is the proof strength of the bolt material

Knowing the tensile force required by the bolt, the tightening torque can be calculated using the equation given below

$$T = K F_i D \quad (14)$$

where,

- T is the torque
- K is a constant approximated to 0.2
- F_i is initial tensile force
- D is the nominal diameter of the bolt.

The pre-torque is applied on the bolted joint using a torque wrench. The torque wrench has an adjustable knob and by setting this knob the torque wrench can precisely apply a specific torque on the bolted joint. The experiments were conducted for three different torque levels: 136 Nm, 108 Nm and 81 Nm. Using the above equation, tightening force for these torques level is calculated as 53 KN, 42 KN and 31 KN

respectively and initial tensile stress on the bolt shank caused by the bolt preload is calculated as 579 MPa, 463 MPa and 346 MPa. These stresses are below the yield strength of the material (634 MPa [54]).

5.2 Results and Comparison

Experiments with UNLV two-stage gas gun were conducted at different projectile velocities and different torque tightness. The test matrix is shown in Table 5.1

Table 5.1: Test Matrix

Test Number	Projectile Velocity (m/s)	Tightening Torque (Nm)
1	5710	135
2	4820	135
3	4760	135
4	5190	108
5	5090	108
6	4540	108
7	5240	81
8	5160	81
9	5040	81

The results comparison of the transient analysis can be divided into four sections: Fast Fourier Transform (FFT) analysis, Shock Response Spectrum (SRS), time

history and damage on the plate. The natural frequencies from FEA and experimental can be obtained from FFT plots. Frequencies corresponding to peaks on these plots are natural frequencies. The FFT program was done in MATLAB and sample program is shown in Appendix D. FFT is found using the formula given below.

$$X(K) = \sum x(j)\, w_n^{(j-1)(k-1)} \quad (15)$$

where,

- $w_n = e^{(-2\pi i)/N}$
- N is the length of input vector
- X is the input acceleration

Shock response spectrum is mainly used for high shock levels. It is a calculated function based on the acceleration time history. It applies an acceleration time history as a base excitation to an array of single degree- of-freedom (SDOF) systems. Each system is assumed to have no mass-loading effect on the base input. The SRS Matlab code was written by T. Irvin [55]. A sample program is show in Appendix E.

FEA acceleration data deviated from acceleration data after 1ms because of modified boundary condition. In experiment the dynamics of angle bracket and the target chamber influence the vibration of the target plate, but these structures are not included in the FEA. Therefore results are compared only up to 1ms. Experiment 4 data was truncated at 0.6ms because of heavy DC shift and noise. Acceleration levels on target plate (pre-joint) are too high for any accelerometer to measure without damaging

itself. So comparing the damage on the target plate would give good confidence on the FE model. Table 5.2, shows the plate damage comparison. Table 5.2 does not include the tightening torque since the damage is a localized phenomenon and depends only on the projectile velocity and not on tightening torque. Table 5.2 also shows that the damage on the target increases with increasing projectile velocity. Figure 5.2 to 5.28 shows the FFT, SRS and acceleration time history results of experiment and FEA.

Table 5.2: Experiment and FEA Damage Area Comparison

Test	Projectile Velocity (m/s)	Bulge (mm)		Percentage Difference	Penetration (mm)		Percentage Difference	Diameter (mm)		Percentage Difference
		Experiment	FEA		Experiment	FEA		Experiment	FEA	
1	4540	1.13	1.22	7.96	5.1	5.9	15.69	15.03	14.69	2.26
2	4760	1.42	1.42	0	6.5	5.8	10.77	15.37	14.5	5.66
3	4820	1.48	1.47	0.68	6.51	6.21	4.61	15.14	17.9	18.23
4	5040	1.66	1.85	11.45	5.84	5.35	8.39	15.9	18.4	15.72
5	5090	2.33	1.91	18.03	7	6.5	7.14	16.9	17.9	5.92
6	5160	1.7	2	17.65	6.26	6	4.15	15.73	19.11	21.46
7	5190	1.88	2.03	7.98	7.03	6.85	2.52	16.15	15.9	1.55
8	5240	2.07	2.1	1.45	6.9	6.2	10.14	16.3	19.9	22.09
9	5710	3.13	2.65	15.34	7.71	8.1	5.06	17.7	15.8	10.73
Average Error (%)				8.95			7.6			11.51
Standard Deviation (%)				6.76			3.89			7.64

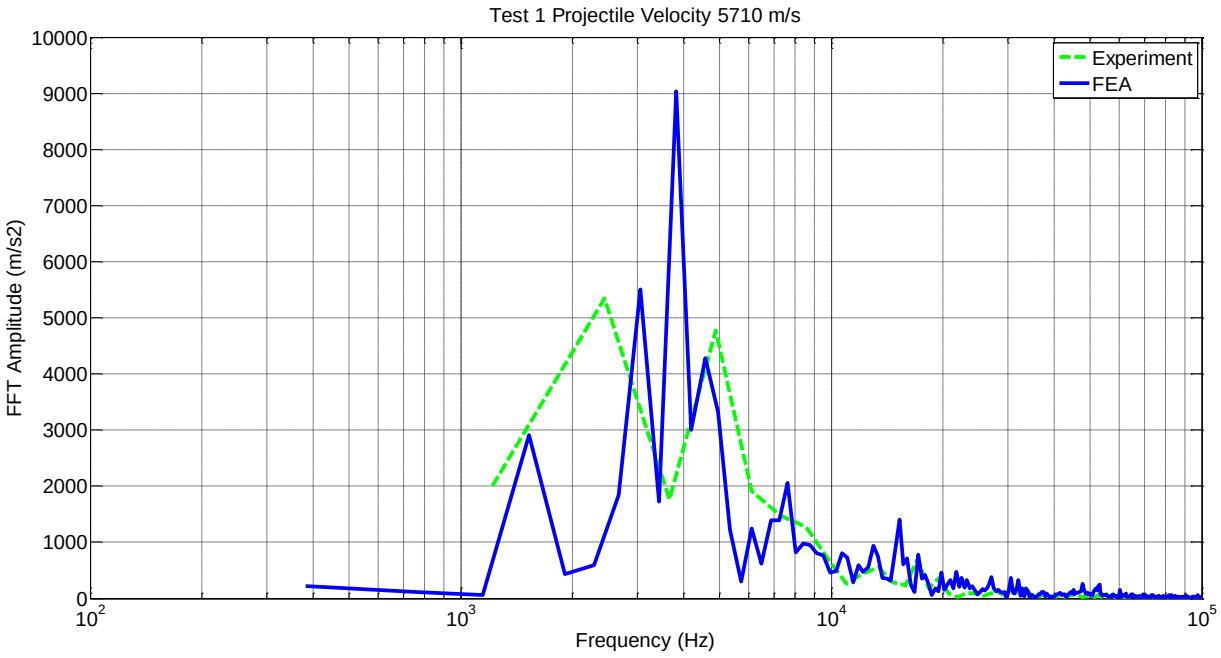

Figure 5.2: Test 1 FFT Comparison

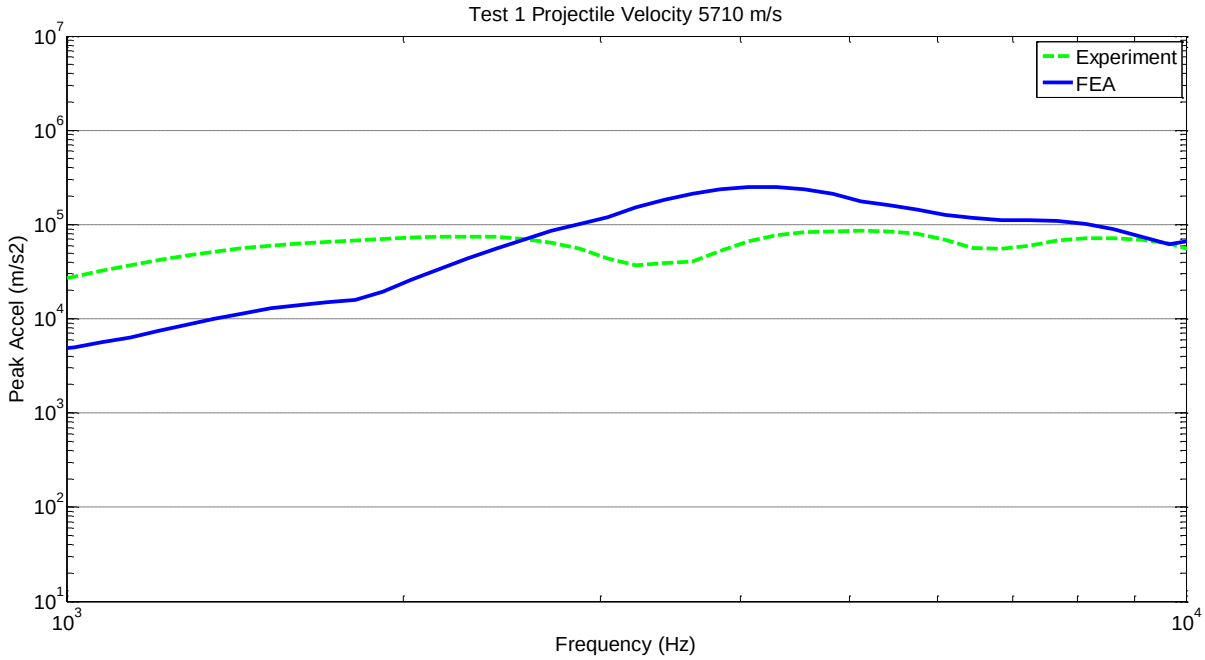

Figure 5.3: Test 1 SRS Comparison

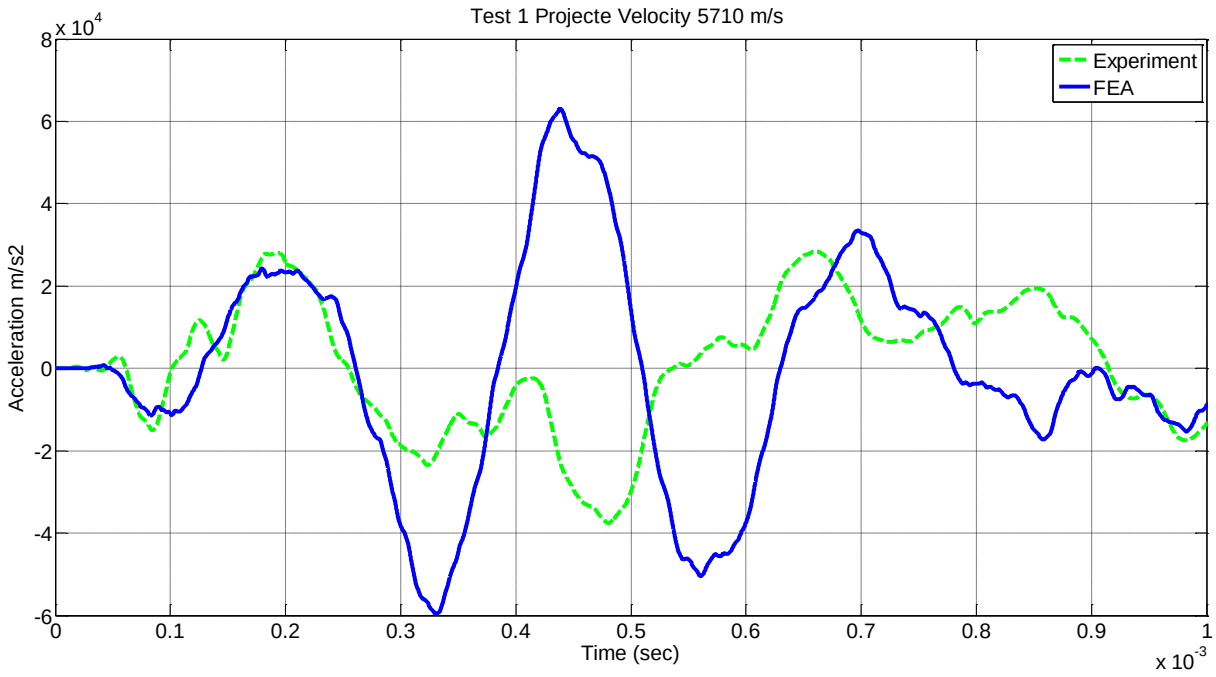

Figure 5.4: Test 1 Time History Comparison

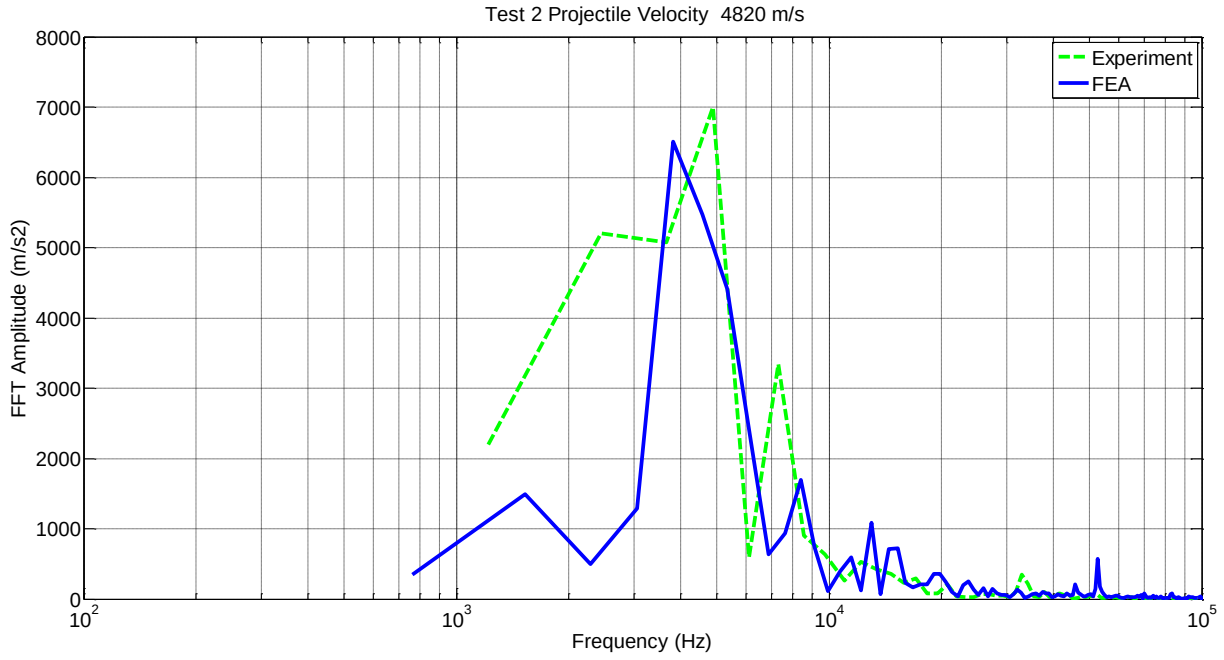

Figure 5.5: Test 2 FFT Comparison

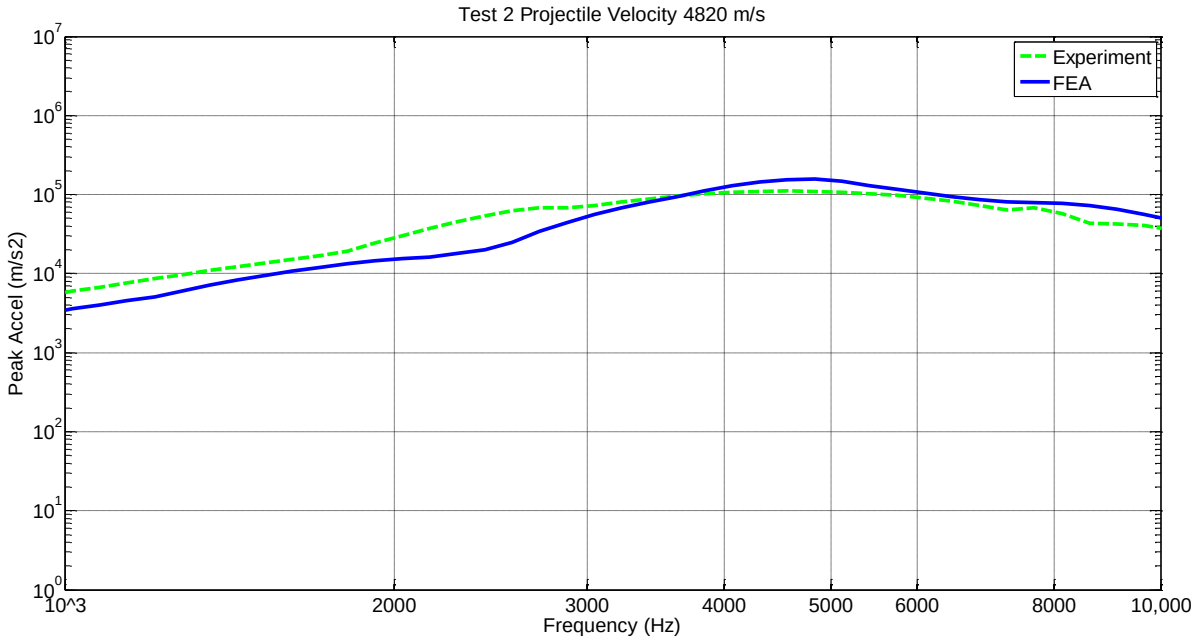

Figure 5.6: Test 2 SRS Comparison

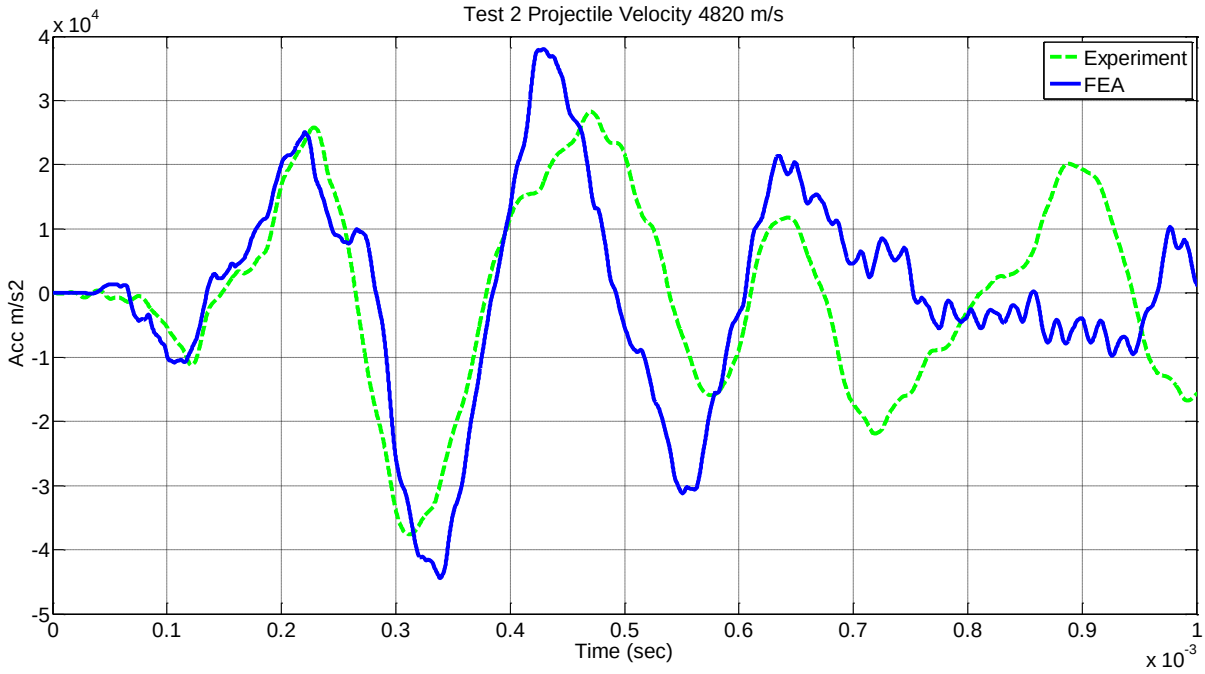

Figure 5.7: Test 2 Time History Comparison

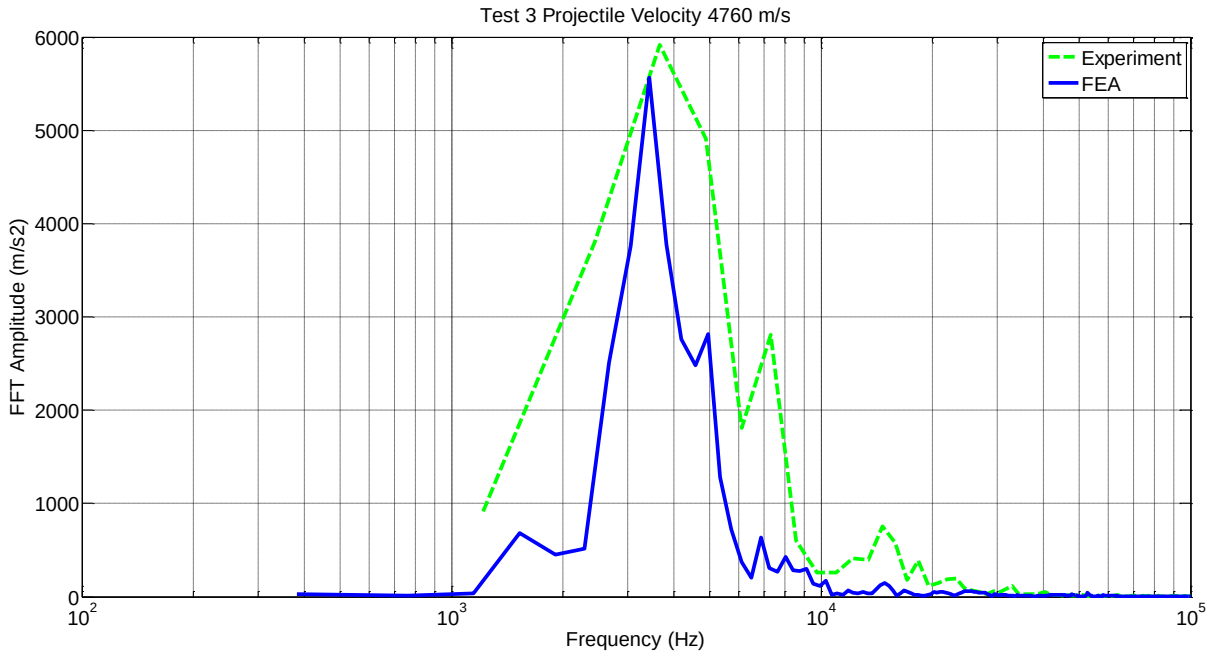

Figure 5.8: Test 3 FFT Comparison

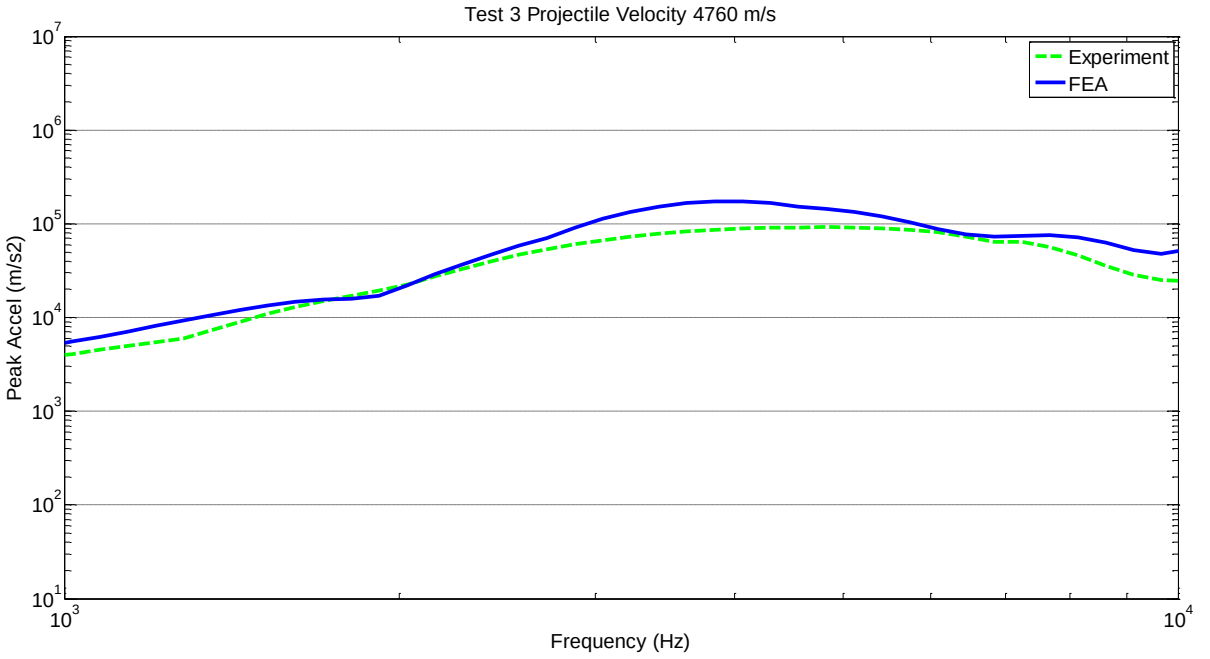

Figure 5.9: Test 3 SRS Comparison

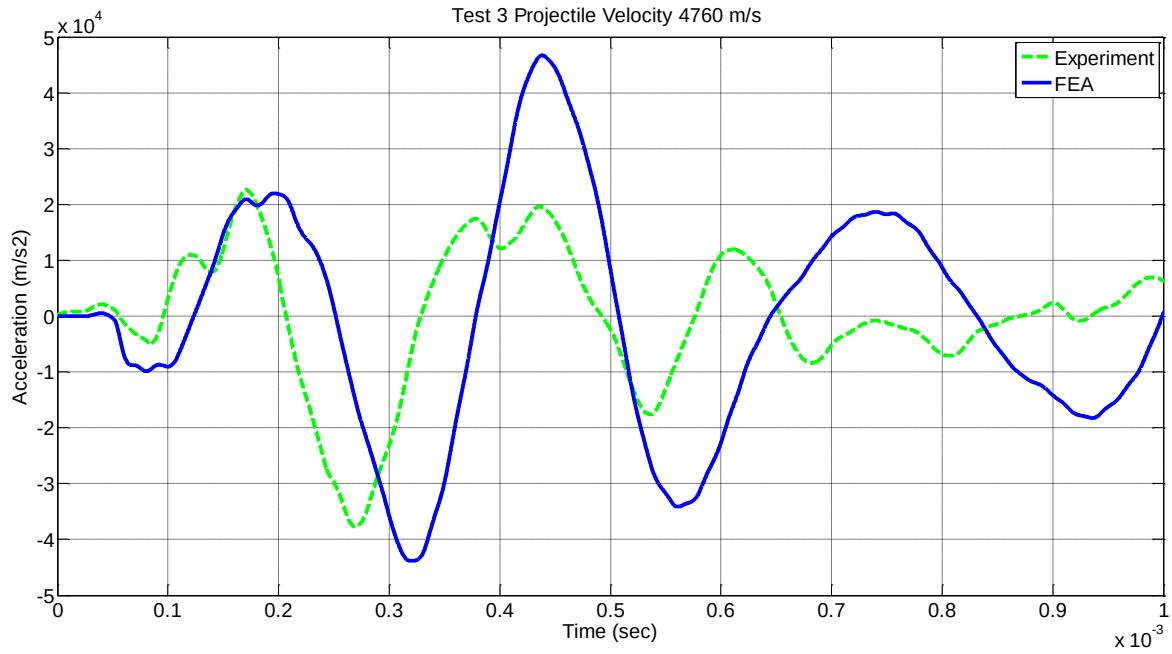

Figure 5.10: Test 3 Time History Comparison

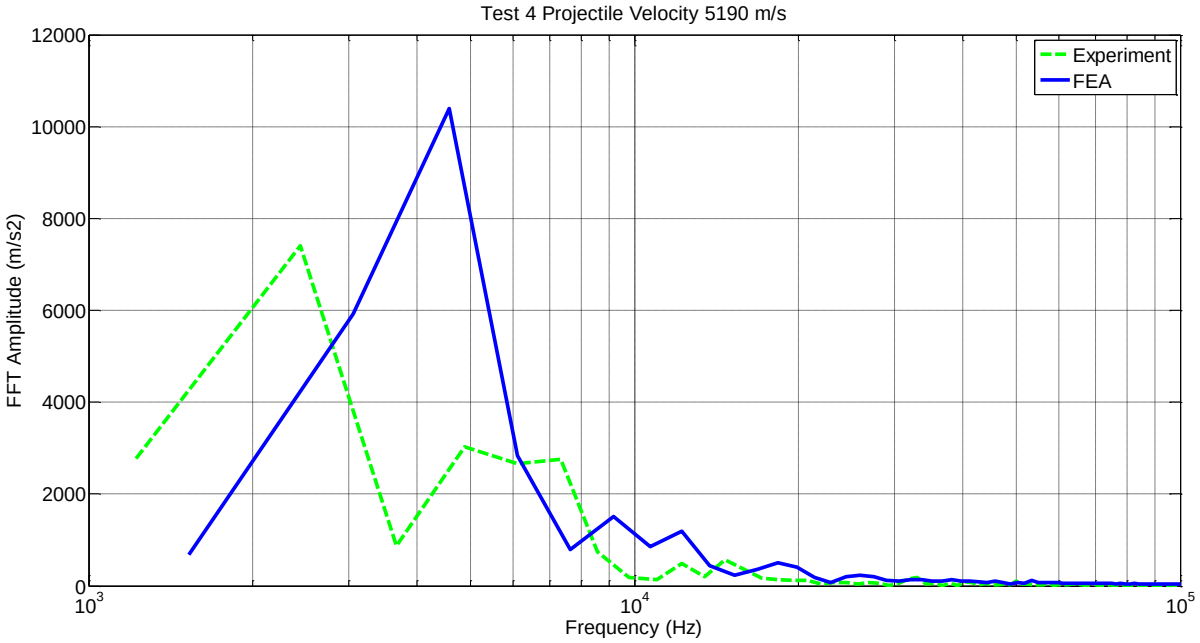

Figure 5.11: Test 4 FFT Comparison

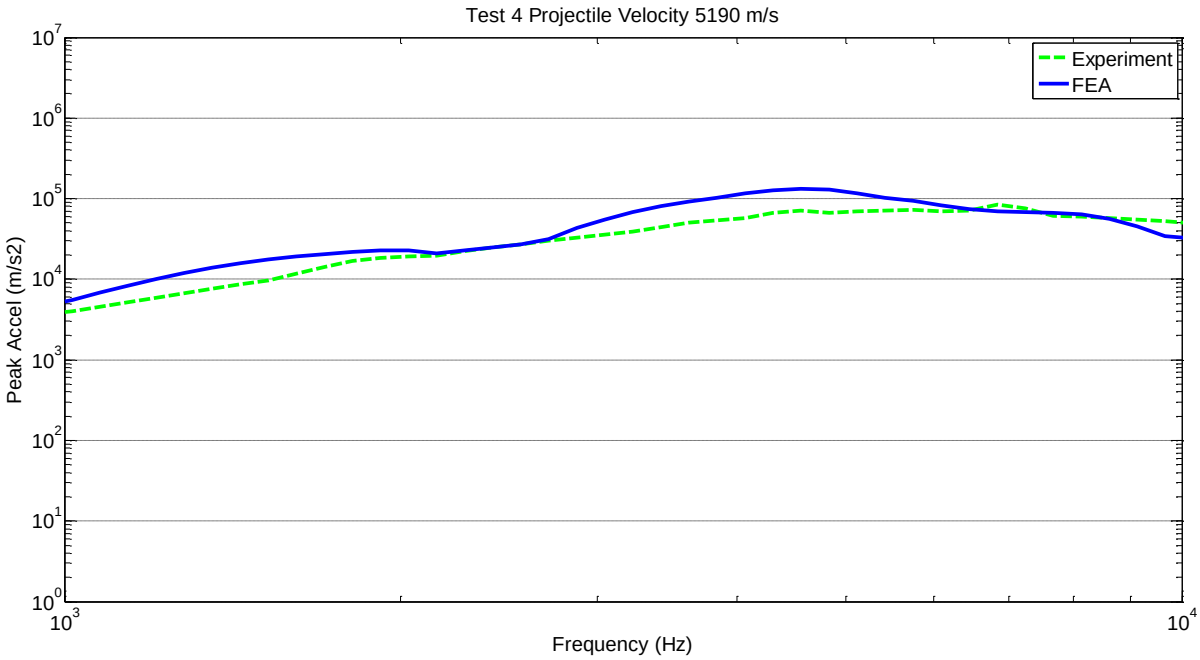

Figure 5.12: Test 4 SRS Comparison

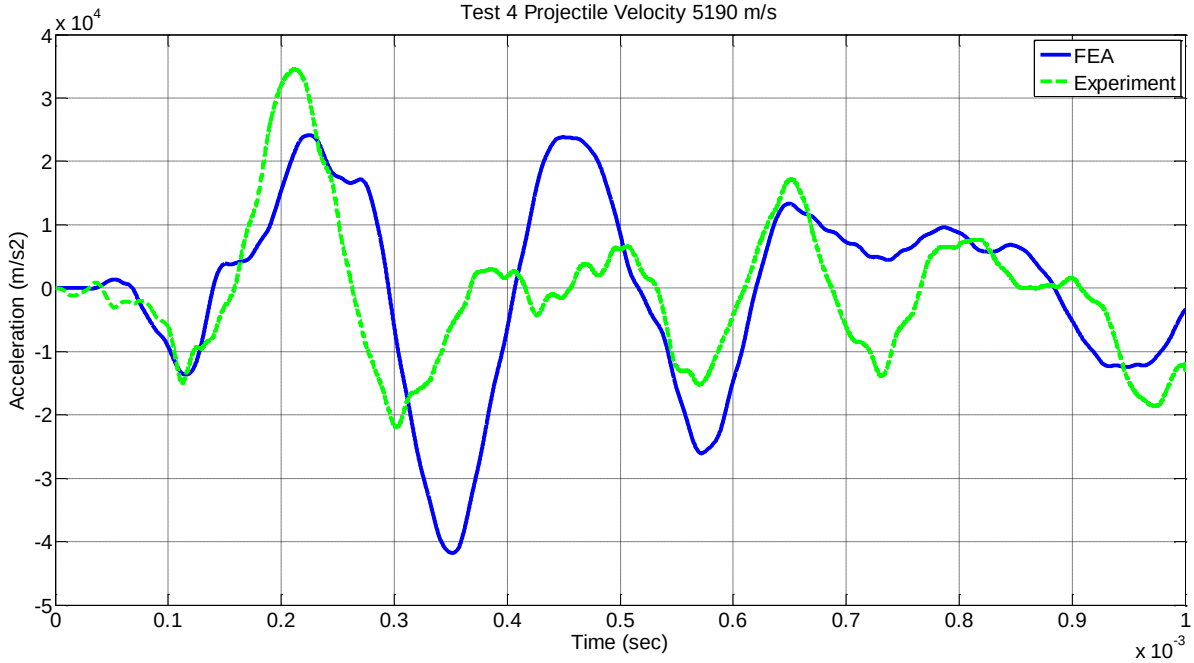

Figure 5.13: Test 4 Time History Comparison

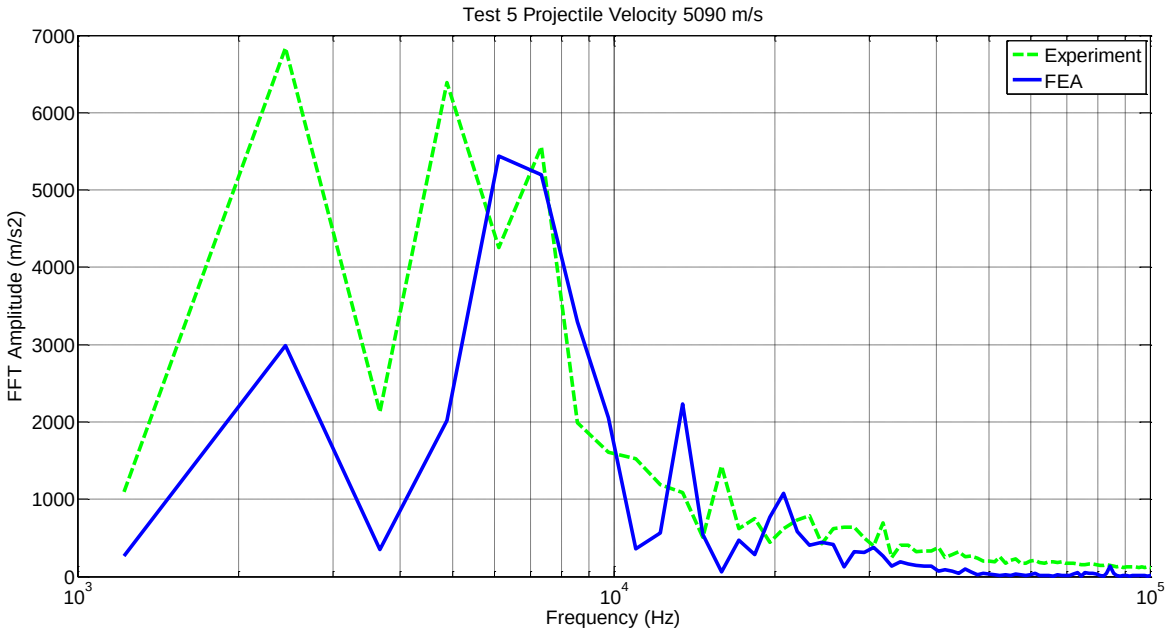

Figure 5.14: Test 5 FFT Comparison

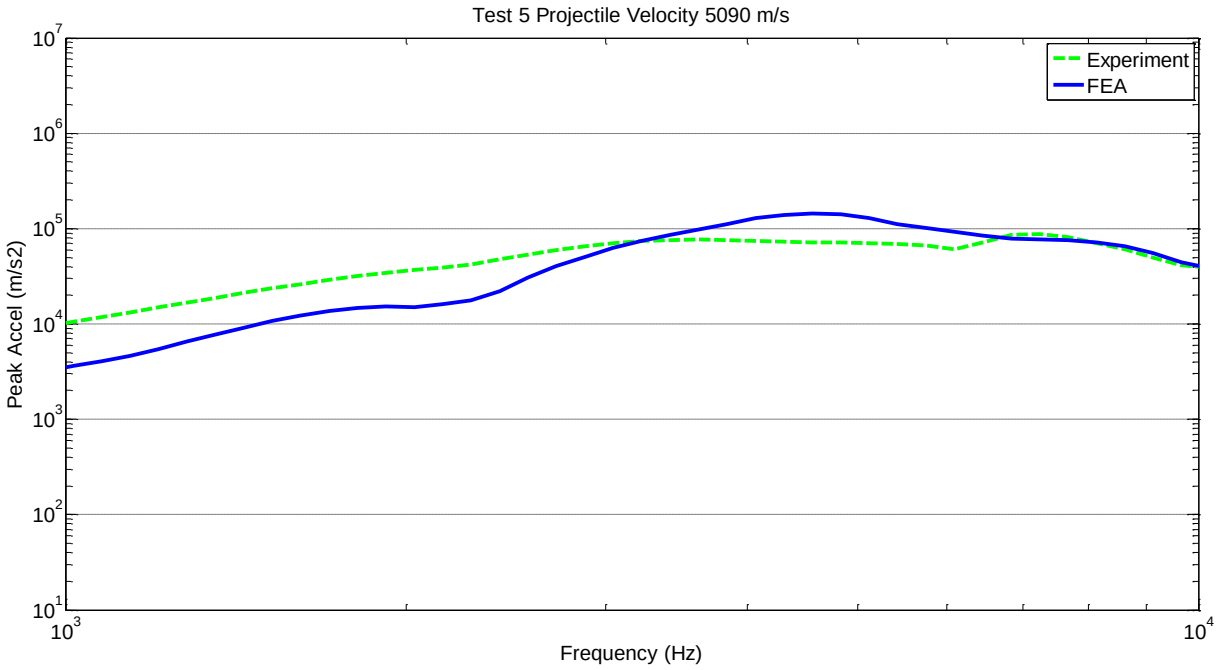

Figure 5.15: Test 5 SRS Comparison

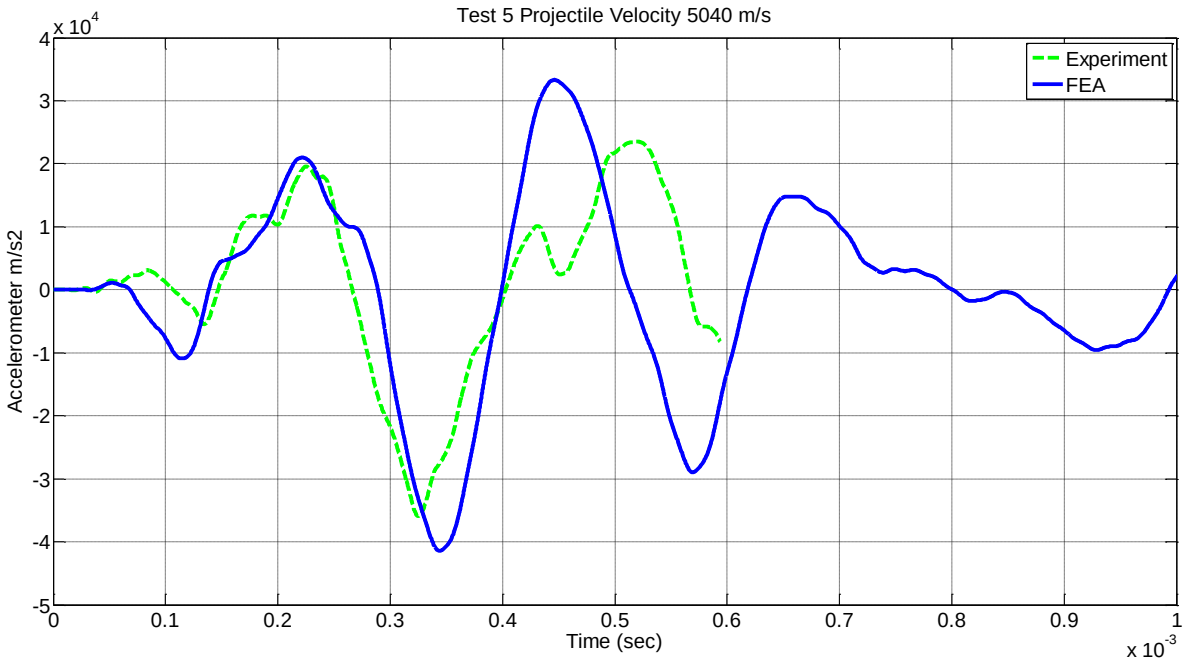

Figure 5.16 : Test 5 Time History Comparison

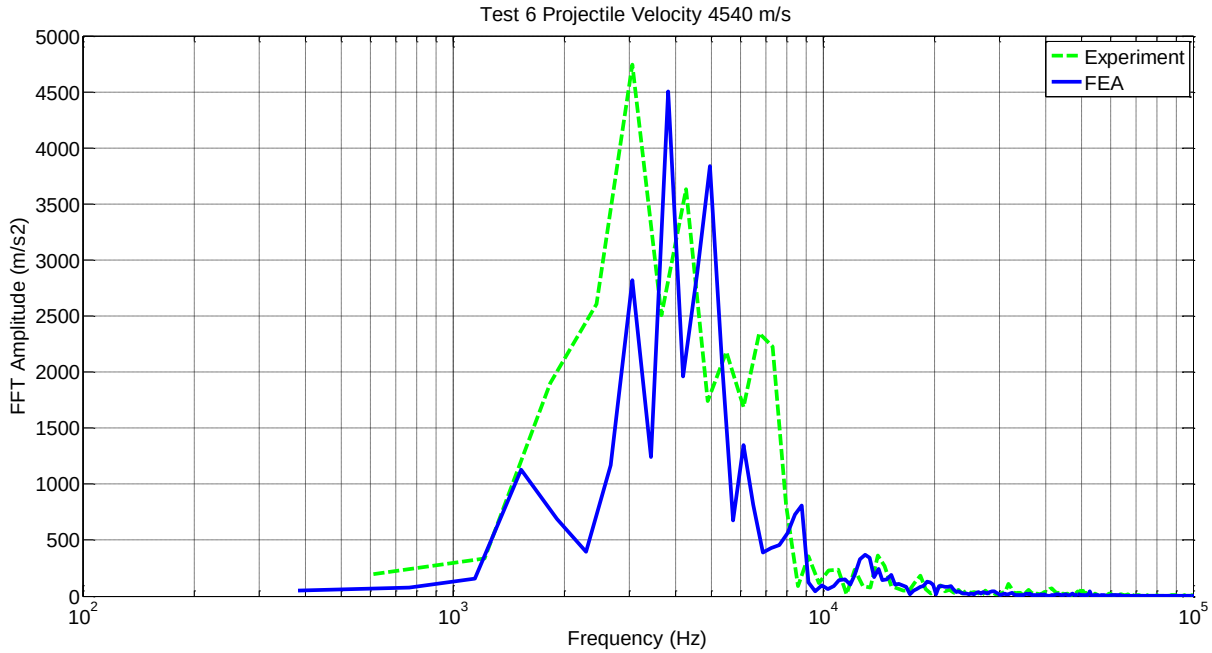

Figure 5.17: Test 6 FFT Comparison

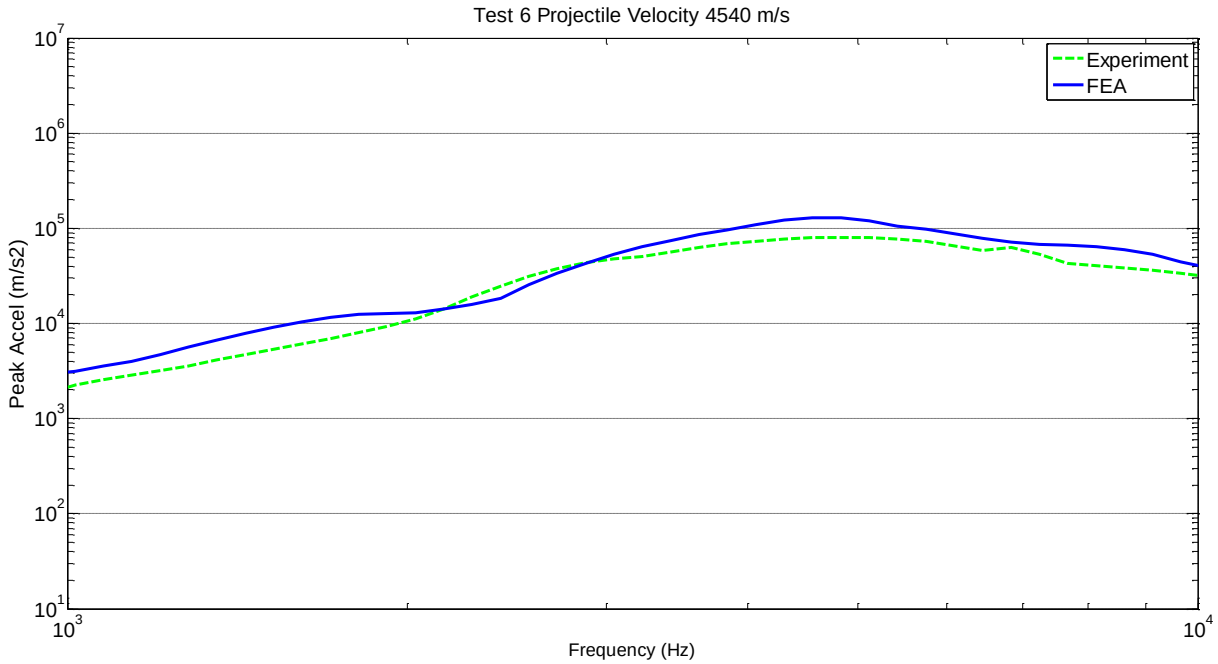

Figure 5.18: Test 6 SRS comparison

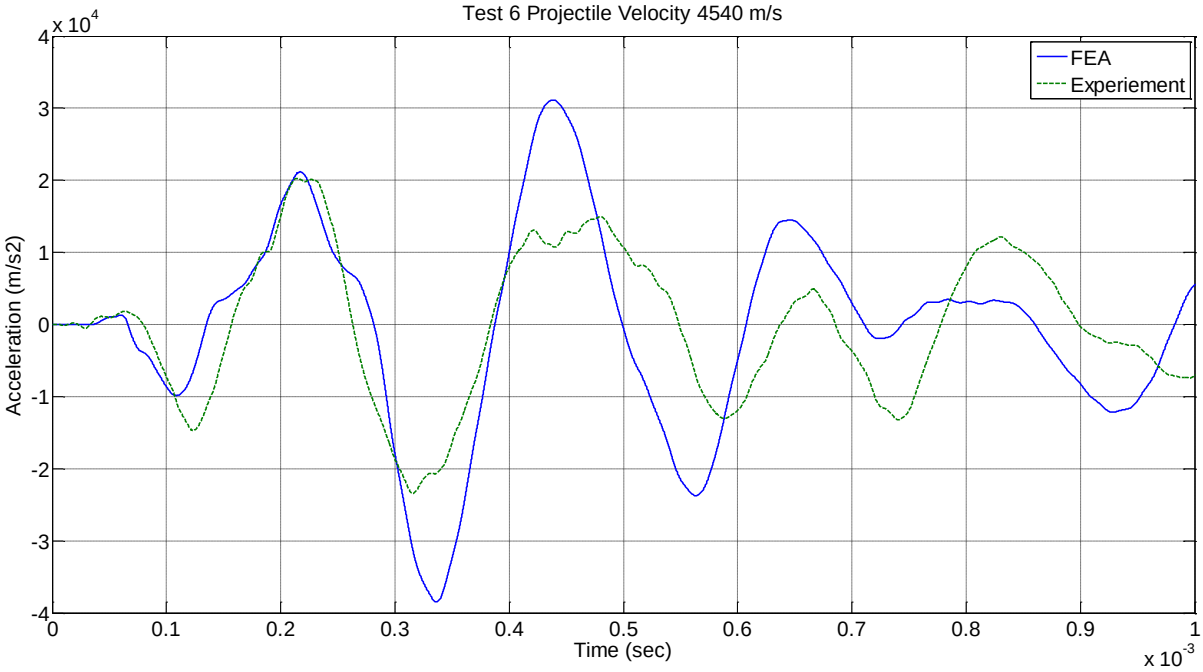

Figure 5.19: Test 6 Time History Comparison

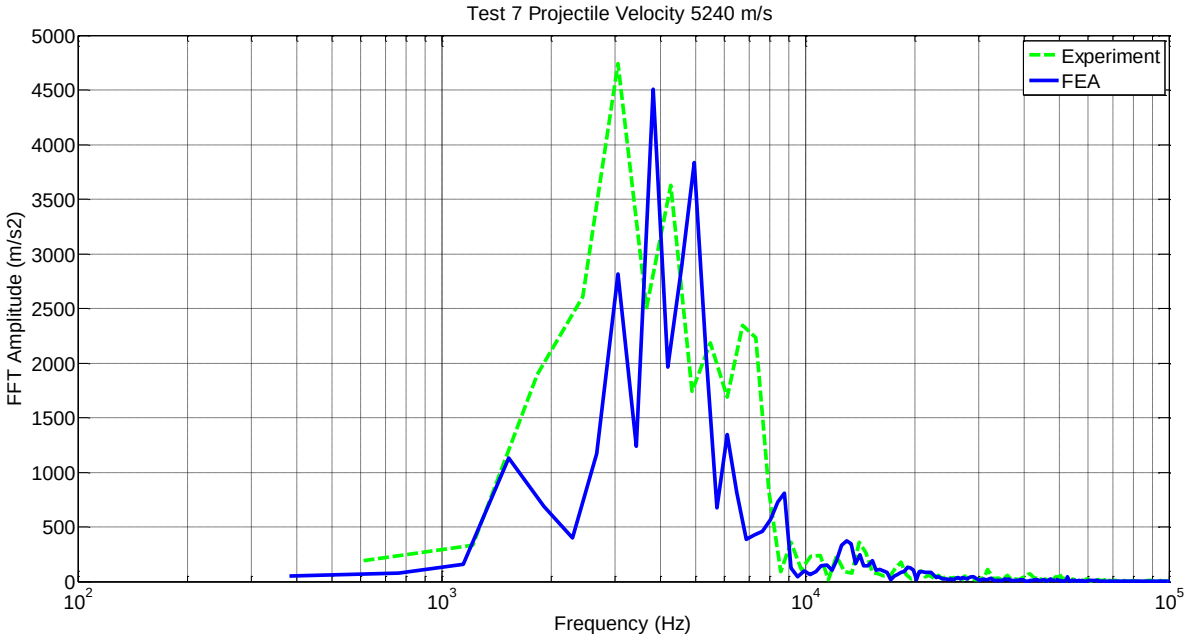

Figure 5.20: Test 7 FFT Comparison

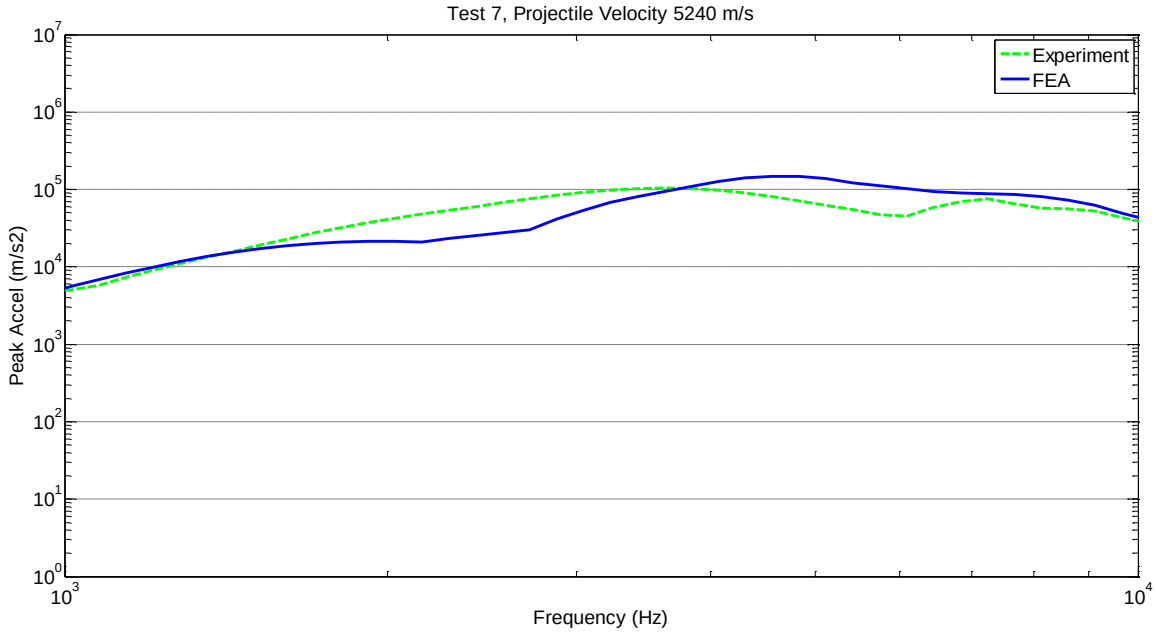

Figure 5.21: Test 7 SRS Comparison

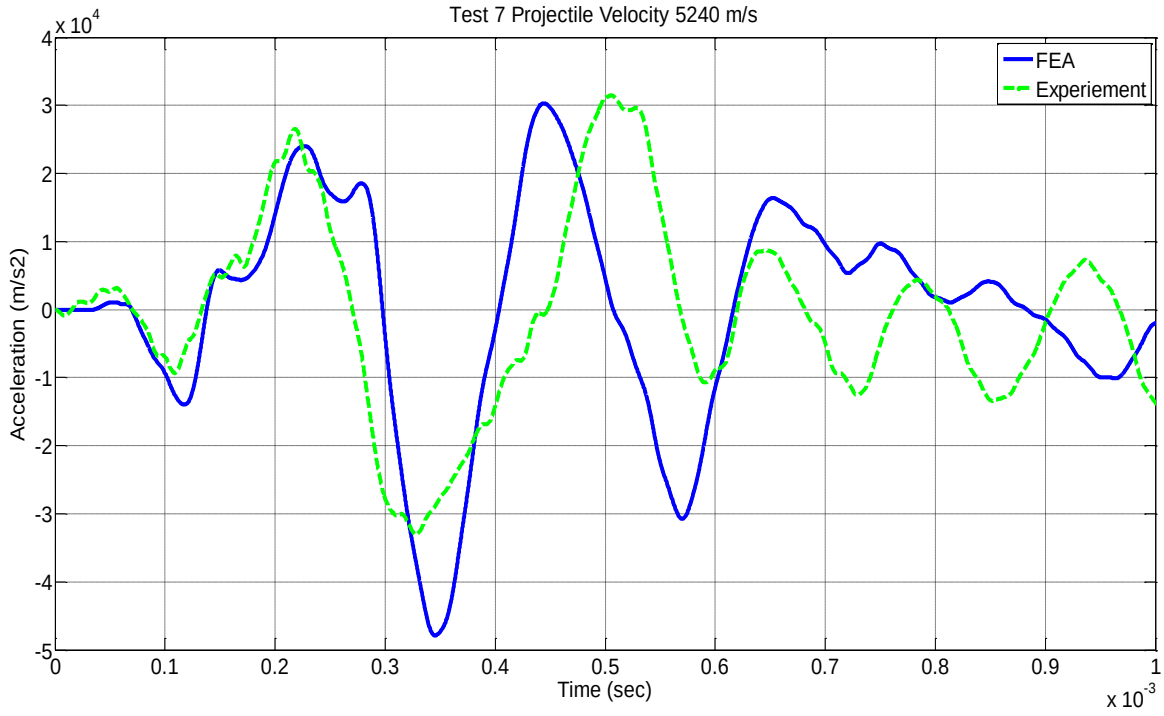

Figure 5.22: Test 7 Time History Comparison

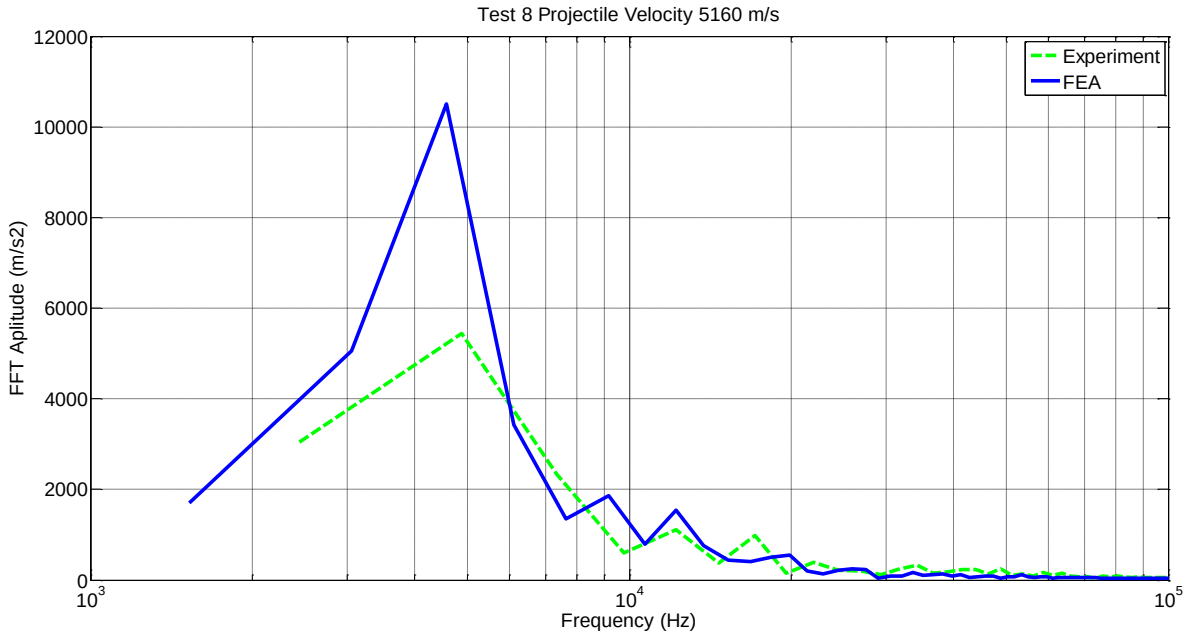

Figure 5.23: Test 8 FFT Comparison

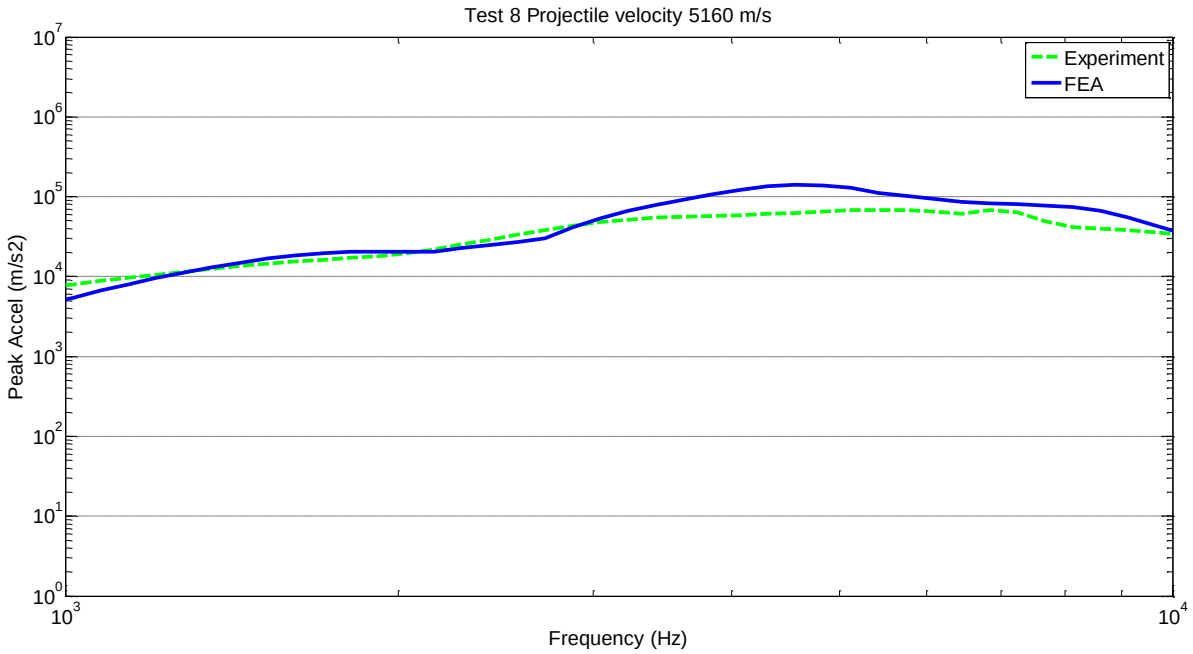

Figure 5.24: Test 8 SRS Comparison

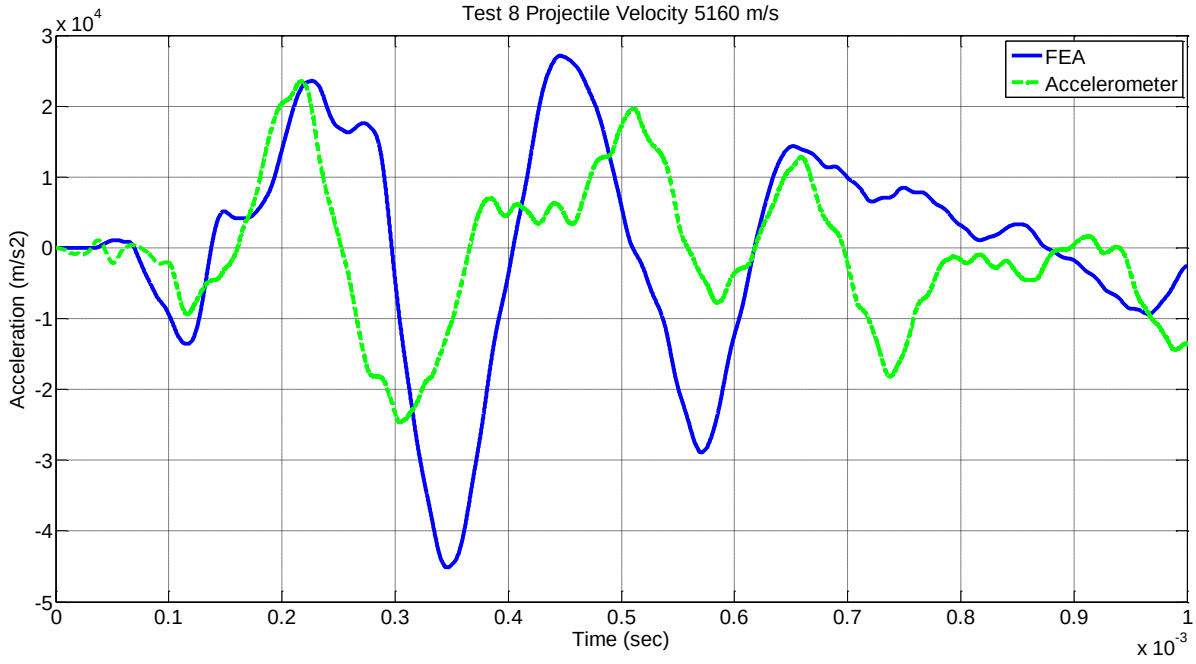

Figure 5.25: Test 8 Time History Comparison

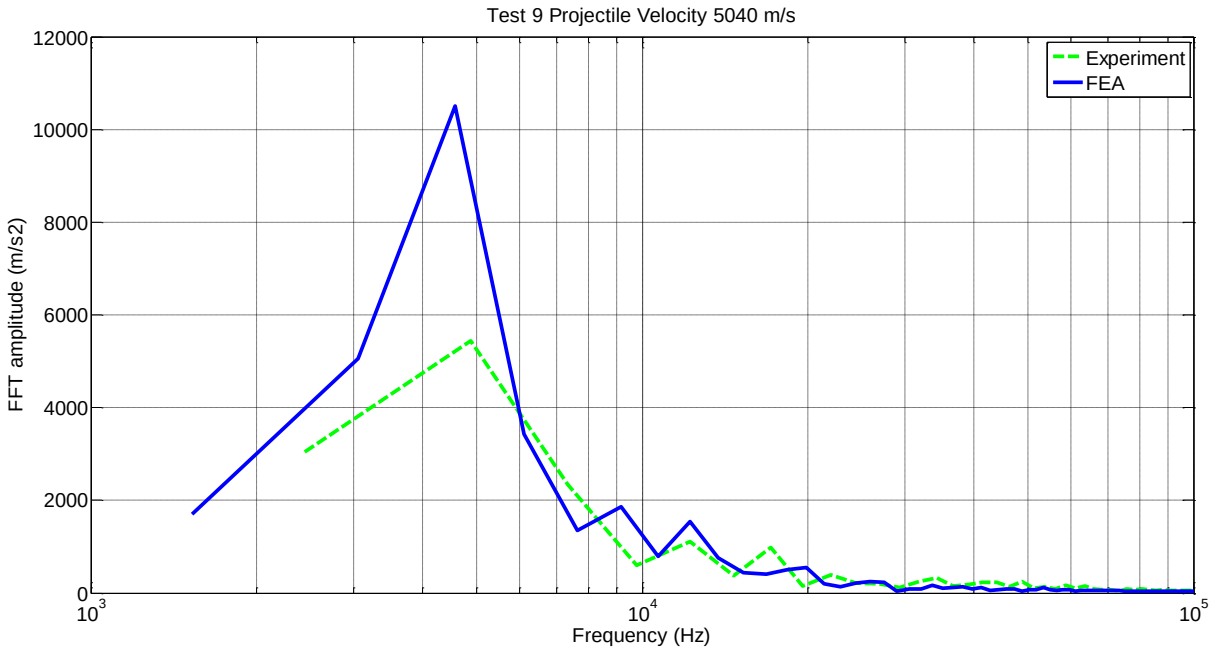

Figure 5.26: Test 9 FFT Comparison

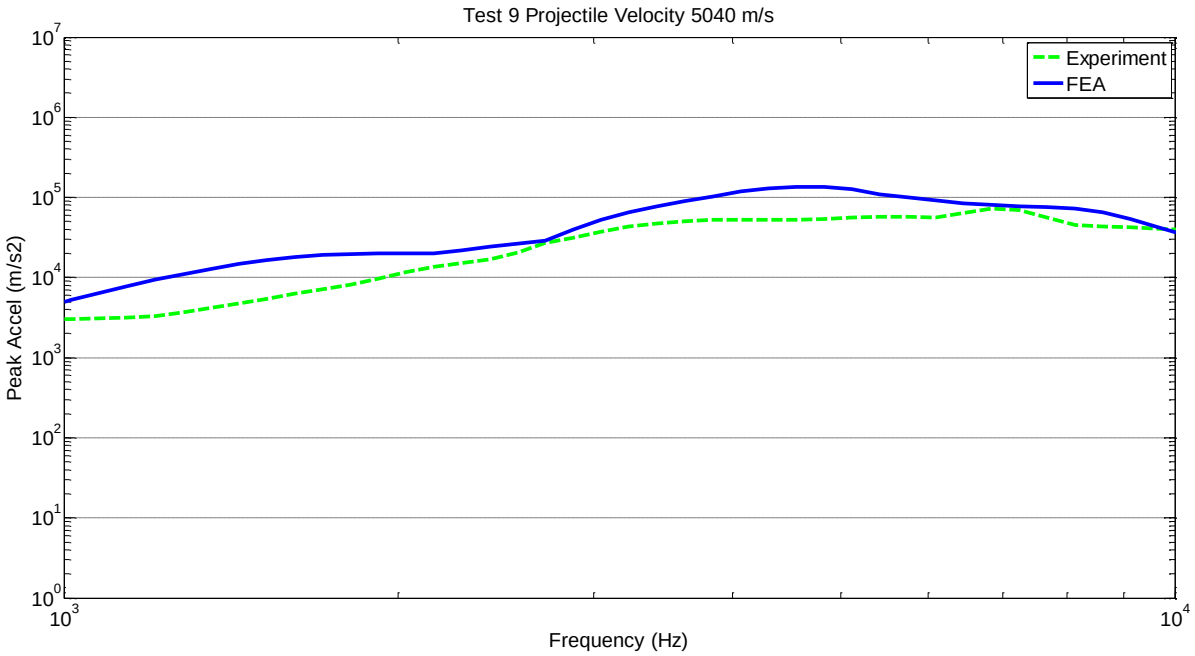

Figure 5.27: Test 9 SRS Comparison

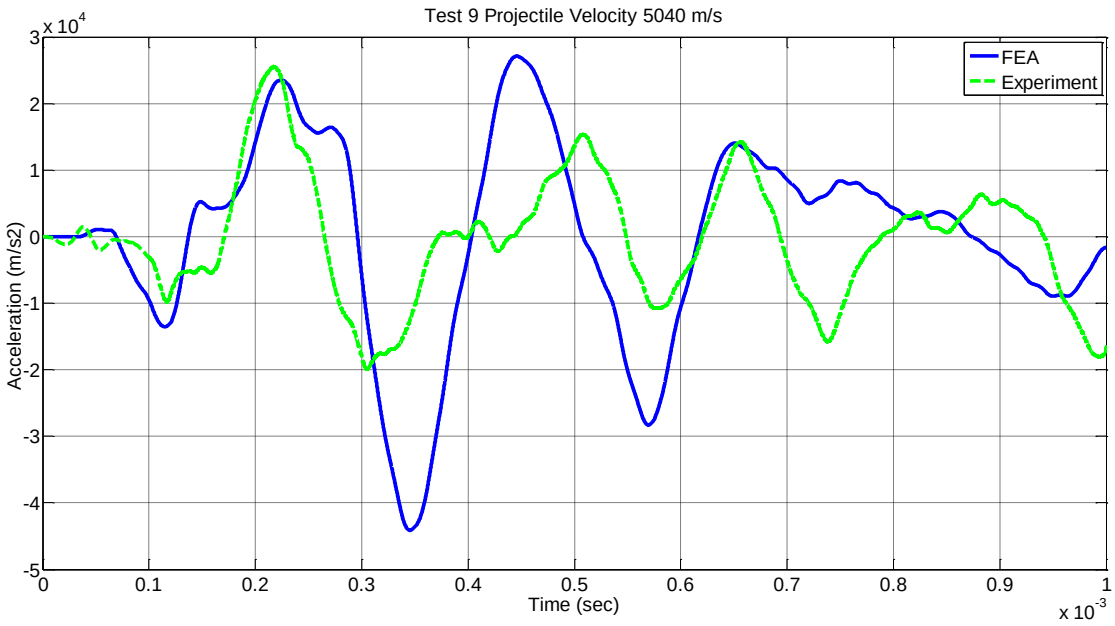

Figure 5.28: Test 9 Time History Comparison

Normalized root mean square deviation (NRMSD), Equation (13), of the SRS data is used to compare the closeness of the FEA results to the experimental data. NRMSD is the root mean square deviation normalized over the range of data and it is represented as a percentage.

$$\mathrm{NRMSD} = \frac{\mathrm{RMSD}}{(\mathrm{x,y})_{\max} - (\mathrm{x,y})_{\min}} * 100 \qquad (16)$$

where, $\mathrm{RMSD} = \sqrt{\frac{\sum_{i=n} (x_i - y_i)^2}{n}}$

x is the Experiment SRS data

y is the FEA SRS data

n is the number of points.

Table 5.3, shows the NRMSD values between experimental and simulated SRS curves for 9 different cases. The results show that the model is able to simulate the experiment for different tightness torque and projectile velocity. The SRS value estimated by the simulation does not exceed the experimental value by more than 17%. The average error for the simulation is around 10% with a standard deviation of 2.47%.

Table 5.3: NRMSD between FEA and Experiment Data

Tightening Torque (Nm)	Projectile Velocity (m/s)	NRMSD (%)
135	5710	16.91
135	4820	7.98
135	4760	12.64
101	5190	10.31
101	5090	10.06
101	4540	8.66
81	5240	10.05
81	5160	10.04
81	5040	10.85
Average NRMSD %		10.83
Standard Deviation		2.47

5.3 Summary of Results

The objective of this part of dissertation is to study shock propagation across a bolted joints subject to high impact loads using the UNLV two-stage gas gun. A test fixture was designed for this purpose. The bolts were preloaded to three different torque levels. A finite element model that combines Lagranian and SPH elements of the bolted structure was created in Ansys-LS-DYNA. Results from the simulation were compared with the experiments based on target plate damage FFT, SRS, and time histories were compared. NRMSD method was used to quantify the FE results. Simulation results agree well with the experiments.

There are few discrepancies in acceleration data, which can be attributed to fixed boundary condition in place of the angle brackets. The acceleration signal starts deviating after 0.1 ms. In real world the angle bracket which holds the target holder plate might have some flexibility. This can be confirmed by the fact that the wave reaches the fixed boundary after 0.1ms in the simulation. And the influence of the entire gas gun dynamics is not considered. Differences in the target plate damage can be attributed to non-available of exact high strain rate material models and damage material model for A36 plate and the projectile (LEXAN). Microscopic material defects might also influence the results. A possible phase transformation of A36 plate is not accounted for.

CHAPTER 6

EXPERIMENTAL SETUP FOR BOLTED JOINTS UNDER MEDIUM IMPACT

6.1 Introduction

Combat military vehicles or structure undergo a high impact/shock loading from mine blast or projectile impact. In these cases, the structure and the bolts experience large shock loads. These loads may or may not yield plastic deformation to bolts and the structure. In the previous chapters, bolted joints were tested under high impact loading with the structure undergoing plastic deformation. A limited research was conducted on plastic deformation of bolts when subjected to impact loading.

When structures with bolted joint are subjected to low impact loading, there won't be any plastic deformation or failure. The only nonlinearity arises from the friction. When structures with bolted joints are subjected to high impact, either the structure or the bolts can undergo plastic deformation. Thus two additional sources of nonlinearity can arise from plastic deformation of the structure, bolts or both.

In chapter three and four of this report, a simple structure with bolted joints was impacted with a high velocity projectile. The structure was subjected to plastic deformation while the bolts didn't. Also the experiments were conducted at different preload on the bolts. Explicit finite element analysis was used to simulate the shock propagation on the bolted joints and the result matched comparably with the experiment.

This chapter focuses on structures when bolted joints are subjected to plastic deformation during impact. This chapter also provides a detailed experimental setup

and finite element modeling technique for conducting impact loading on structure with bolted joint. A drop weight tower was used to impact the bolted joints to a medium impact.

6.2 Impact Testing Machine

The impact is applied on to the fixture by means of gravity load. To have the repeatable and controlled impact, Dynatup Instron 8250 drop weight impact tower is used as test equipment for performing the impact tests as shown in Figure 6.1. Drop heights varying from 0.0508m to 1.016 m can be achieved in this machine. Mass of the drop assembly may also be adjusted based on the requirement, by changing the support plates in the crosshead. The weights can be varied from 2.5 kg to 45.3 kg. For this study, a mass of 4.5 kg is used at different heights. Procedures to operate the Instron Dynatup 8250 in gravity driven automatic mode is given in Appendix F. The drop weight mechanism has three parts: weight, impactor and impactor holder as shown in Figure 6.2. The impactor is a steel cylinder with diameter and lengths of the impactor are 0.0254m. The impactor holder is a cylindrical disc with a diameter and length of 0.0381m and 0.034m respectively. Mass of impactor and impactor holder is 0.10kg and 0.25kg respectively.

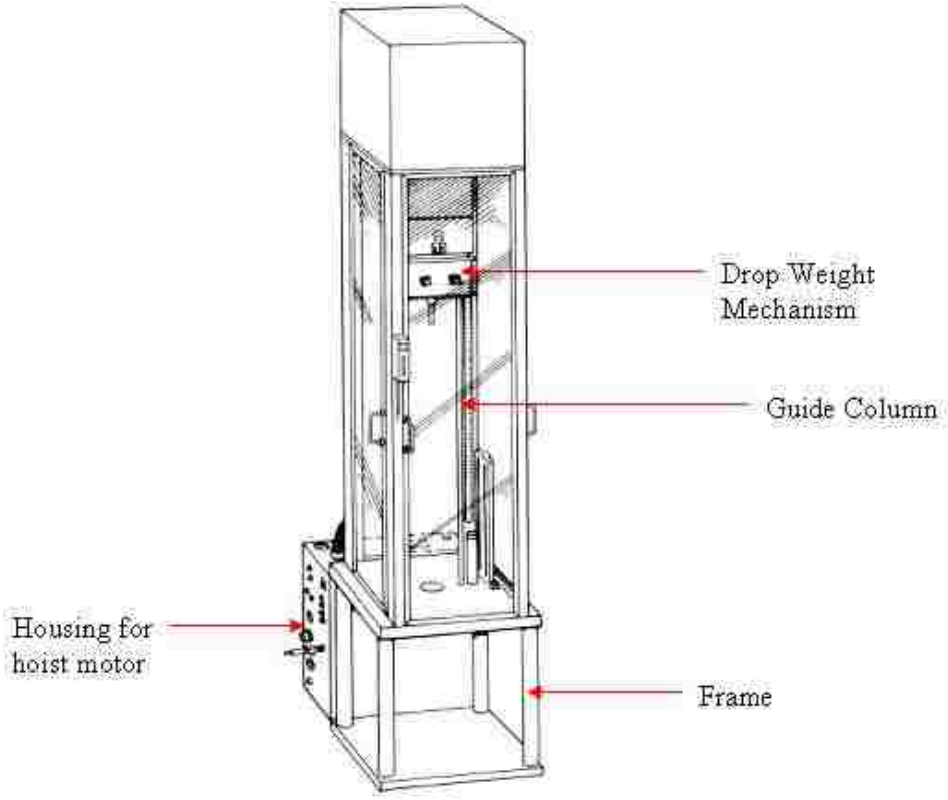

Figure 6.1: Instron Dynatup 8250 Drop Weight Tower [55]

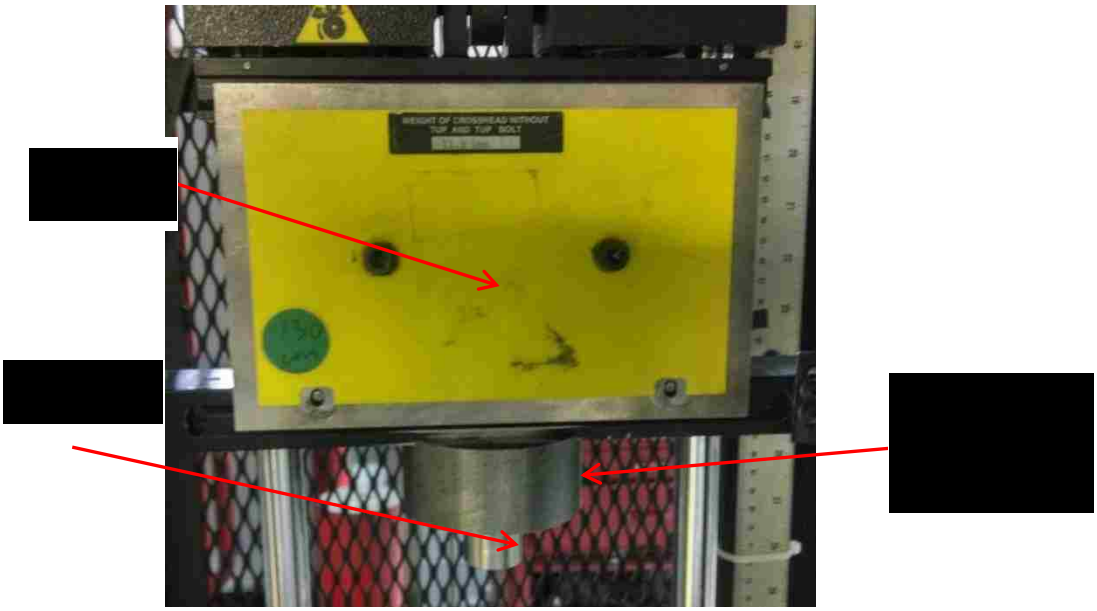

Figure 6.2: Drop Weight Mechanism

6.3 Test Fixture

For the study of bolted joints under medium impact, a fixture is developed as shown in Figure 6.3. The fixture has five components: Base, guide, body with flange, lid and bolts. The fixture is designed in a way that bolts are subjected to pure tensile load under impact. The purpose of the guide is to center the body and flange with respect to the drop weight impact mechanism. The lid and flange are held together by four 8-18 screws. The screws are made up of SS 304 material and the rest of the fixture is made up of structural steel. Figure 6.4a, 6.4b and 6.4c shows the dimensions of the fixture. The base has a ¼- 28 threaded through hole at the center. A ¼ - 28 screw is used to secure the load cell and base together.

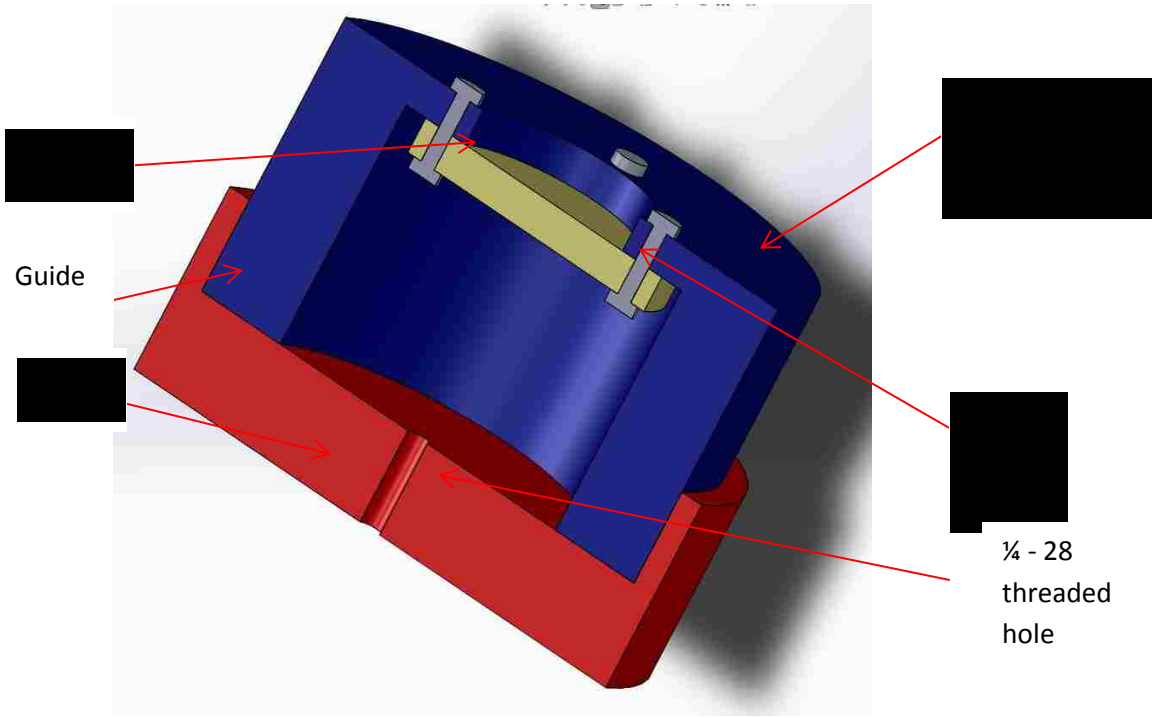

Figure 6.3: Section View of Fixture

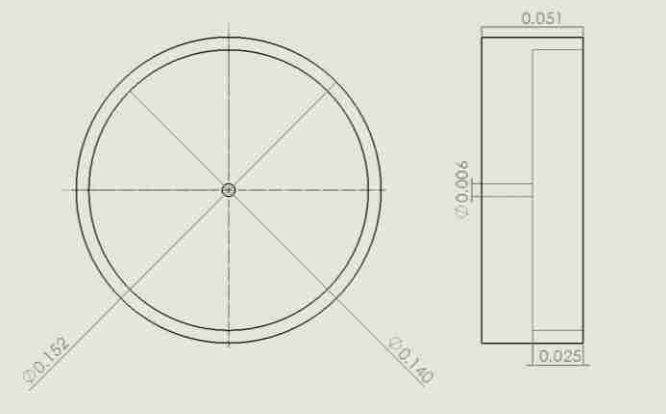

Figure 6.4a: Base (Dimensions in m)

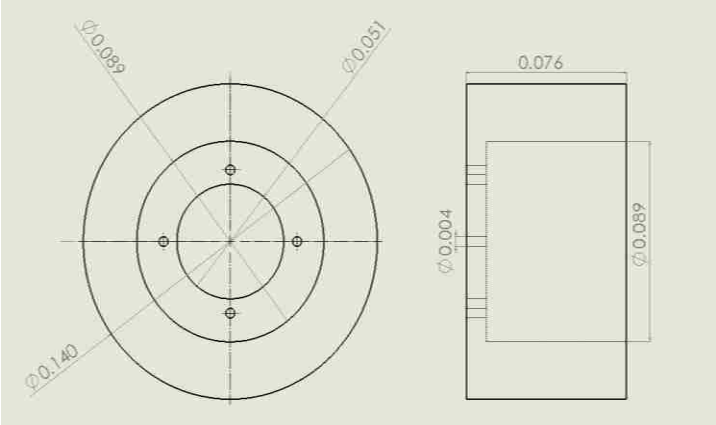

Figure 6.4b: Body with Flange (Dimensions in m)

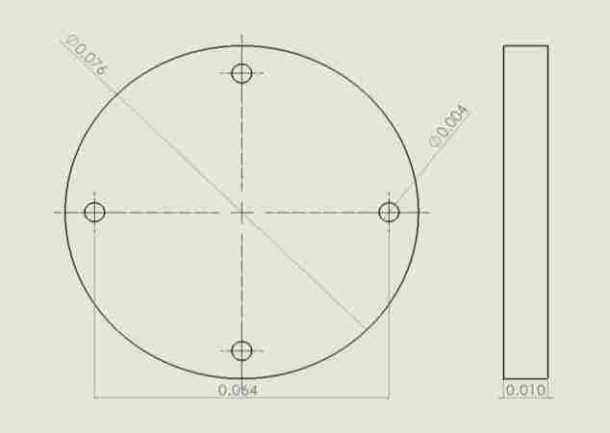

Figure 6.4c: Lid (Dimensions in m)

The base is connected to a PCB Piezotronics force transducer Model: 200M50 (Figure 6.5), through a ¼ - 28 threaded screw. The specifications of the load cell are listed in Appendix G. The load cell is fixed to the body of drop weight tower using a ¼ - 28 threaded screw. The base and body with flange are held together by two c-clamps as shown in Figure 6.6 to avoid losing contact between the body and the base during impact. The two c-clamps are positioned opposite to each other.

Figure 6.5: PCB Piezotronics (Model: 200M50) Force Transducer

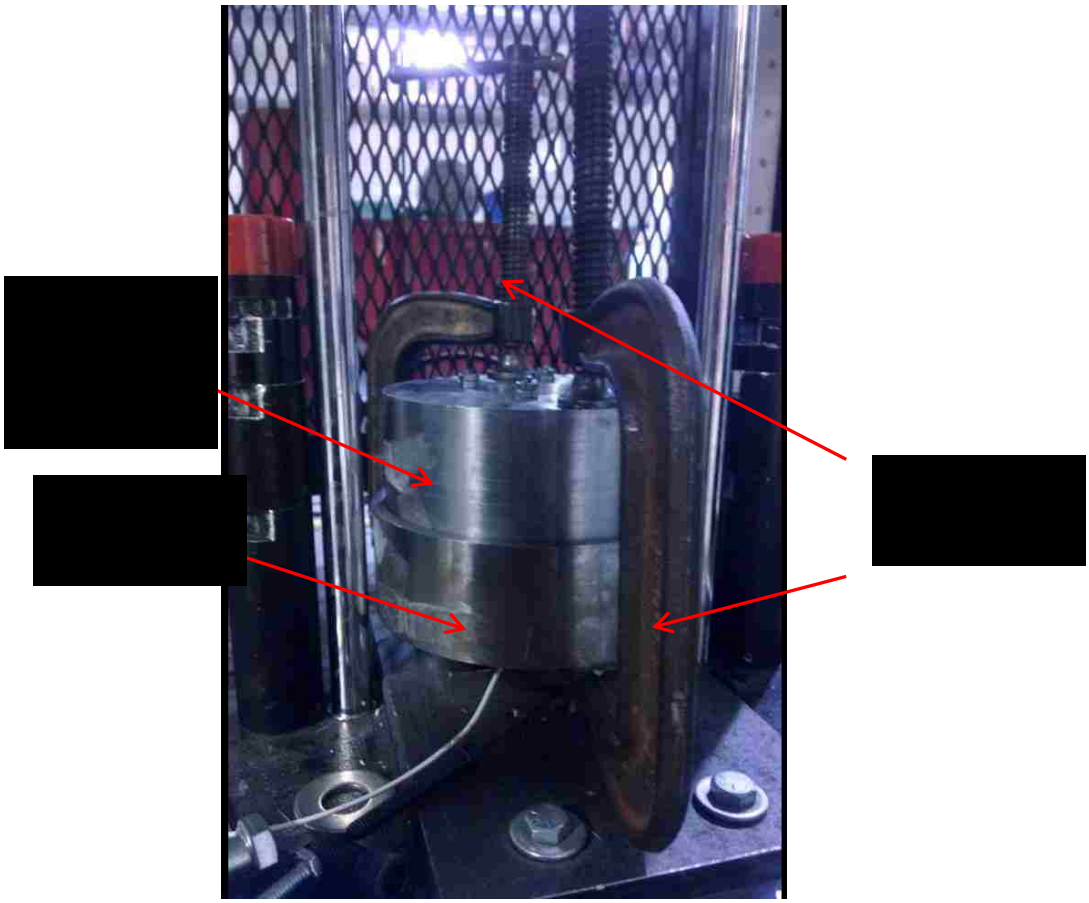

Figure 6.6: Test Fixture with C-Clamps

The same Dytran 3200b accelerometer used in the gas gun experiment is used to measure the acceleration and is fixed to the body as show in Figure 6.7. The accelerometer and force sensor are connected to a data acquisition system through Dytran 4103C signal conditioner and PCB 482A21 signal conditioner respectively. Output of the signal conditioners were captured using DL 750 scopecorder oscilloscope. The experimental setup for medium impact testing is shown in the Figure 6.8.

Figure 6.7: Accelerometer Location

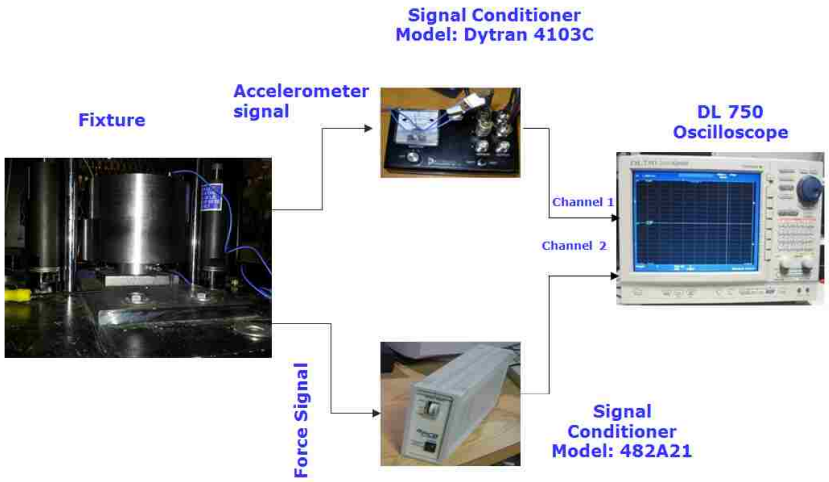

Figure 6.8: Experimental Setup

The experiments were conducted at two different torque levels: 0 Nm and 1 Nm. Using the equation (13) and (14) discussed in Chapter 5, the tightening force for 1Nm torque level is calculated as 1868.2 N and the initial stress on the bolt shank caused by the preload is 207MPa. These stresses are below the yield strength of the material (310

MPa [56]). The drop height of the weights was also changed to change the strain rate on the bolts. The test matrix for the drop weight tower experiments are listed in Table 6.1. Drop velocity and impact energy are calculated using the equation given below,

$$\mathrm{V} = \sqrt{2\,\mathrm{g}\,\mathrm{h}} \tag{17}$$

where, V is the velocity

g is the acceleration due to gravity

h is the drop weight

$$E = \frac{1}{2}\, m\, v^2 \tag{18}$$

where, E is the kinetic energy

m is the mass

v is the velocity

Table 6.1: Test Matrix

Test	Drop height (m)	Tightening Torque (N-m)	Drop Velocity (m/s)	Kinetic Energy (J)	Number of Repetitions
1	0.050	1	0.99	2.20	3
2	0.050	0	0.99	2.20	3
3	0.254	1	2.23	11.18	3
4	0.254	0	2.23	11.18	3
5	0.508	1	3.15	22.32	3
6	0.508	0	3.15	22.32	3

6.4 Experiment Results

Figure 6.9 and 6.10 shows a typical acceleration and force profile in time domain from an experiment conducted at 0.508 m drop and 0 torque respectively. The signal is

measured for 10ms at a sampling rate of 5E6 samples per second. The acceleration results were filtered using a low pass Butterworth filter at 10,000 Hz, since the accelerometer has a range from 0.35 to 10,000 Hz. The results were not high passed filtered as there was no DC shift in the accelerometer signal. The results are show in Figure 6. 11.

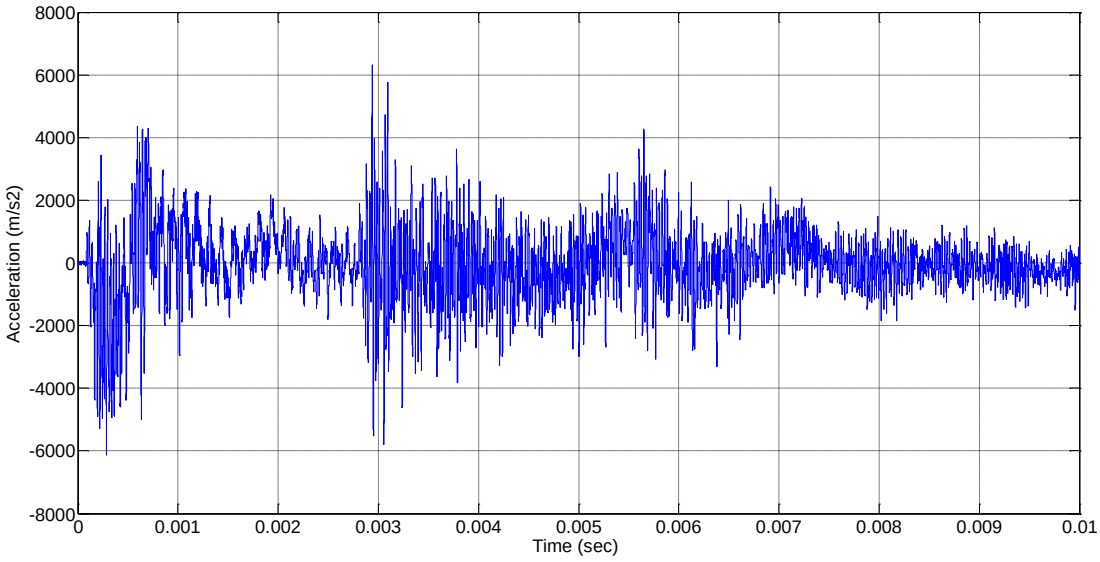

Figure 6.9: Typical Unfiltered Acceleration Data for 0.508 m Drop and 0 Nm Torque

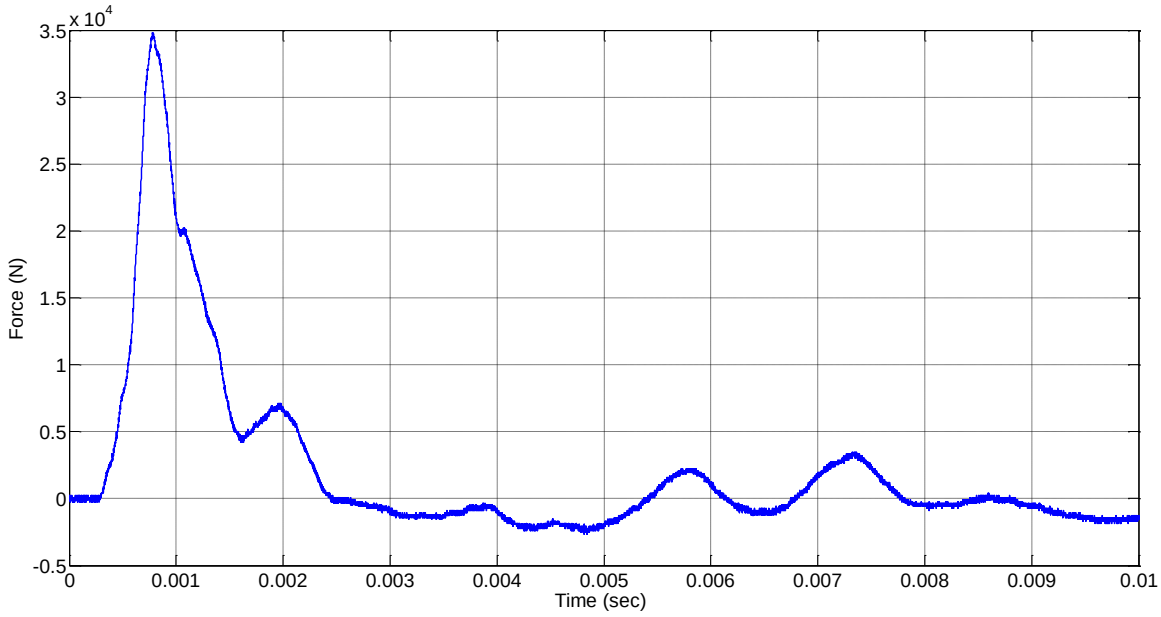

Figure 6.10 Typical Force Data for 0.508 m Drop and 0 Nm Torque

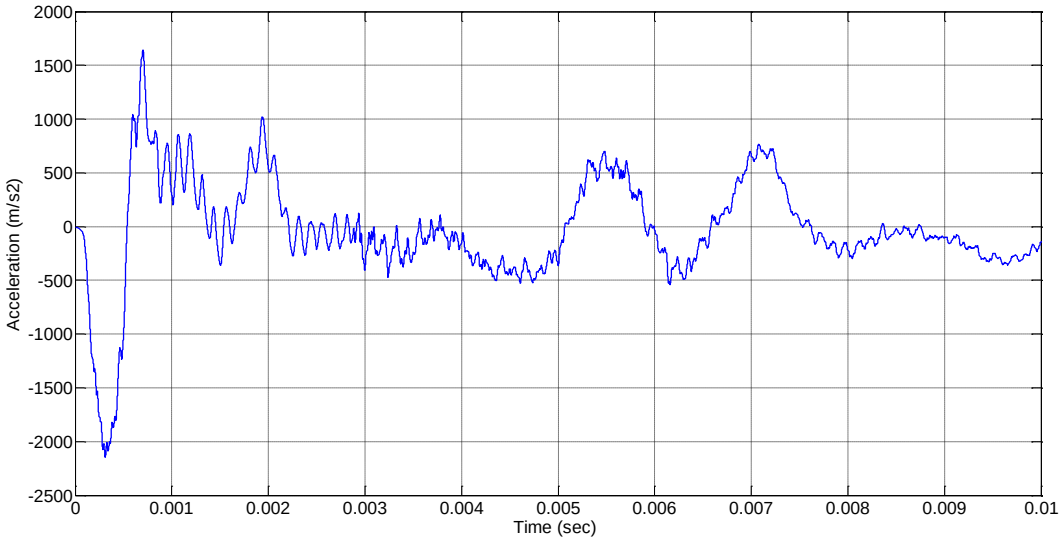

Figure 6.11: Typical Filtered Acceleration Data for 0.508 m Drop and 0 Nm Torque

Plastic deformation of the bolts is calculated by measuring the length of the bolt before and after the experiment using a Vernier caliper. The plastic strain is calculated

using the given equation. The average plastic strain is calculated using the following equation,

$$e = \frac{l_f - l_i}{l_i} \quad (19)$$

where, e is the plastic strain

l_f is the final length of the bolt

l_i is the initial length of the bolt

Table 6.2 shows the plastic strain in bolts for different loading conditions. The results indicate that the plastic strain and the standard deviation increase as the drop height increases. The increase in the deviation with drop height can be attributed to the misalignment of the railing which guides the weight.

Table 6.2: Plastic Strain on Bolts

Drop Height (m)	Tightening Torque (Nm)	Experiment Average Plastic Strain (%)	Standard Deviation (%)
0.050	1	0.13	0.095
0.050	0	0.17	0.087
0.254	1	0.45	0.176
0.254	0	0.42	0.187
0.508	1	1.16	0.490
0.508	0	1.47	0.309

CHAPTER 7

FINITE ELEMENT ANALYSIS OF MEDIUM IMPACT

7.1 Objective

Finite element Analysis (FEA) was performed to simulate the experiment and study the behavior of the joints when they are subjected to plastic deformation. The objective of this study is to reduce the need for experimental testing by developing procedures that allow the use of FEA to simulate impact.

All the computation analysis was done on 64 GB, 48 cores Linux server located at UNLV. Same unit system is used as explained in chapter 3. ANSYS workbench and LS-Prepost was used as a preprocessor to create and mesh the 3D model of fixture. Lagrangian finite element method approach is used for modeling the fixture since the deformation is not large.

7.2 Model Development and Meshing

Similar to the experiment, the FEA model has four basic components: Base, body with flange, lid and bolts. The model also includes the drop weight mechanism and the load cell. Guide component was not included in the model as it doesn't affect the dynamics of the impact. Load cell, base and body with flange are modeled as single part and weights, Impactor holder and impactor were modeled as single part. Finite Element Langrangian model was created in Solid Works as shown in Figure 7.1. The solid works model was imported into ANSYS WorkBench for meshing.

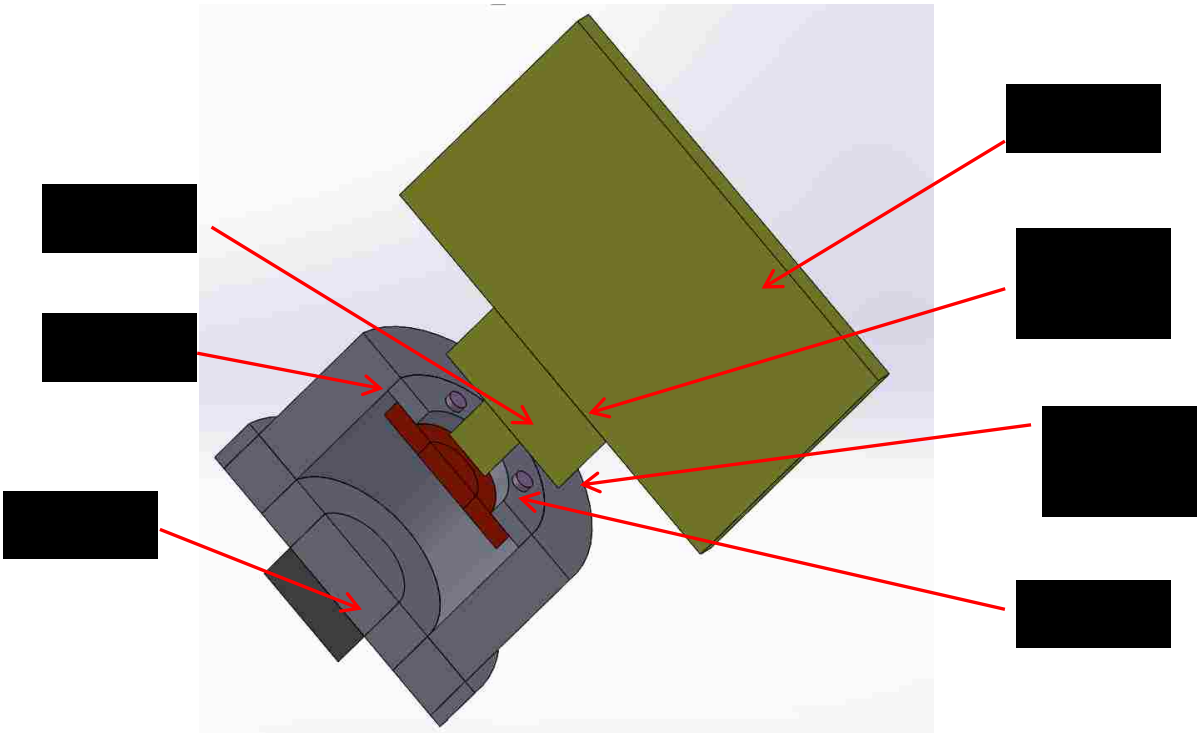

Figure 7.1: Test Fixture

All the components were meshed using Multizone option available in ANSYS Workbench. To reduce the size of the model, quarter plane of symmetry is considered. Table 7.1 shows element sizing and number of elements for each component. Figure 7.2 shows the meshed model of the entire fixture and Figure 7.3 shows the meshed model of 8-18 screw.

Table 7.1: Lagrangian Element Size and Number of Elements

Part	Element Size (10^{-3} m)	No. of elements
Base	3	17,694
Load Cell	3	1,925
Body with Flange	0.8	45,279
Lid	0.5	28,561
Impactor	0.8	9,207
Impactor Holder	3	4,561
Weights	3	6,160
Bolt	0.2	46,776

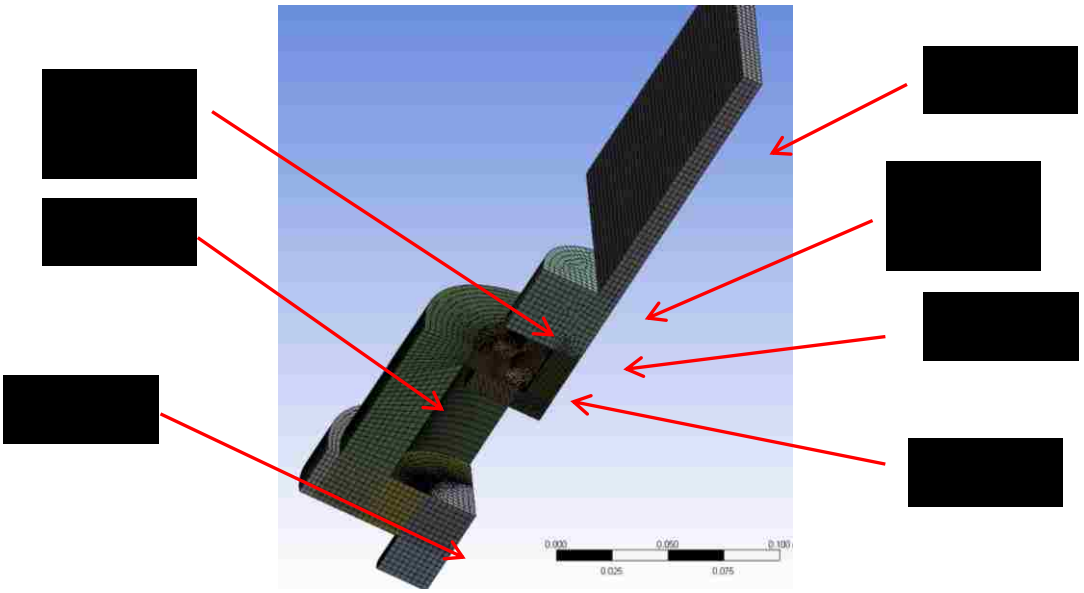

Figure 7.2: Meshed Geometry of the Fixture

Figure 7.3: Meshed model of 8-18 Screw with Nut

An input file (.k) of the whole setup was created from ANSYS WorkBench. The input file was imported to LS-Prepost for the creation of SPH elements.

7.3 LS-Dyna Input Card

Same set of Ls-Dyna input cards as described in Chapter 4 is used in used to describe the model. I addition to the cards used in Chapter 4, following cards have been added and modified for simulation of drop weight experiment.

1. Cards defining output
2. Contact cards
3. Material cards
4. Damping

7.3.1 Cards Defining Output

Acceleration is measured in a node that corresponds to the accelerometer location as show in Figure 7.4. Acceleration is also measured around the corresponding nodes for consistency. The output is recorded using DATABASE_HISTORY_NODE. The force is measured at the bottom of the base plate, as shown in Figure 7.5, using DATABASE_CROSS_SECTION_SET card. The input for DATABASE_CROSS_SECTION_SET card is the node set and element set pertaining to the area where the force is measured. The acceleration and force signal are sampled at 2E6 samples/sec.

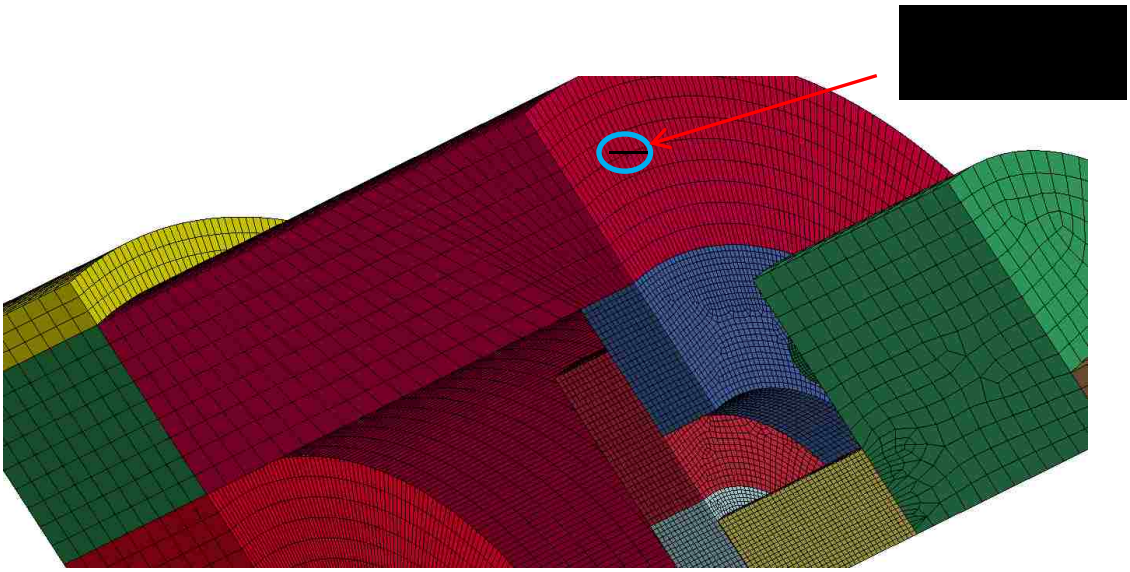

Figure 7.4: Experiment Fixture with Accelerometer location

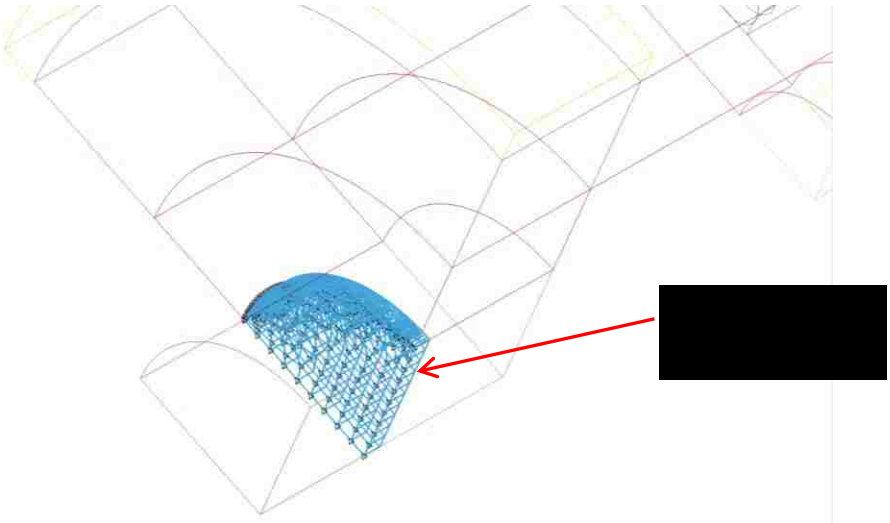

Figure 7.5: FEA Model with Force Output

7.3.2 Cards Defining Contact

Surface to surface contact is defined between bolts and flange, flange and lid, bolt and lid and impactor and lid.

7.3.3 Material Model

In this FEA model, two types of material model were used to define the parts. MAT_PLASTIC_KINEMATIC is used to define the base, body with flange, weight, impactor and impactor holder. This material model is used to define the elastic-isotropic behavior of solid and shell elements. Properties of structural steel are used to define these parts. Material properties are given in Table 7.2.

Table 7.2: Material Properties of Structural Steel used in Model

Parameter	Structural Steel
Density (Kg/m^3)	7850
Young's Modulus (GPa)	200
Poisson's Ratio	0.3
Yield Strength (MPa)	750
Tangent Modulus (GPa)	10

The bolts are subjected to much higher strain rate when compared to other parts. As described in Chapter 4, a constitutive relation that accounts for high strain rate is essential of describing the material, but the temperature change in these experiments are minimal, therefore thermal effects can be neglected. MAT_SIMPLIFIED_JOHNSON_COOK material model is used for defining bolt property. In this simplified model, thermal effects and damage are ignored. The dynamic flow stress is expressed as:

$$\sigma_y = \left(A + B\,\epsilon^{pn}\right)\left(1 + C\ln(\dot{\epsilon})\right) \quad (20)$$

where, $\sigma_y$is the flow stress.

A is the yield stress under quasi-static conditions, B and n are strain hardening parameters, m controls the temperature dependence and C the strain rate dependence.

ϵ^p is the equivalent plastic strain.

$\epsilon^{\cdot}$ is the effective plastic strain given by $\frac{\epsilon^{p}}{\text{EPSO}}$; where EPSO is the reference strain rate

The values of Johnson and Cook parameter for bolt is given in Table 7.3

Table 7.3: Simplified Johnson and Cook Material Property for SS 304

Parameter	**SS 304 Bolt[57]**
Density	7850 Kg/m^3
Young's Modulus	200 GPa
A	310 MPa
B	1000 MPa
N	0.65
C	0.07
Failure Strain	0.28
Reference Strain Rate	1

Material property of the load cell is given in Table 7.4. MAT_PLASTIC_KINEMATIC is used to define the material properties of load cell. Identification and verification of this material model is explained in Appendix F.

Table 7.4: Material Properties of Load cell

Parameter	Structural Steel
Density (Kg/m^3)	7850
Combined Young's Modulus (GPa)	1.08
Poisson's Ratio	0.3
Yield Strength (MPa)	750
Tangent Modulus (GPa)	10

A constant stiffness proportional damping and mass proportional damping is applied of $289.23s^{-1}$ and 7.23E-4s is applied for the parts. Evaluation of this parameter and explanation of stiffness proportional damping and mass proportional damping is given in Appendix F.

7.4 Simulation Results

The FEA model for fixture was run with the load cell parameters determined in previous section. Figure 7.5 and 7.6 shows the FEA result for 0.508m drop with no preload on the bolts. The acceleration around the corresponding node is also measured and the results were consistent.

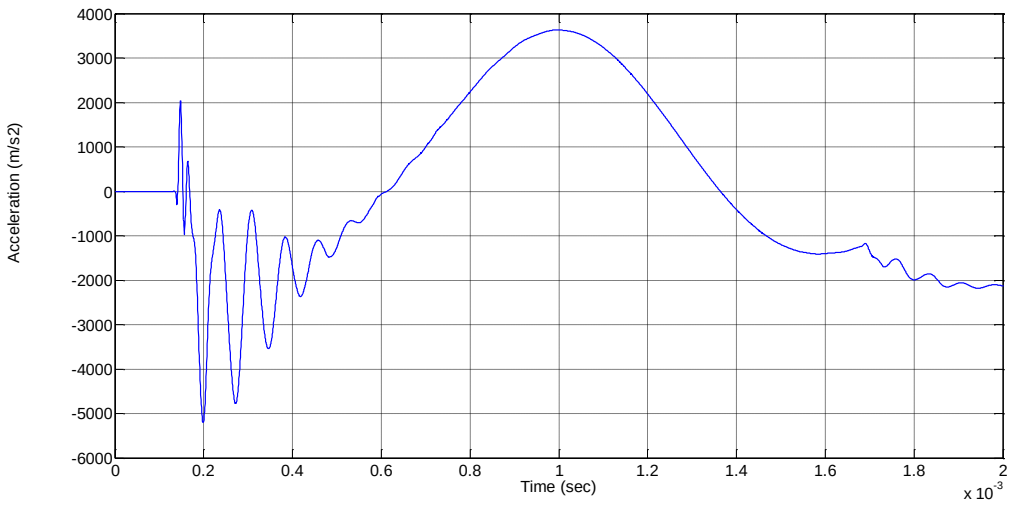

Figure 7.6: Typical Unfiltered FEA Acceleration Data

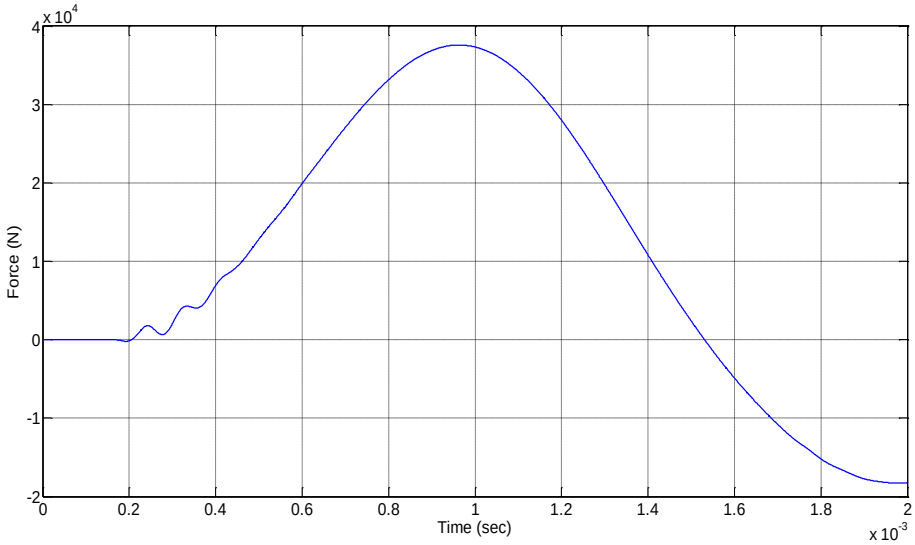

Figure 7.7: Typical Unfiltered FEA Force Data

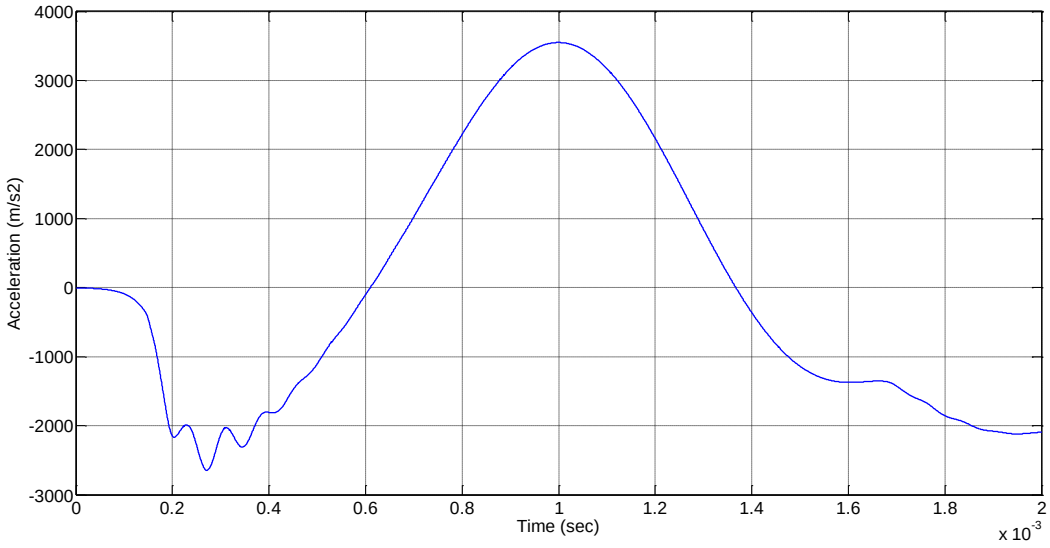

Figure 7.8: Typical Filtered Acceleration Data

CHAPTER 8

RESULTS AND COMPARISON

Experiments were conducted with drop weight tower experiment at different drop height and bolt torque tightness. FE analysis was done for these experiments as explained in Chapter 7. The FE analysis is verified using three experiment parameters: Bolt plastic strain, acceleration, impact force.

Table 8.1, shows the comparison of plastic strain comparison on bolts. The table shows that the plastic deformations on bolts are not depended on the applied torque. The table also shows that as the drop height increases, the plastic strain increases. Figure 8.1 to 8.6 shows the acceleration and force time history results for experiment and FEA.

Table 8.1: Plastic Strain on Bolts

Drop Height (m)	Tightening Torque (Nm)	Experiment Average Plastic Strain (%)	FEA Plastic Strain (%)
0.050	1	0.13	0
0.050	0	0.17	0
0.254	1	0.45	1.56
0.254	0	0.42	1.52
0.508	1	1.16	3.17
0.508	0	1.47	3.16

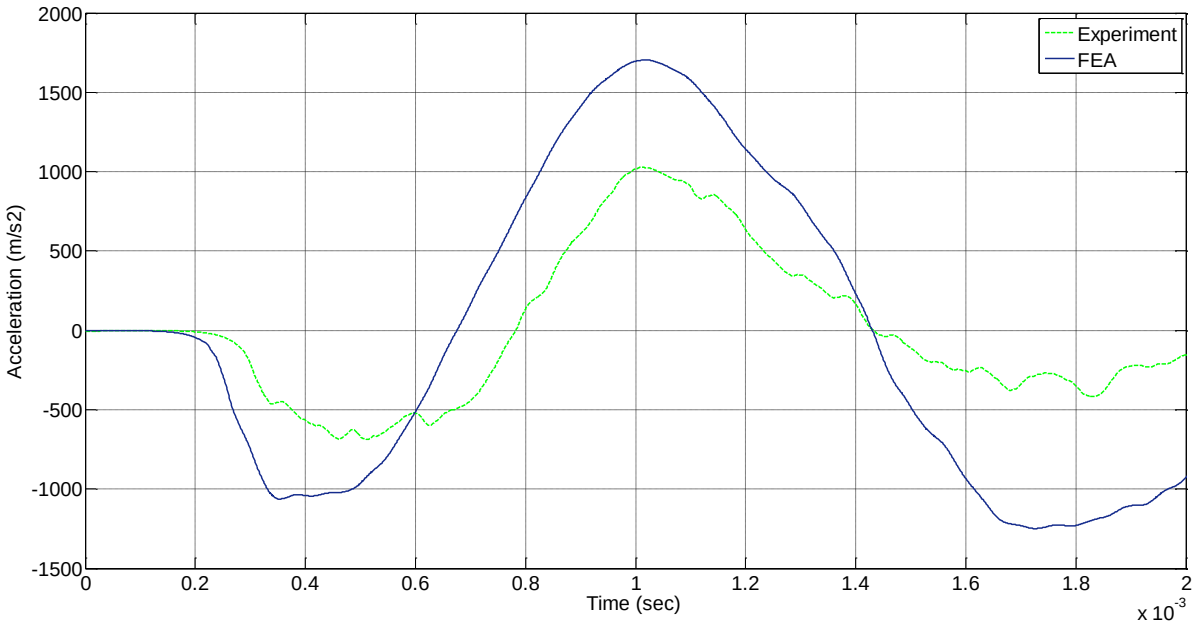

Figure 8.1a: Acceleration Time History for Drop Height of 0.050m and 1 Nm Torque

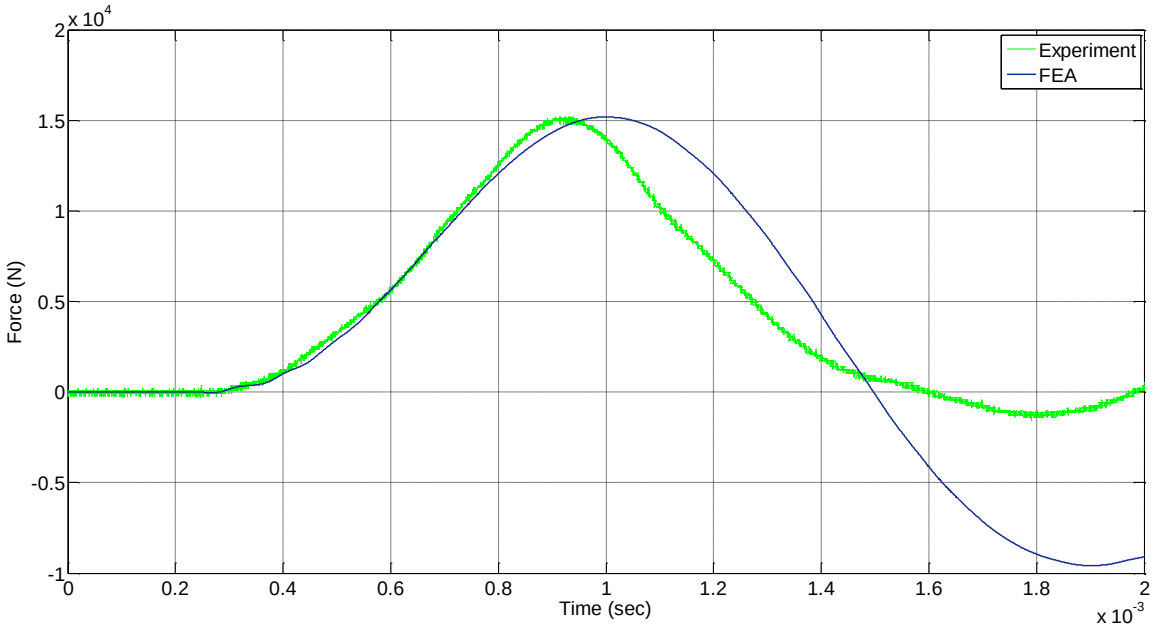

Figure 8.1b: Force Time History for Drop Height of 0.050m and 1 Nm Torque

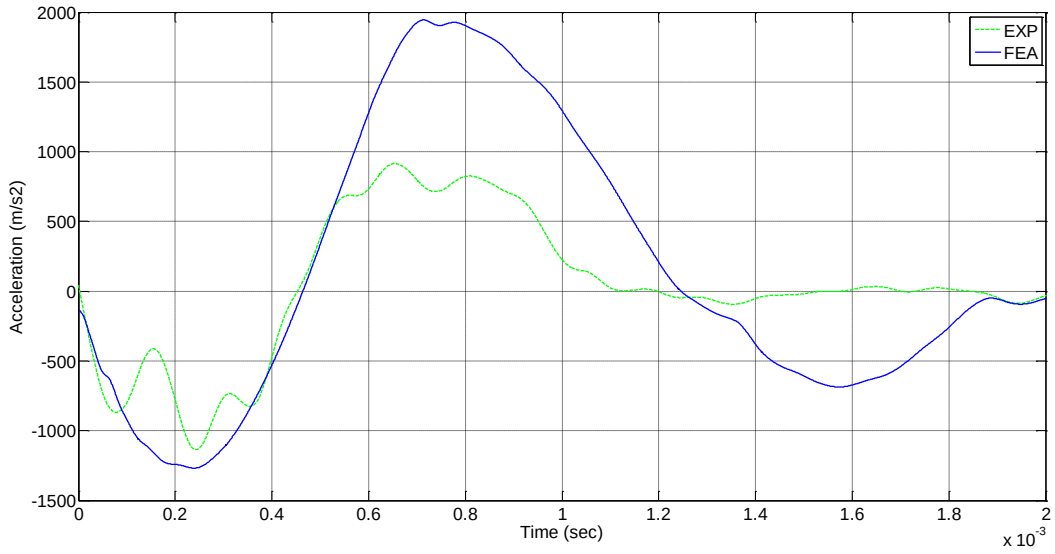

Figure 8.2a: Acceleration Time History for Drop Height of 0.050m and 0 Nm Torque

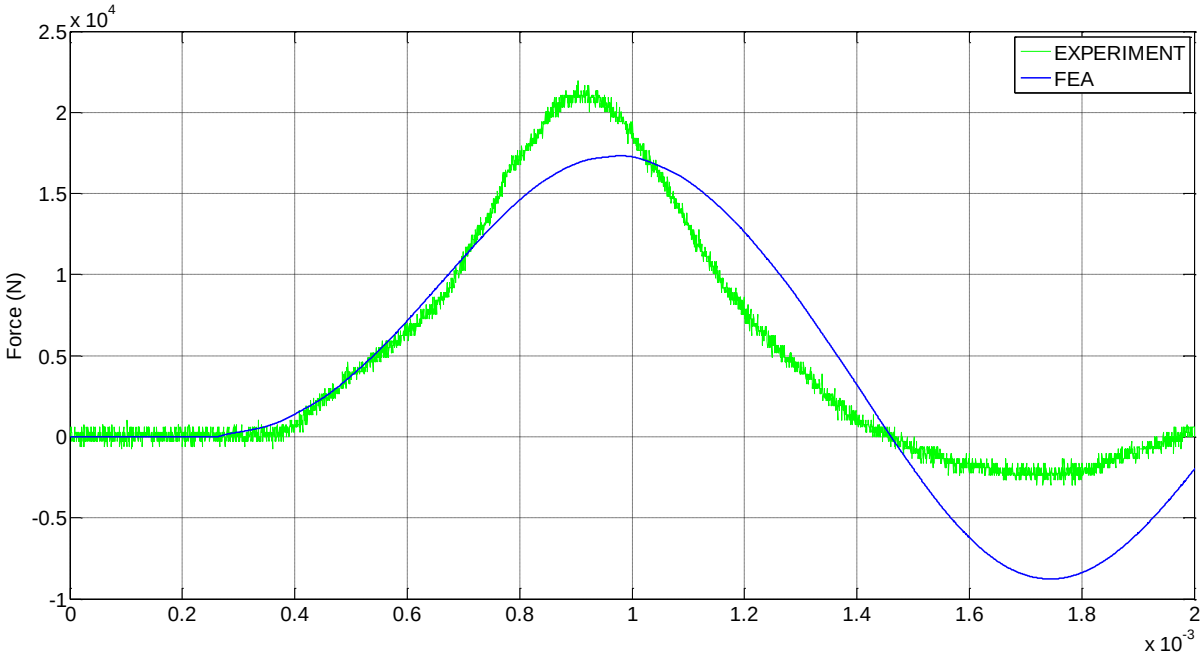

Figure 8.2b: Force Time History for Drop Height of 0.050m and 0 Nm Torque

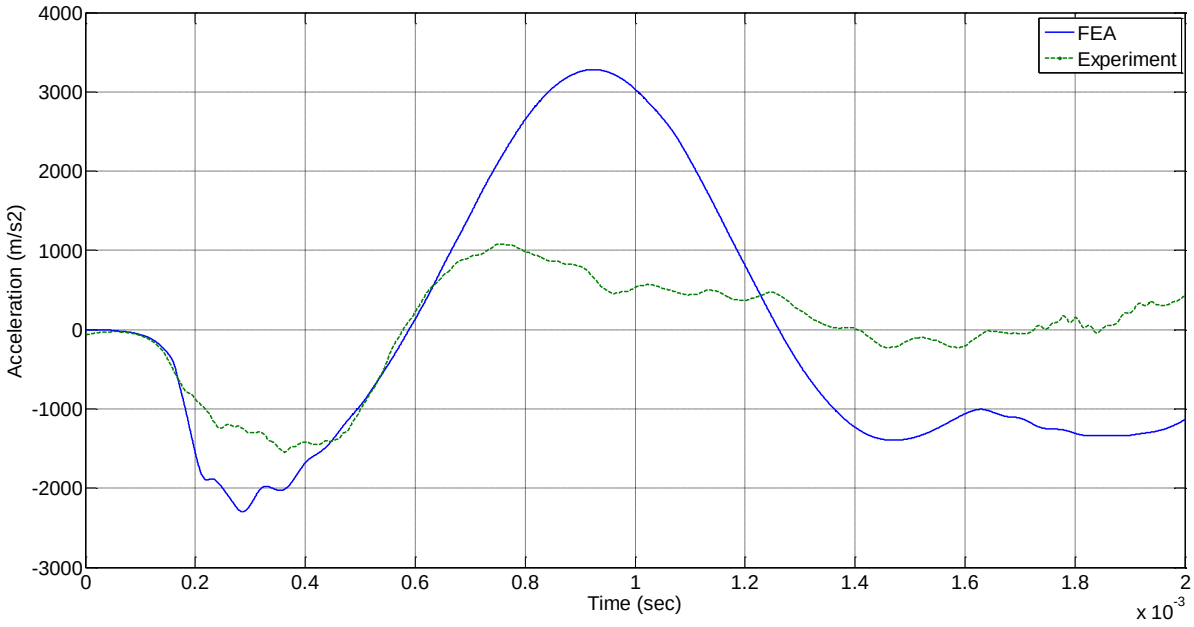

Figure 8.3a: Acceleration Time History for Drop Height of 0.254m and 1 Nm Torque

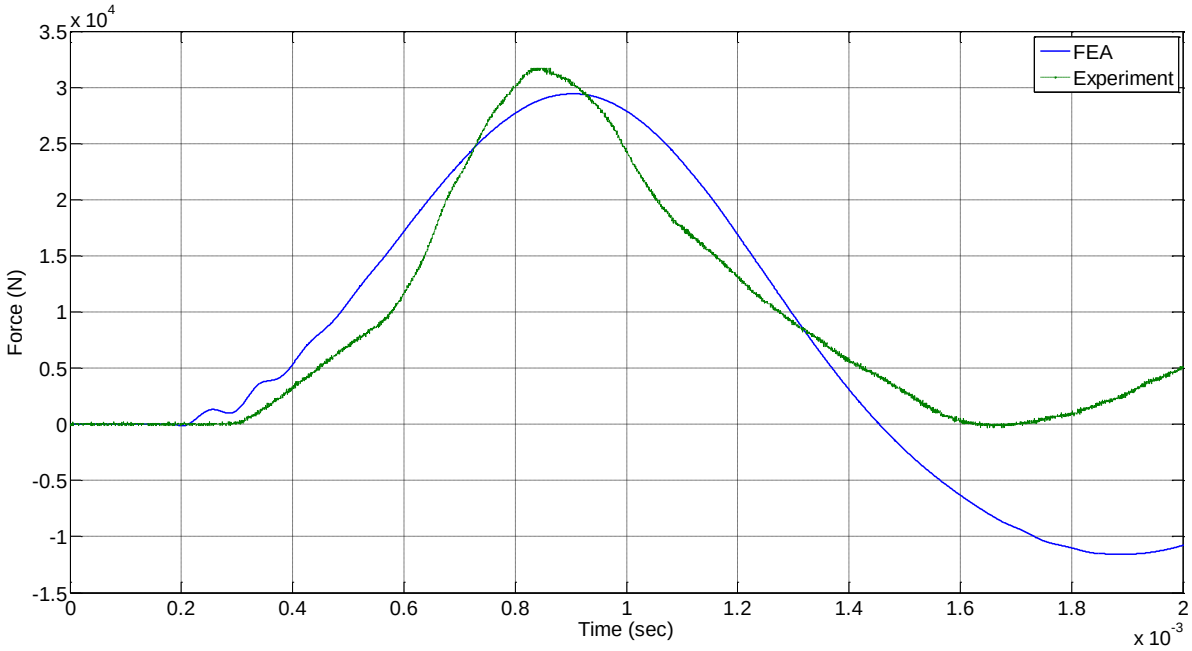

Figure 8.3b: Force Time History for Drop Height of 0.254m and 1 Nm Torque

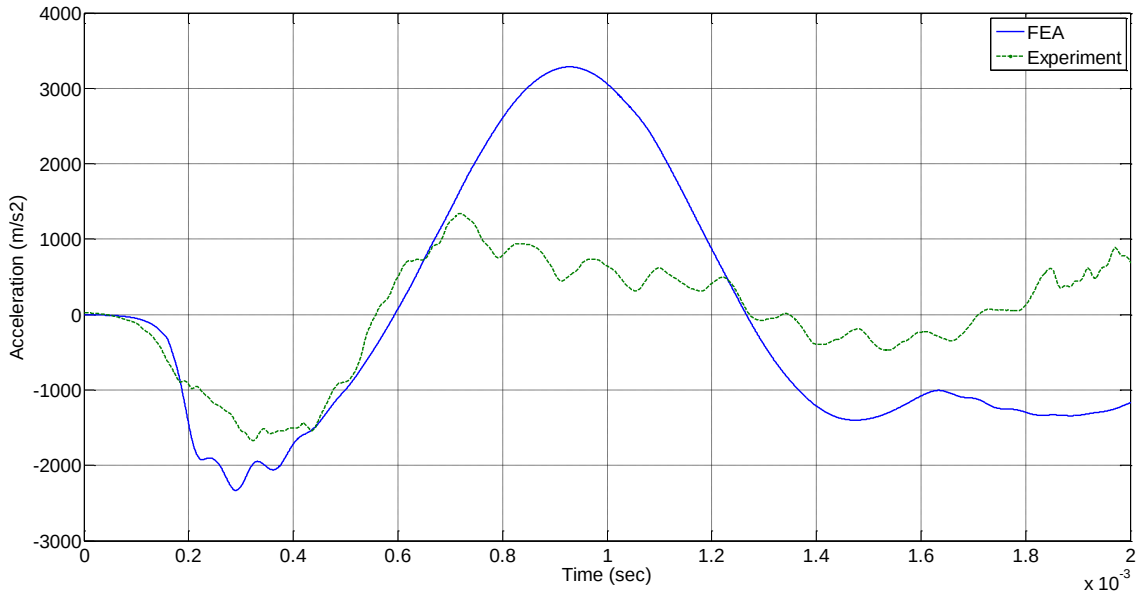

Figure 8.4a: Acceleration Time History for Drop Height of 0.254m and 0 Nm Torque

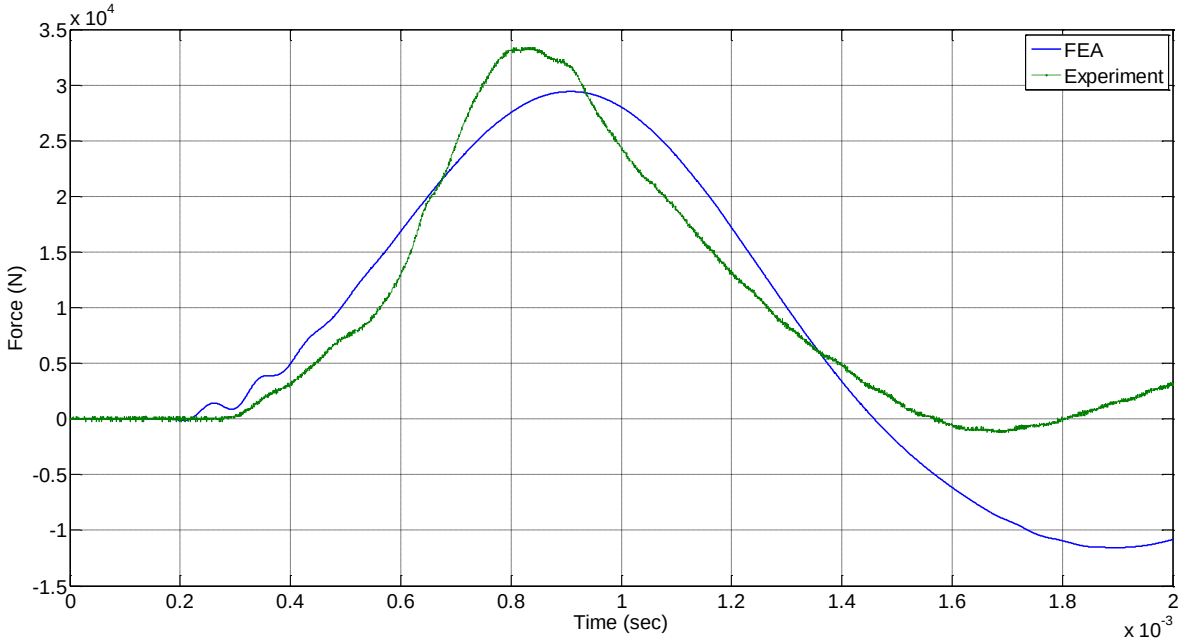

Figure 8.4b: Force Time History for Drop Height of 0.254m and 0 Nm Torque

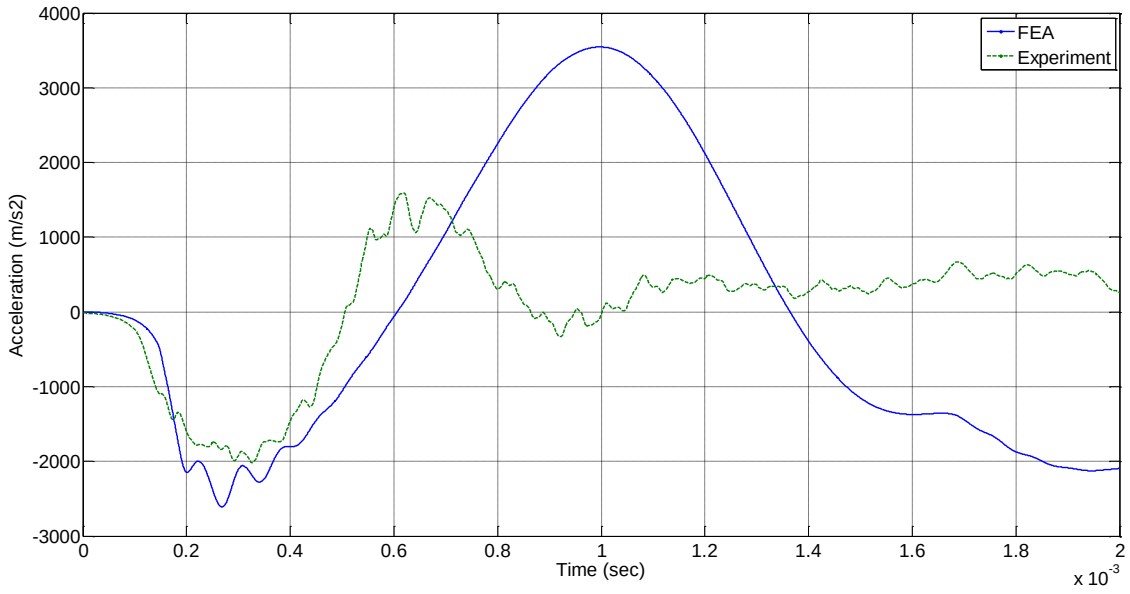

Figure 8.5a: Acceleration Time History for Drop Height of 0.508m and 1 Nm Torque

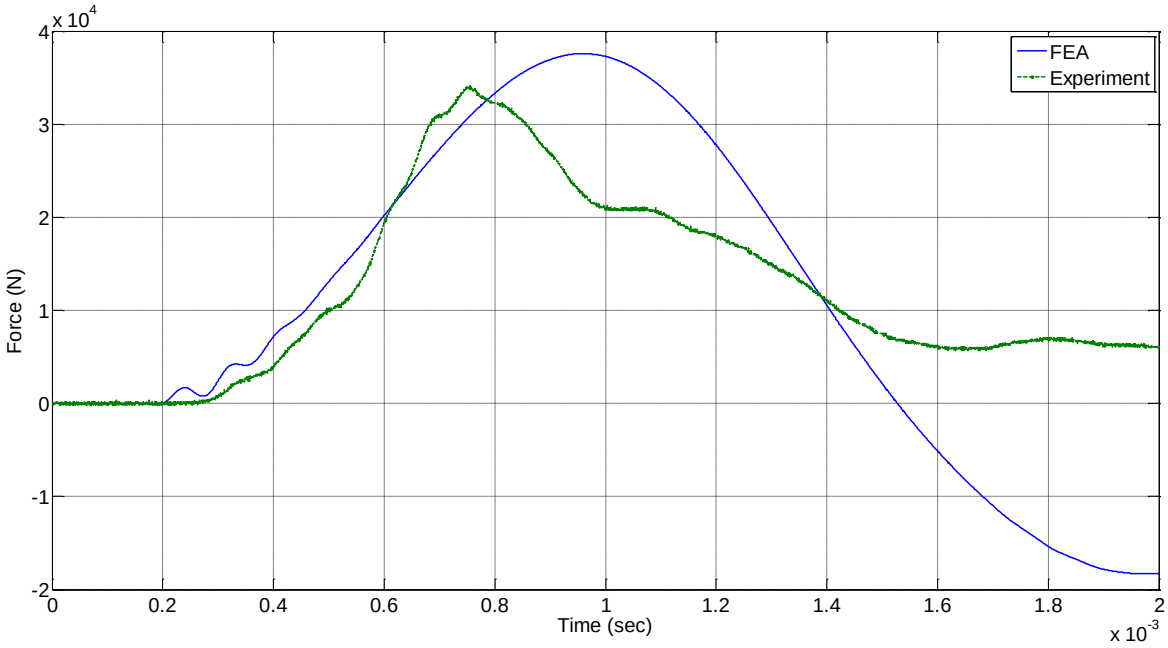

Figure 8.5b: Force Time History for Drop Height of 0.508m and 1 Nm Torque

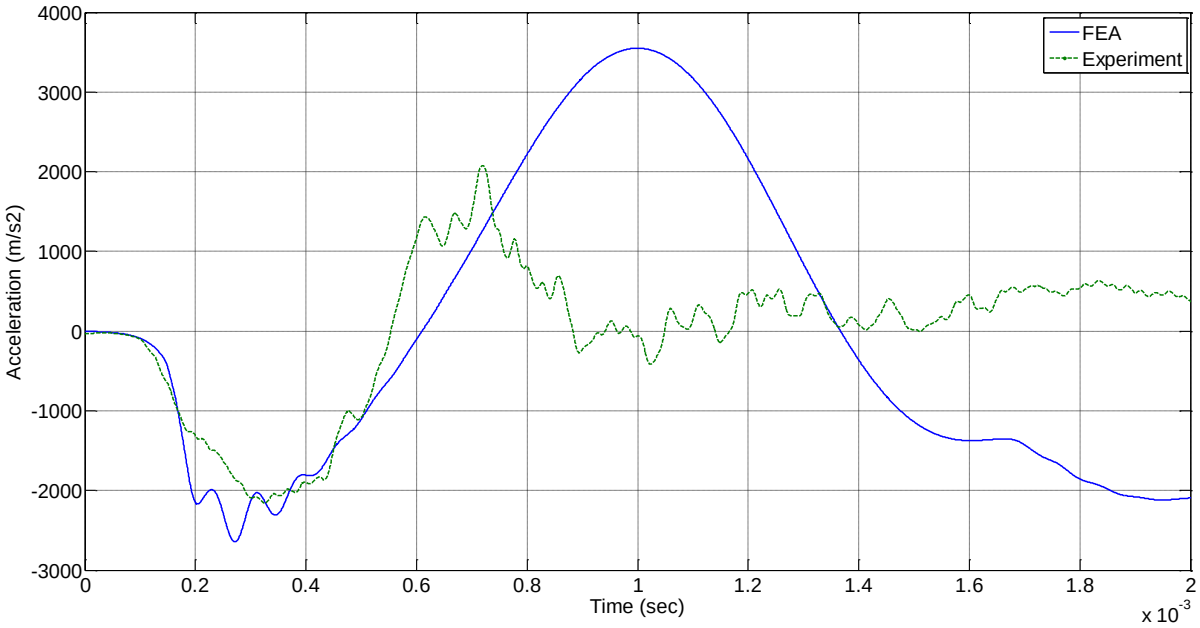

Figure 8.6a: Acceleration Time History for Drop Height of 0.508m and 0 Nm Torque

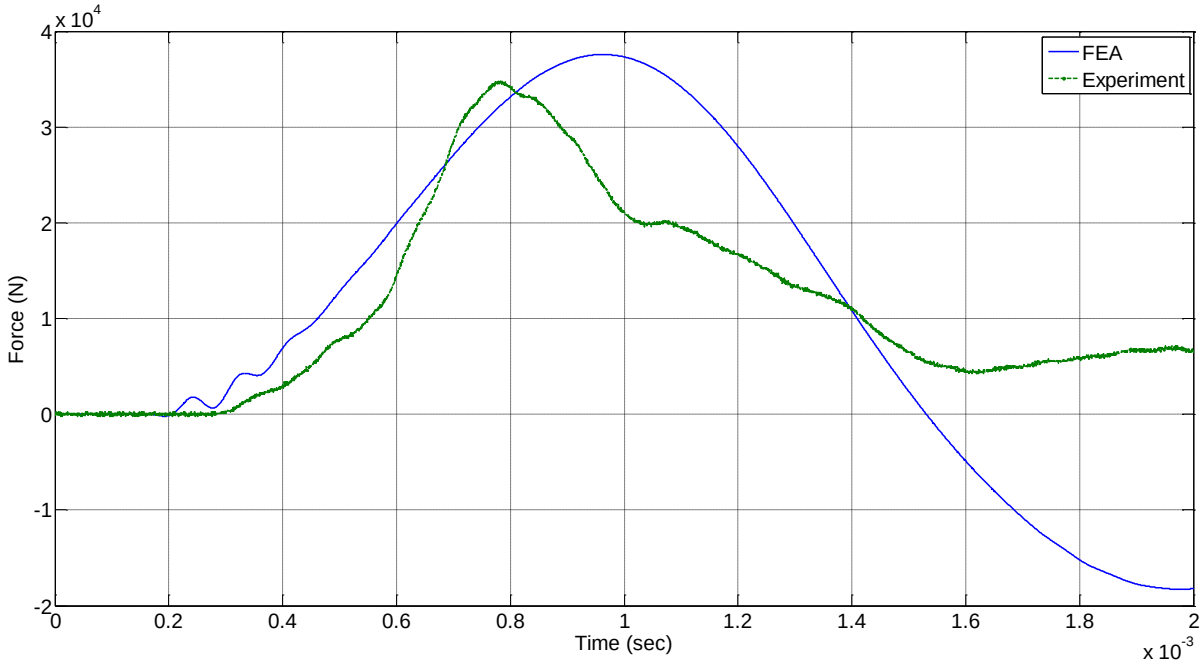

Figure 8.6b: Force Time History for Drop Height of 0.508m and 0 Nm Torque

Normalized root mean square deviation (NRMSD) of acceleration and force data is used to compare the closeness of the FEA results with experimental data as explained in equation 16, Chapter 6. Table 8.2, shows the NRMSD values between experiment and simulation for the different drop heights and torque tightness.

Table 8.2: NRMSD between FEA and Experiment data

Drop Height (m)	Tightness Torque (Nm)	NRMSD Acceleration (%)	NRMSD Force (%)
0.050	1	14.90	16.04
0.050	0	13.40	17.11
0.254	1	24.67	18.05
0.254	0	23.57	27.60
0.508	1	31.09	23.35
0.508	0	30.07	37.37
Average NRMSD %		22.95	23.25
Standard Deviation %		6.78	7.47

The results from Table 8.1 and 8.2 indicate that the model is able to simulate the experiment with certain degree of accuracy. The acceleration and force estimated didn't exceed the experimental value by 30% and 37% respectively. The average error for

acceleration and force is 22.95% and 23.25% respectively and 6.78% and 7.47% standard deviation.

8.2 Summary of Results

The objective of this part of the dissertation was to study the shock propagation across bolted joints when bolts are subjected to plastic deformation. A test fixture was designed in much a manner that the bolts undergo plastic deformation from pure tensile load. The bolts were preloaded to two different torque levels and the heights of the drop weights were also varied. Acceleration and force signals were measured from the impact. Plastic strain of the bolts was also measured. The material model for the load cell with drop weight tower was experimentally determined using a simple steel cylinder. The damping factor was calculated using half power bandwidth method. A finite element model for the bolted joint fixture was created in Ansys-LS-DYNA. All applicable contacts were defined in the FEA model. Damping calculated from the steel cylinder was used in FE model. In this FE model the damping was included using Rayleigh stiffness proportional and mass proportional damping criteria. Results from the simulation were compared with experiment based on plastic strain on bolts, acceleration and force time histories. NRMSD method was used to quantify the FE results.

There were few discrepancies with the FE model results. The results indicate that the drop weight tower assembly dampens the energy much more than calculated. Modelling the entire drop weight tower with the base would be very difficult. The

variation in the result can be also attributed to the stress concentration in the bolts, loosening of the nuts on impact and the impact center not being center of the fixture.

CHAPTER 9

SUMMARY, CONCLUSION AND FUTURE WORK

This chapter provides the summary and outline of the research performed. It discusses the tool developed for simulating structures bolted joints under high and medium impact conditions. Finally, recommendations for future work that would on this research are discussed.

9.1 Research Summary and Conclusion

Bolted joints are common type of fasteners used in many applications, including military vehicles and blast containment vessel. These bolted joints can be subjected to high impact loads from projectile impact or blast load. An extensive literature review showed that there has been little work done on the shock propagation through bolted joints. The focus of most of the earlier research was on slip mechanism or damping in bolted joint. Few researchers considered time history analysis of low impact loading conditions. On the other hand, little research was done on bolted joints when bolted structure is subjected to plastic deformation. The objective of this research is to understand and develop a tool for simulating structures with bolted joints when subjected to high impact loading.

Two types of structures are considered in this study:

- Structures with bolted joints that are subjected to high shock loads, where shock speeds were higher than elastic wave speed and,

- Structures with bolted joints that are subjected to medium shock loads and undergoes plastic deformation.

The first part of the research focused on structure with bolted joints subjected to high impact loading. The experiments were conducted using Two-Stage Gas Gun facility at UNLV. A36 steel was used for target and target holder material and four ½" grade 5 bolts were used for connecting these plates. The targets were impacted with Lexan polycarbonate projectile around the speed of 5000 m/s. The experiments were conducted at three bolt tightness levels: 135 Nm, 108 Nm, 81 Nm. Accelerometer was used to measure the post-joint acceleration. The measured accelerations were also verified using a Planar Doppler Velocimetry (PDV). Damage caused by the impact on the plate was also measured.

A Finite Element (FE) model was created to simulate experiments using ANSYS-LS-DYNA. Since the Lagrangian method was not suitable due to mesh distortion and instability arising from penetration, a Smoothed Particle Hydrodynamics (SPH) was used. The projectile and a cylindrical volume of 40 mm on the centered at the impact point are modelled with SPH particle while rest of the fixture was modelled using Lagrangian method. To accurately model the high strain rate and temperature effects due to projectile impact, Johnson Cook material model with Mie-Grüneisen equation of state were used for defining the material properties of the target and the projectile.

The FE results were compared to experimental ones using Fast Fourier Transform (FFT) analysis, Shock Response Spectrum (SRS), acceleration time history and

damage on target plate. The experimental and FE results matched accurately. The average error for plate deformation was 9.3% with a standard deviation of 6.09%. Normalized root mean square deviation (NRMSD) method of SRS data was used to compare the closeness of FE results with experiment. The average NRMSD was 10.83 % with a standard deviation of 2.47%

The focus of the second part of this research was on understanding the plastic deformation of bolts when subjected to impact loading. For this purpose, a test fixture consisting of base, body, flange and circular lid was designed to mimic the top of a cylindrical container. The flange and lid was connected using four SS 304 8-18 screws. The rest of the fixture were made of 4030 structural steel. The fixture was designed in such a way that the bolts are subjected to only tensile loading. The experiments were conducted using Instron drop weight tower with a 4.5 kg drop weight, which was maintained the same for all the experiments. The height of the drop was varied from 0.05m to 0.508m. Two torque levels were used for the experiment: 0 and 1 Nm. Each set of experiments were repeated thrice to ascertain the repeatability and consistency of the experiment. One accelerometer was used to measure the acceleration after the joint and force signal was measured using a force sensor, located at bottom of the fixture. The bolt lengths were measured before and after the experiment and the plastic strain was calculated.

The impact fixture model with bolts was modeled in ANSYS-LS-DYNA. Johnson – Cook material model was used to define the bolts. Experimentally obtained material

property and damping ratio values were used for load cell. In LS-DYNA both Rayleigh mass and stiffness proportional damping constants were used to define the overall damping ratio. Acceleration and force signals from FE were compared to the experiment. Plastic strains on the bolts were also compared. NRMSD method was done on acceleration data and the average was found to be 22.95% with a standard deviation of 6.78%. These results show that finite elements method can be used to simulate structures with bolted joints subjected to high impact loading, where the structure or the bolts undergo plastic deformation.

9.2 Future Work

- Exploring different modeling techniques for accurately modelling plastic deformation on bolts and shock propagation onto the structure after plastic deformation.
- This research focused on simulating the bolted joints by measuring the post-joint acceleration from impact. Measuring and simulating pre-joint acceleration along with post-joint acceleration will help us in understanding energy dissipation through joints.
- Exploring bolted connection study on composite structures under high impact.
- Stress concentration factor can have huge impact on plastic deformation of bolts when subjected to high impact loads. Study on effect of stress concentration factor in bolts during transient load can aid in improving the model for simulating plastic deformation of bolts.

- Another important aspect for structures with bolts when subjected to blast load is sudden rise in temperature. Understanding the cause and effect of temperature on bolted joints will help in better design of these structures.

APPENDIX A

MEASUREMENT OF DAMAGE PARAMTER

Impact crater dimensions (diameter of the crater, depth of penetration and bulge) were measured using slide calipers. Three measurements were taken for each parameter and an average value was considered for final parameter. Distance between the flat surface of the plate and peak point of the bulge was considered as the height of the bulge. Rulers were used to measure this distance and finally an average was considered. All the measurements were taken in inch scale and then converted to millimeter scale. Figure A.1, shows all documentations of how physical measurements were made of the impacted plate.

Impact crater diameter measurement

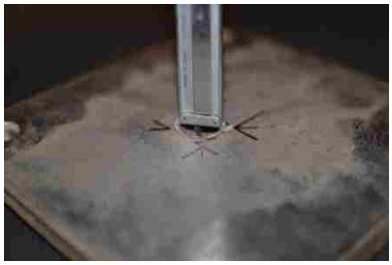

Depth of penetration measurement

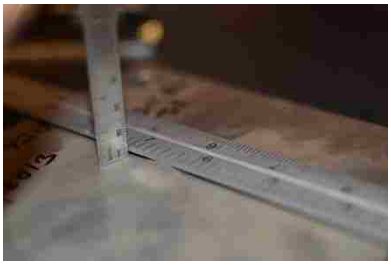

Bulge measurement

Figure A.1: Physical Measurement of Impacted Plate

APPENDIX B

ACCELEROMETER VERIFICATION USING PLANAR DOPPLER VELOCIMETRY

For high impact test using UNLV two stage gas gun, acceleration as high as 2E5 m/s2 were measured. The acceleration signal also contained higher frequencies. Accelerometer used for this application is a Dytran 3200B, which is low impedance voltage mode type accelerometer. The main sensing unit is a piezo crystal. High impedance generated by the crystal is converted to low impedance voltage by an integral IC electronics system. These accelerometers are generally linear at low velocities and when the frequencies are below the rated frequencies. But high accelerations and frequency, it is necessary to validate the accelerometer. So it was decided to use Planar Doppler Velocimetery (PDV), developed by NSTec for validation.

The PDV system used for the validation is a hytrodene velocimetery [58]. This technique makes use of Doppler shift theory. The Doppler shift is the difference between the frequency at which light leaves a source and the frequency seen by the observer. The difference is caused by the relative motion of the observer and the source and the shift in the frequency of the reflected light is proportional to the velocity of the source. A schematic of a PDV system used in UNLV is shown in Figure B.1

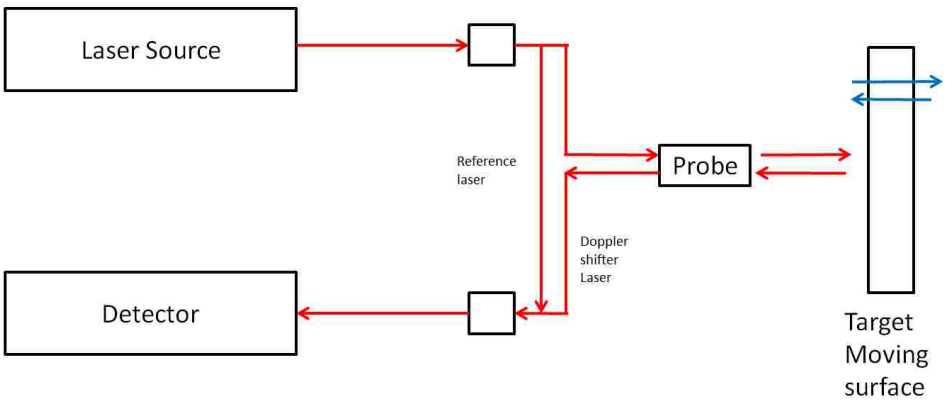

Figure B.1: Schematic of PDV System

The Doppler shifted light combined with the reference light, creating a beat frequency (frequency difference between two waves) is proportional to the target velocity and is given by $f = 2v/\lambda$, where λ is the wavelength of the source laser and v is the velocity. The frequency content of the PDV signal is typically calculated using a sliding short-time Fourier transform (STFT). The velocity of the target was provided by NSTec after data reduction.

Figure B.2, shows the laser probe positioned close to the accelerometer in the target plate. The laser probe was around 9mm from the accelerometer.

Figure B.2: PDV Laser Probe.

Accelerometer data was integrated using Matlab. Figure A.3 and A.4 shows the comparison of velocities for Test 5 and Test 9 with projectile velocity of 4540 m/s and 5040 m/s respectively. These figures show that the accelerometer is able to detect high acceleration and frequencies.

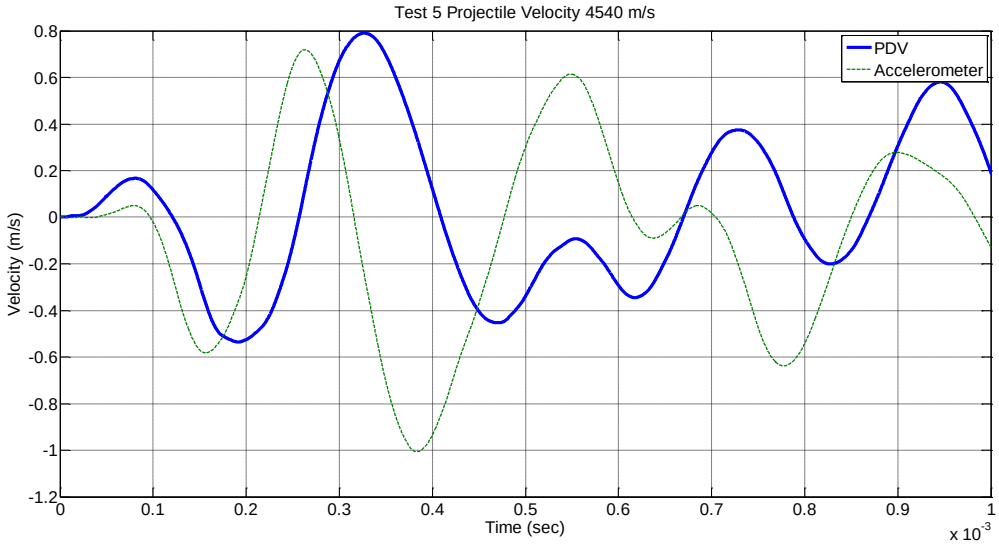

Figure B.3: Test 5 Velocity Comparison

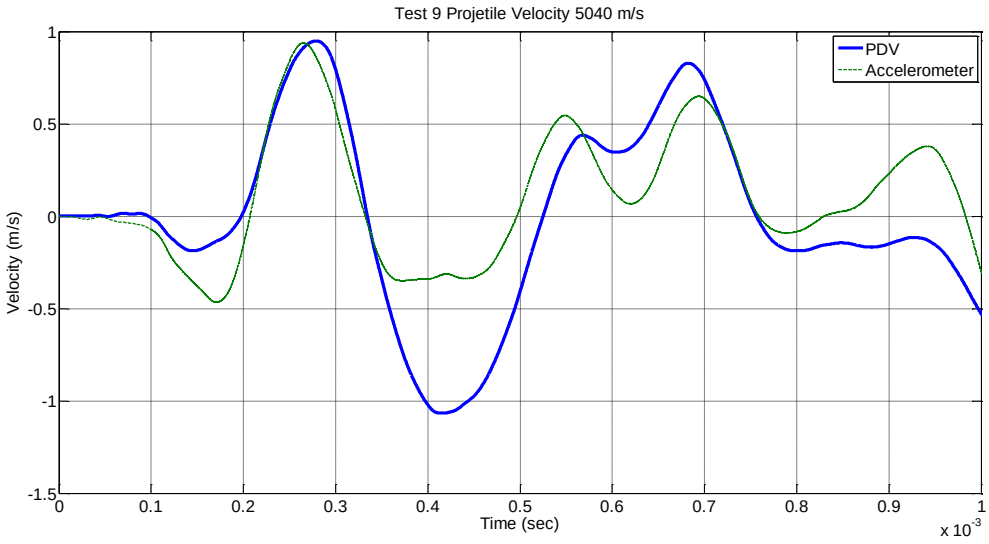

Figure B.4: Test 9 Velocity Comparison

APPENDIX C

FILTERING EXPERIMENTAL DATA

Typically accelerometers convert acceleration into electrical signal using a sensing unit and the vibration occurs around a fixed point and has zero mean over the time. But accelerometers have an unwanted phenomenon called drift which is caused by a small DC bias. The drift can be clearly seen when the acceleration signal is integrated to velocity. Velocity is calculated from acceleration signal using cumulative trapezoidal method. Figure C.1, shows a typical unfiltered acceleration signal and Figure C.2, shows the velocity signal calculated from acceleration. Figure C.2 suggests that the target holder's velocity increases with respect to time and it doesn't indicate that the vibration is around a fixed point. Both these figures clearly indicate the presence of DC shift in the signal.

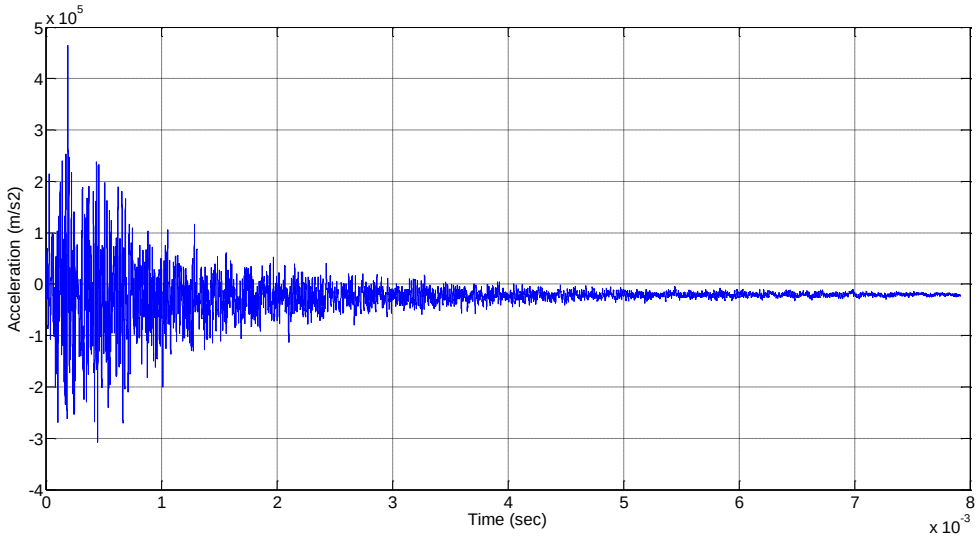

Figure C.1: Typical Unfiltered Acceleration Signal

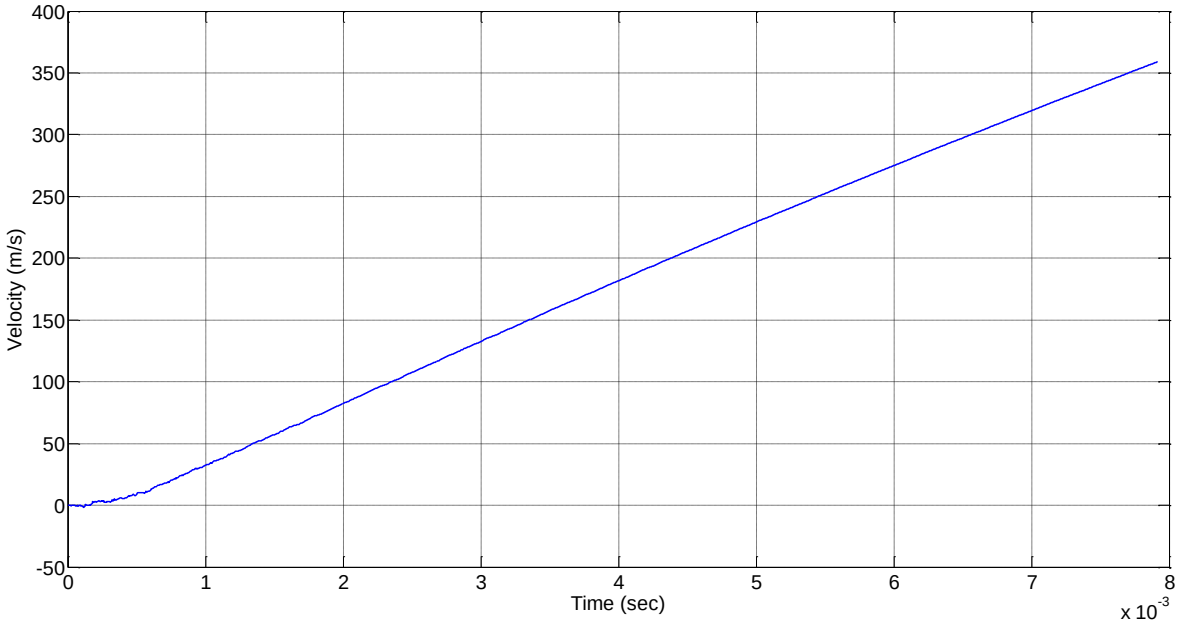

Figure C.2: Typical Unfiltered Velocity Signal

To solve the problem of drift, a high pass filter is used to remove the DC shift (DC component) from the acceleration signal. The acceleration signal is low pass filtered at 10,000 Hz. This is done since the accelerometer has limit at 10,000 Hz. The frequency of vibration due to impact is around 4000 Hz, as shown in Figure C.3. Therefore it was decided to limit the high pass filter frequency to 3000 Hz. Table C.1, shows the average velocity of vibration with respect to high pass filter frequency. For a signal without DC shift the average value is zero. The table clearly indicates that the average value decreases with increase in high pass filter frequency. The average velocity of the high pass filter frequency of 3000 Hz is -0.0059 m/s. Figure C.4 to C.9 shows the velocity signal filtered at different frequencies. Figure C.8, shows that using a high pass filter at 3000 Hz, completely removes the DC shift from the signal. High pass filtering the

acceleration signal at 3000 Hz also agrees well with the PDV signal as shown in Appendix B.

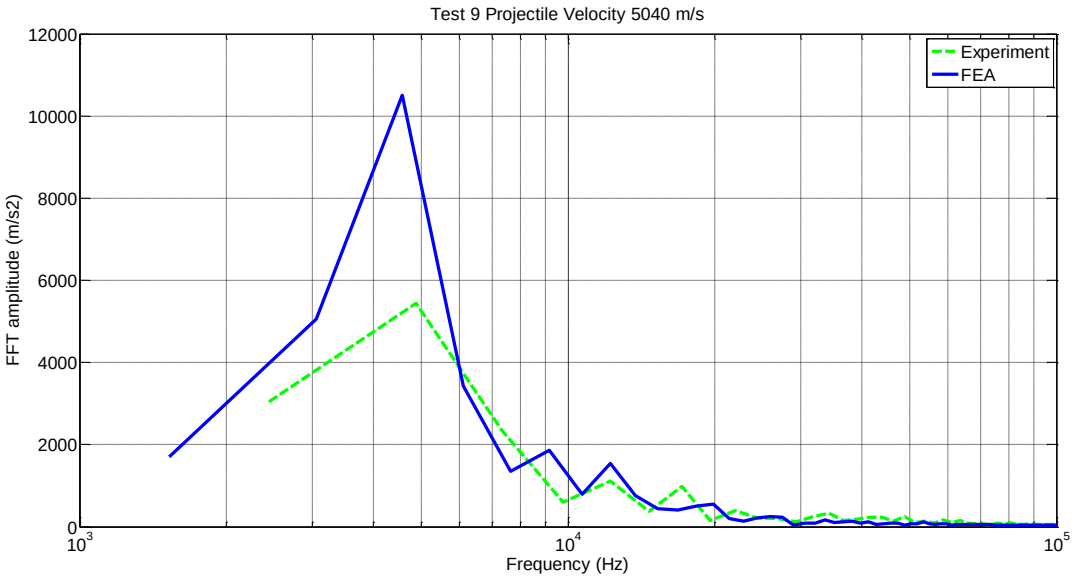

Figure C.3: Typical FFT Signal of Experiment and FEA

Table C.1: Average Velocity

High Pass Filtering Frequency (Hz)	Average Velocity (m/s)
0	-91.13
50	-47.26
500	-0.94
1000	-0.21
2000	-0.0415
3000	-0.0059

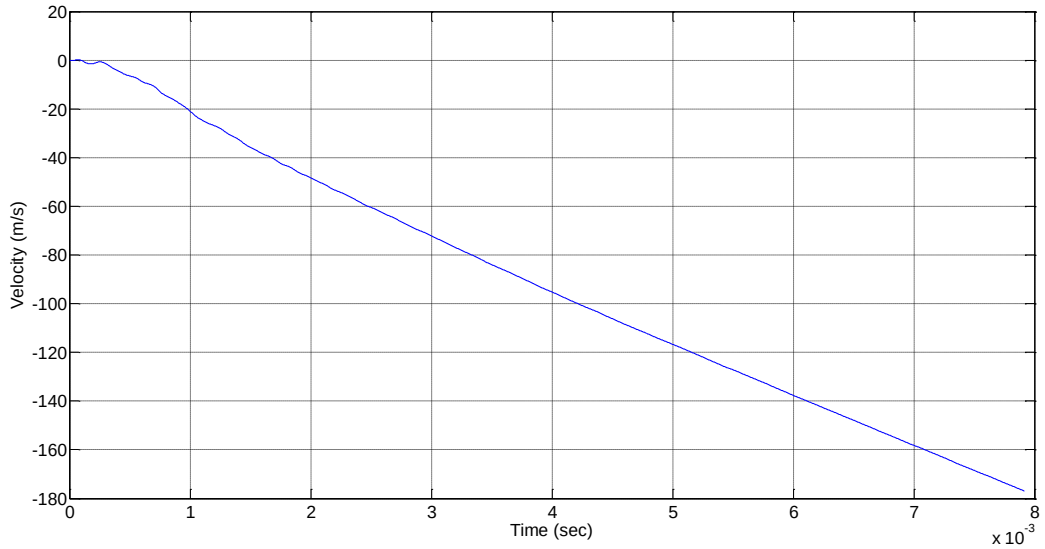

Figure C.4: Typical Velocity Signal Filtered from 0Hz to 10,000Hz

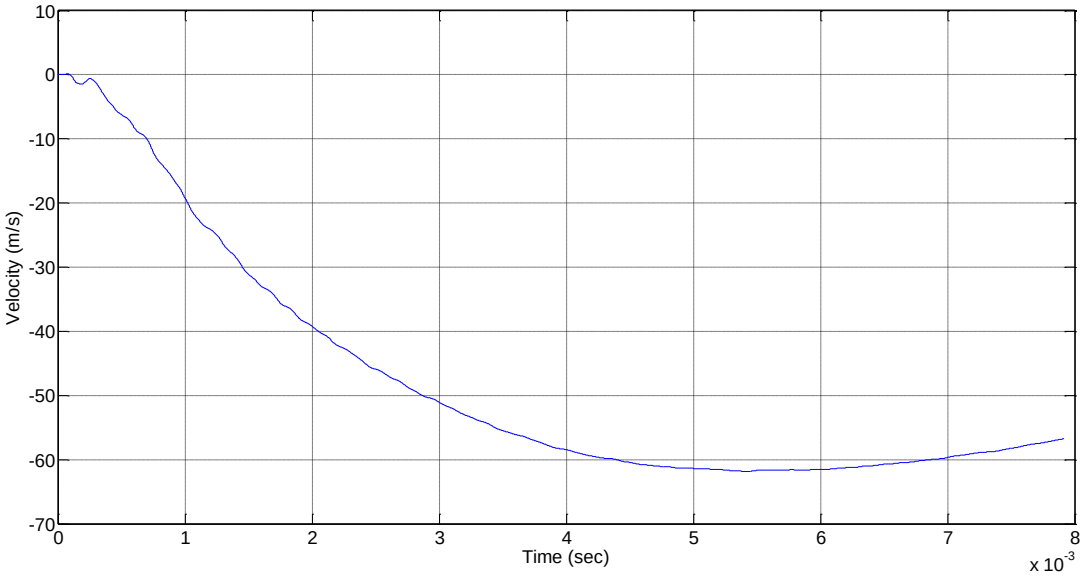

Figure C.5: Typical Velocity Signal Filtered from 50Hz to 10,000Hz

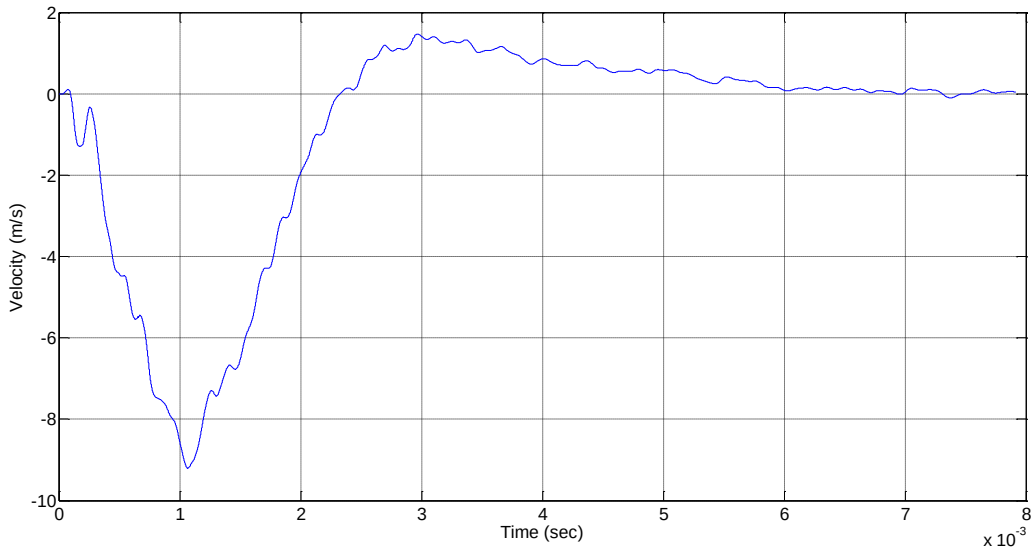

Figure C.5: Typical Velocity Signal Filtered from 500Hz to 10,000Hz

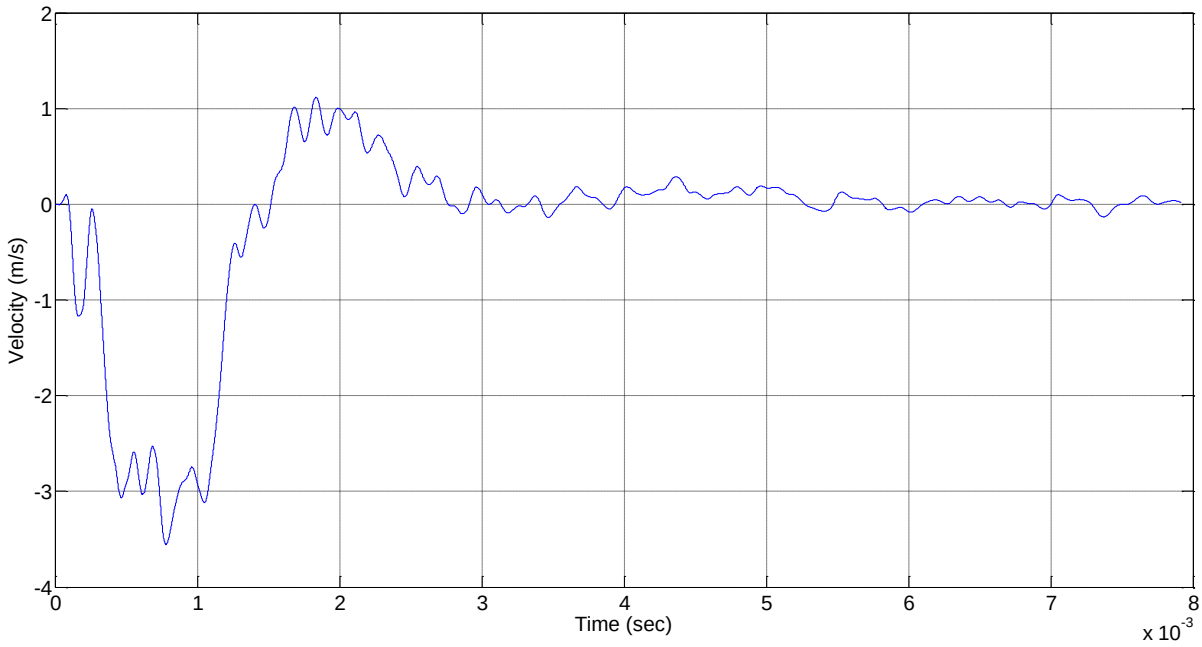

Figure C.7: Typical Velocity Signal Filtered from 1000Hz to 10,000Hz

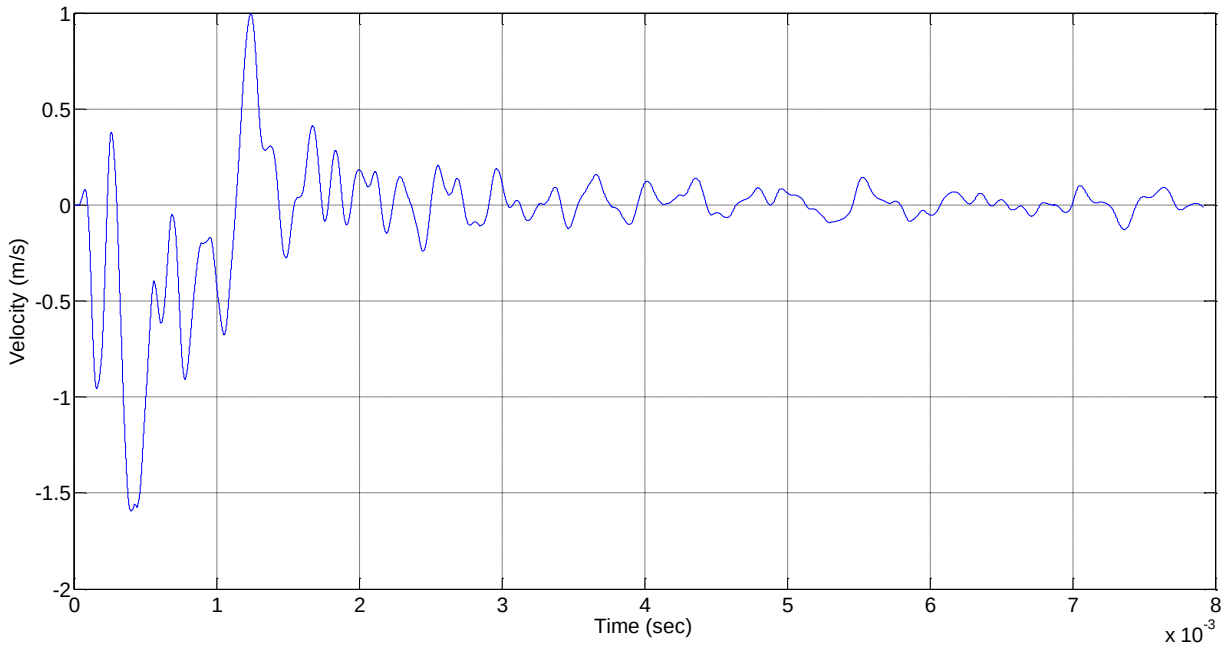

Figure C.8: Typical Velocity Signal Filtered from 2000Hz to 10,000Hz

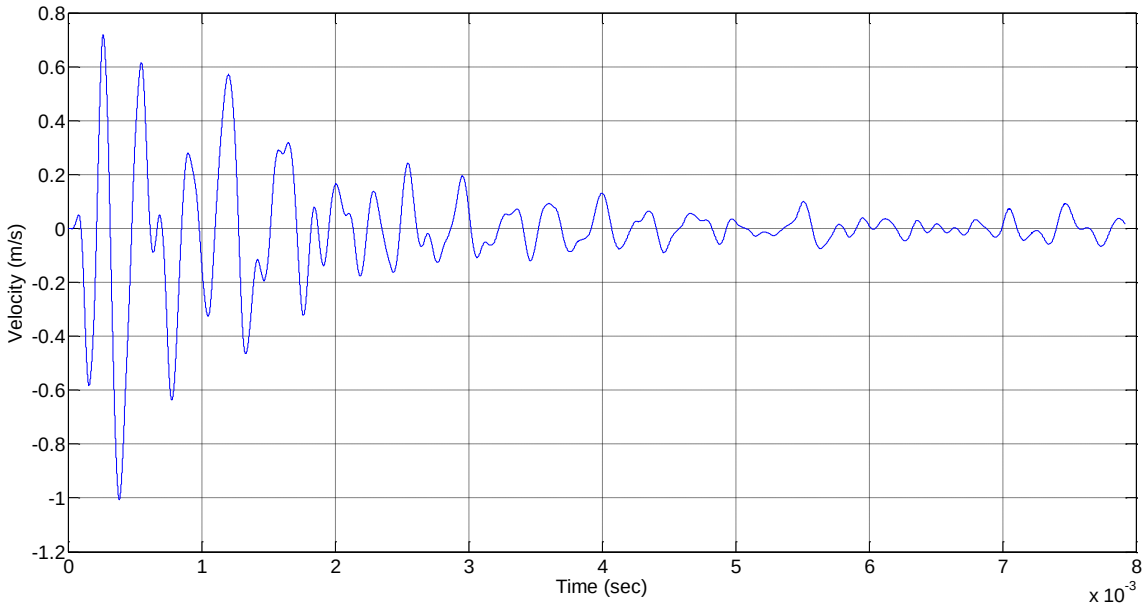

Figure C.9: Typical Velocity Signal Filtered from 3000Hz to 10,000Hz

APPENDIX D

SAMPLE FFT AND FILTERING CODE IN MATLAB

```
% Acc is the acceleration data.

        sampfreq_S1= 10*10^6; % Sampling rate
        pointnum_S1= 16384;
        % Or any number. Better if it is 2^n where n is an integer
        freq_S1= (0:pointnum_S1-1)/pointnum_S1*sampfreq_S1;

% Applying FFT
        IH_S1=fft(Acc(1:1+pointnum_S1-1,1),pointnum_S1)/pointnum_S1;

% Plotting frequency data
        figure('position',[50 100 1200 700]);
        semilogx(freq_S1(1:Number2),abs(IH_S1(1: Number2)),'r- ','linewidth',2);hold
on;
        % Number2 should be less than half of pointnum

% Filtering
        %Shifting the data to remove zero shift
        % 1 to 1801 is the idle region, where acceleration is zero.
        shift = Acc(1:1801);
        ad = mean(shift);
        Shift_Acc = Acc-ad;

% Filtering the shifted data
        [c_S1,d_S1] = butter(1,[filtering frequency/Sampling rate, 'bandpass');
        filtered_Acc = filter(c_S1,d_S1, Shift_Acc);
```

Where, filtered_Acc is the filtered acceleration of the data.

APPENDIX E

SAMPLE SRS CODE IN MATLAB

```
% t and y are time and acceleration data respectively
% dt and sr are the time step and sampling rate respectively

        fn(1) = 10;        % Minimum frequency
        damp = 0.05;    % Damping ratio of 5% applied
         tmx = max(t);
         tmi = min(t);
         tmax = (tmx- tmi) + 1./fn(1);
        limit = round( tmax/dt );
        n=limit;
        yy=zeros(1,limit);
        for i=1:length(y)
                yy(i)=y(i);
        end

        for j=1:1000
%
                omega=2.*pi*fn(j);
                omegad=omega*sqrt(1.-(damp^2));
                cosd=cos(omegad*dt);
                sind=sin(omegad*dt);
                domegadt=damp*omega*dt;
%
                 if(ialgorithm==1)
                        a1(j)=2.*exp(-domegadt)*cosd;
                        a2(j)=-exp(-2.*domegadt);
                         b1(j)=2.*domegadt;
                        b2(j)=omega*dt*exp(-domegadt);
                        b2(j)=b2(j)*( (omega/omegad)*(1.-2.*(damp^2))*sind -
2.*damp*cosd );
                        b3(j)=0;
%
                else
                        E=exp(-damp*omega*dt);
                        K=omegad*dt;
                        C=E*cos(K);
                        S=E*sin(K);
                        Sp=S/K;
%
                        a1(j)=2*C;
```

```
                a2(j)=-E^2;
                b1(j)=1.-Sp;
                b2(j)=2.*(Sp-C);
                b3(j)=E^2-Sp;
        end
        forward=[ b1(j),  b2(j),  b3(j) ];
        back   =[     1, -a1(j), -a2(j) ];
%
        resp=filter(forward,back,yy);
%
        x_pos(j)= max(resp);
        x_neg(j)= min(resp);
%
        jnum=j;
        if  fn(j) > sr/8.
                break
        end
        fn(j+1)=fn(1)*(2. ^ (j*(1./12.)));
end


if max( abs(x_neg) ) > srs_max
        srs_max = max( abs(x_neg ));
 end
srs_min = min(x_pos);
if min( abs(x_neg) ) < srs_min
        srs_min = min( abs(x_neg ));
 end

  srs_max = max(x_pos);
if max( abs(x_neg) ) > srs_max
        srs_max = max( abs(x_neg ));
end
srs_min = min(x_pos);
if min( abs(x_neg) ) < srs_min
        srs_min = min( abs(x_neg ));
end

figure(1);
plot(fn,x_pos,'-')
ylabel('Peak Accel (m/sec^2)');
xlabel('Natural Frequency (Hz)');
set(gca,'MinorGridLineStyle','none','GridLineStyle',':','XScale','log','YScale','log');
ymax= 10^(round(log10(srs_max)+2));
```

```
        ymin= 10^(round(log10(srs_min)-0.6));
        fmax=max(fn);
        fmin=fmax/10.;
%
        fmax= 10^(round(log10(fmax)+0.5));

        if  fn(1) >= 0.1
                fmin=0.1;
         end
         if  fn(1) >= 1
                fmin=1;
         end
         if  fn(1) >= 10
                fmin=10;
        end
        if  fn(1) >= 100
                fmin=100;
        end
        L2k_x = [10000,10000,10000];
        L2k_y = [0.01,ymax/2,ymax];
        hold on; loglog(L2k_x,L2k_y,'-r');
        axis([1000,fmax,ymin,ymax]);
```

APPENDIX F

INSTRON DYNATUP 8250 OPERATION PROCEDURE

1. Attach the desired weight set to the crosshead.
2. Set the control pendent switches to AUTO GRAV and, if a pneumatic clamp is installed, set the clamp ON/OFF switch to ON. When the AUTO switch is pressed, the crosshead automatically rises to the height determined by the magnetic switch. Set the pneumatic assist air pressure using the regulator on the top of the rear motor enclosure.
3. Remove any tools, other foreign objects, and the safety “H” bar from the enclosure and close the doors. The “ARM” button illuminates.
4. Press and hold the “ARM” button. The audible alarm sounds while still holding the ARM button, press the “FIRE” button. The latch hook opens allowing the crosshead to fall and strike the specimen.
5. The latch assembly automatically retrieves the crosshead and raises it back to the height of the magnetic switch.
6. Insert safety “H” bar.
7. Remove the specimen.

APPENDIX G

PROPERTIES OF LOAD CELL AND DROP WEIGHT TOWER EVALUATION

PCB load cell Model: 200M50 is positioned on the drop weight tower as shown in Figure G.1. The specifications of the load cell are listed in Table G.1.The load cell is securely connected to the base of the machine using a ¼- 28 screw. The drop weight tower equipment in turn is secured to the floor. The load cell and the drop weight tower act as a huge spring, so it is necessary to calculate the stiffness of the load cell and drop weight tower.

Table G.1: PCB load cell Model: 200M50 Specification

Sensitivity (± 15%)	22.48 mV/KN
Measurement Range	222.40 KN
Maximum Static Force	333.60 KN
Diameter	53.90 mm
Height	19.00 mm
Electrical Connector	10- 32 Coaxial Connector
Mounting Thread	¼ - 28 Thread

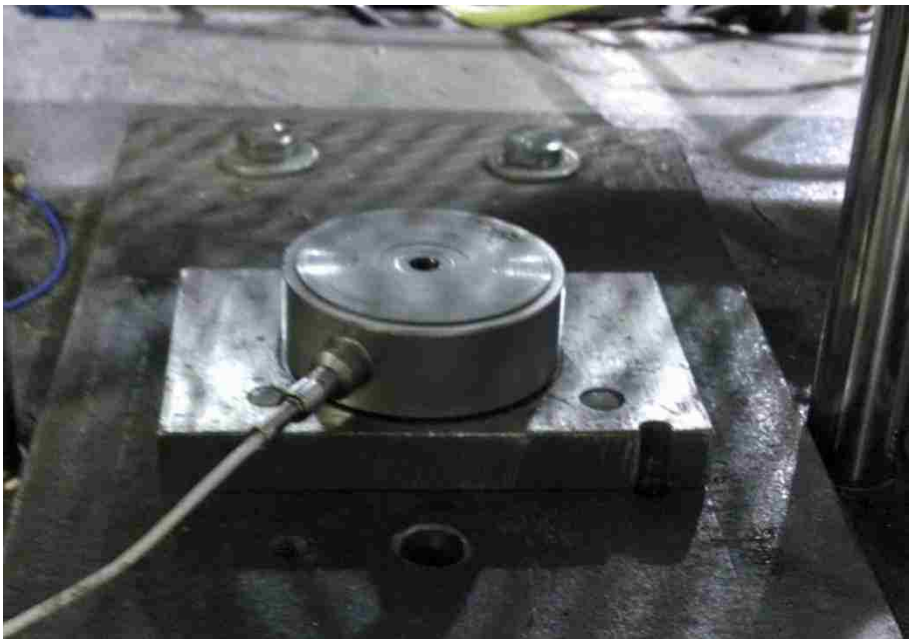

Figure G.1: PCB Load Cell

The stiffness of the load cell combined with drop weight tower can be calculated using the frequency of the vibration. To calculate the frequency of vibration, a simple cylindrical steel specimen with 0.026m radius and 0.099m length, as show in Figure G.2, is used. The cylinder has the same dimension as the load cell. The steel cylinder is attached to the load cell through a ¼- 28 thread. The steel cylinder is impacted on the top with a hammer and the acceleration is measured using a PCB 352C22 accelerometer attached to the cylinder as shown in Figure G.3.

Figure G.2: Steel Cylinder

Figure G.3: Steel Cylinder with Accelerometer

A typical unfiltered acceleration signal is shown in Figure G.4. The acceleration results are low pass filtered at 10,000 Hz, since the acceleration has a range of 0.35 Hz to 10,000 Hz. The results are shown in Figure G.5.

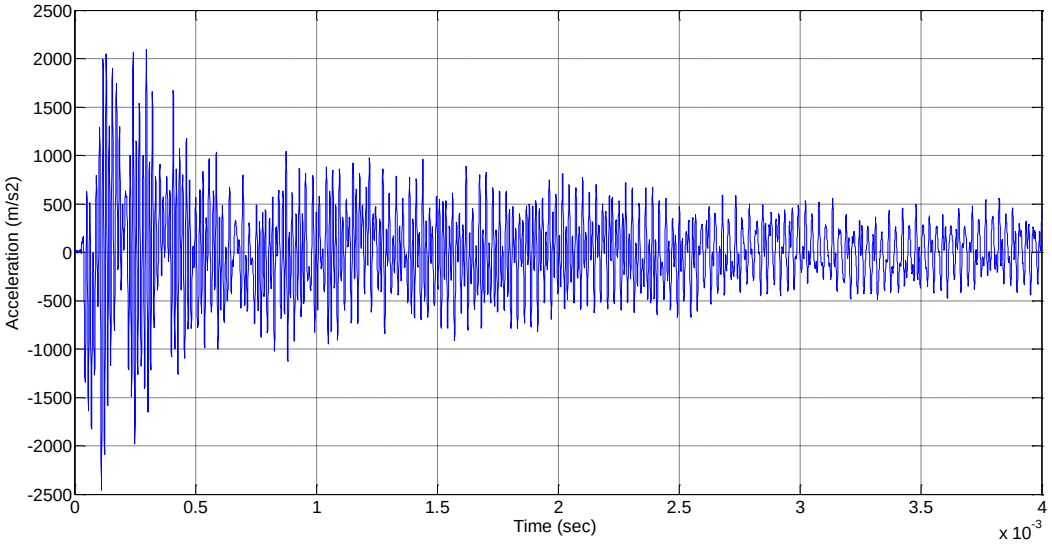

Figure G.4: Typical Unfiltered Acceleration

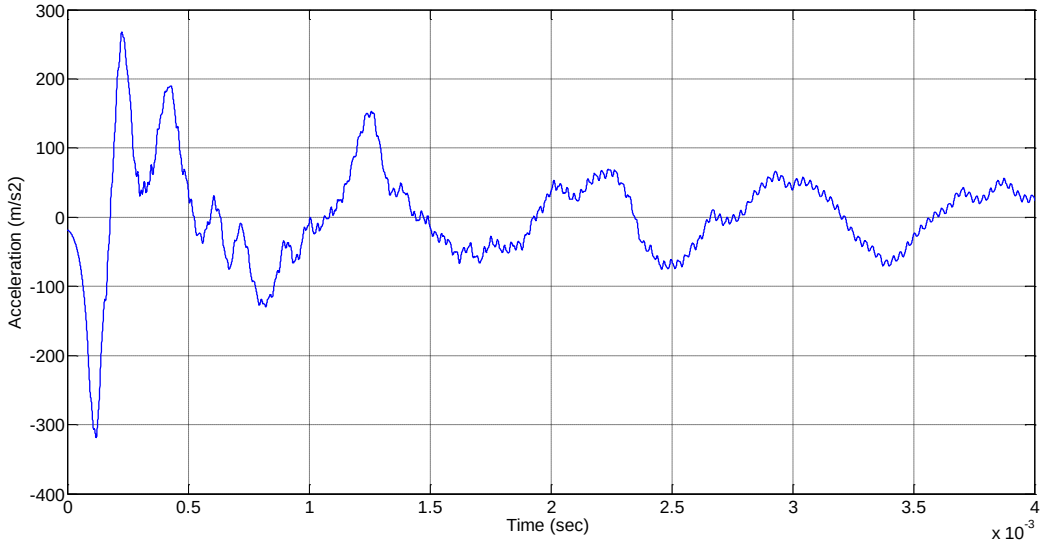

Figure G.5: Typical Filtered Acceleration

Frequency of vibration was found using FFT analysis on acceleration signal, as explained in Chapter 6. The results are shown in Figure G.6. The frequency obtained from the plot is 1221 Hz. This frequency corresponds to combined frequency of steel cylinder, load cell and drop weight tower.

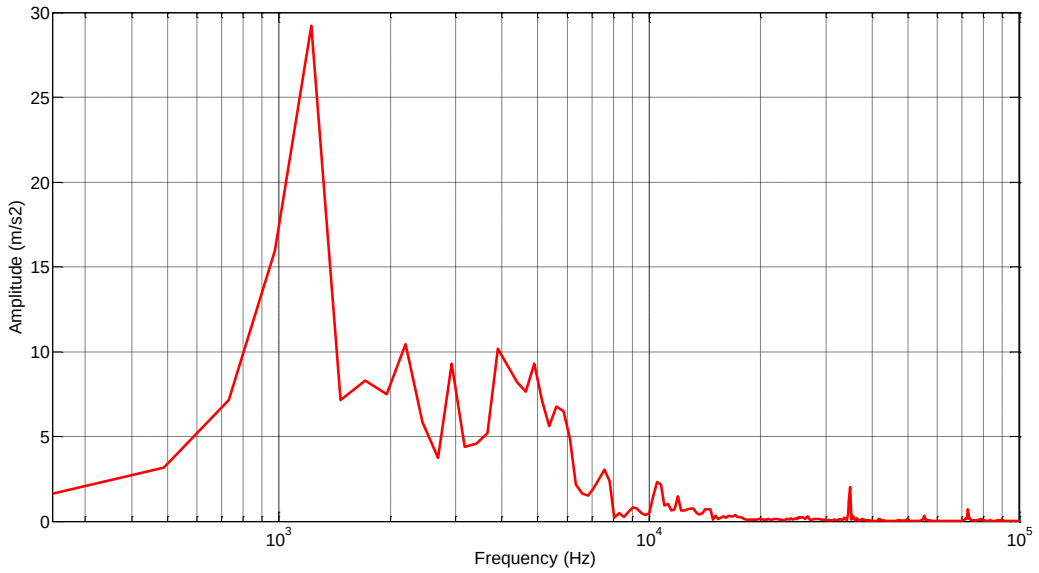

Figure G.6: FFT of Acceleration Signal

Knowing the combined frequency of the cylinder and load cell with drop weight tower, the equivalent stiffness can be calculated using the equation given below.

$$\omega = \frac{1}{2\pi}\sqrt{\frac{K}{m}} \qquad \text{(G.1)}$$

where ω is the frequency in Hz,

K is the stiffness

$m = m_{load\ cell} + m_{Cylinder}$

$$m = m_{\text{load cell}} + m_{\text{cylinder}} = (\pi r^2 h \rho) + (\pi r^2 h \rho) = (\pi * 0.0269^2 * 0.019 * 7850) + (\pi * 0.0269^2 * 0.099 * 7850) = 2.14 \text{ kg}$$

From equation E.1, the stiffness can is calculated as shown below

$$K_{eq} = 4 \omega^2 \pi^2 m = 1.26 \text{ E8 N/m} \quad \text{(G.2)}$$

Cylinder, load cell and the drop weight tower can be considered as spring in the series and can be represented as equivalent spring as shown in the Figure G.7.

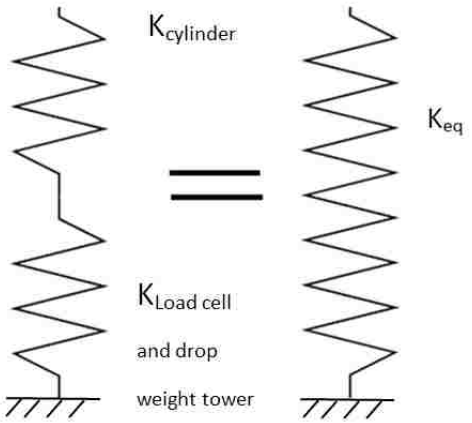

Figure G.7: Springs in Series

The stiffness of the equivalent spring is shown in equation below.

$$\frac{1}{K_{eq}} = \frac{1}{K_{\text{cylinder}}} + \frac{1}{K_{\text{Load cell+drop tower}}} \quad \text{(G.3)}$$

Stiffness of the steel cylinder is calculated as shown below

$$K_{\text{cylinder}} = \frac{AE}{L} = 4.45\text{E9 N/m} \quad \text{(G.4)}$$

where K_{cylinder} is the stiffness of the cylinder

A is the cross section area of the cylinder

E is Youngs modulus (2 E11 N/m^2)

L is the length (0.099m)

Knowing the stiffness of the cylinder and equivalent stiffness, the stiffness of the load cell and drop weight tower is calculated as 1.297 E8 N/m using equation G.3. And from the calculated stiffness of the load cell and drop weight tower, combined modulus is calculated from equation G.4. The Young's modulus of load cell and drop weight tower is calculated as 1.08E9 N/m^2. Load cell material property used for this model is given in Table G.2.

Table G.2: Calculated Material Properties of Load cell

Parameter	Structural Steel
Density (Kg/m^3)	7850
Combined Young's Modulus (GPa)	1.08
Poisson's Ratio	0.3
Yield Strength (MPa)	750
Tangent Modulus (GPa)	10

G.2 Damping Ratio Calculation

There are extensive amount of literature concerning the theory of structural dynamics that cannot be reviewed within the scope of this dissertation. However, the

research in this area yielded different methods to study the structural dynamics of a system as listed below.

1. Time Domain Analysis

- Logarithmic Decrement Analysis [59].
- Hilbert Transform Analysis [60].

2. Frequency Domain Analysis

- Moving Block Analysis [61].
- Half Power Bandwidth [62].

Half Power Bandwidth method, which is most commonly used, and simple method is used for the evaluation of the damping coefficient. Results from the hammer impact on steel cylinder are used in calculating damping ratio using the Half-Power Bandwidth method [62].

Half-Power Bandwidth method is used in frequency domain. The method is based on the observation that the shape of the frequency spectrum is controlled by the amount of damping in the system. Therefore it is possible to estimate the damping ratio from the properties of the frequency curve. Damping ratio is calculated by identifying the two frequencies that neighbor the first natural frequency of the system and whose magnitude is equal to $R_d/\sqrt{2}$, Figure G.8. The damping ratio is calculated according to the following equation:

$$\xi = \frac{f_2 - f_1}{f_2 + f_1} \tag{G.5}$$

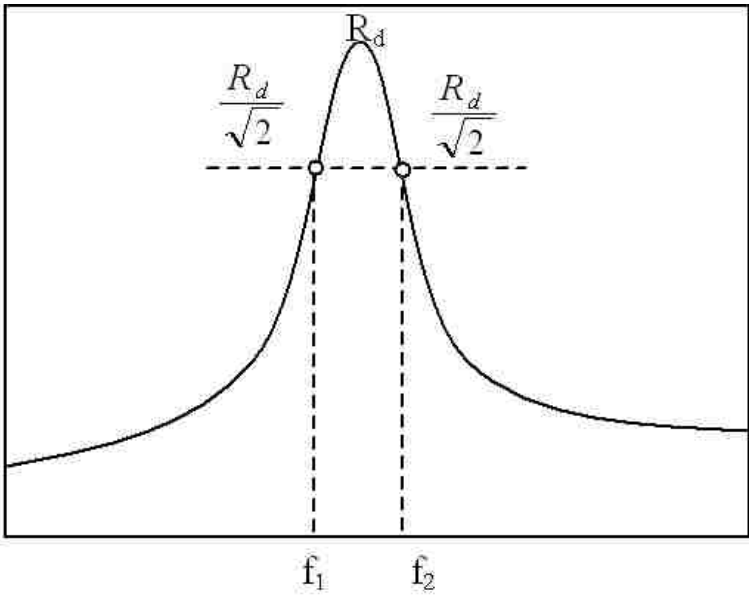

Figure G.8: Half-Power Method to Estimate Damping

The half power band width method is applied to the first natural frequency as shown in Figure G.9. The f_1 and f_2 obtained from the plot are 1066 Hz and 1305 Hz respectively. Using Equation G.5, the damping ratio is calculated as 10.08%.

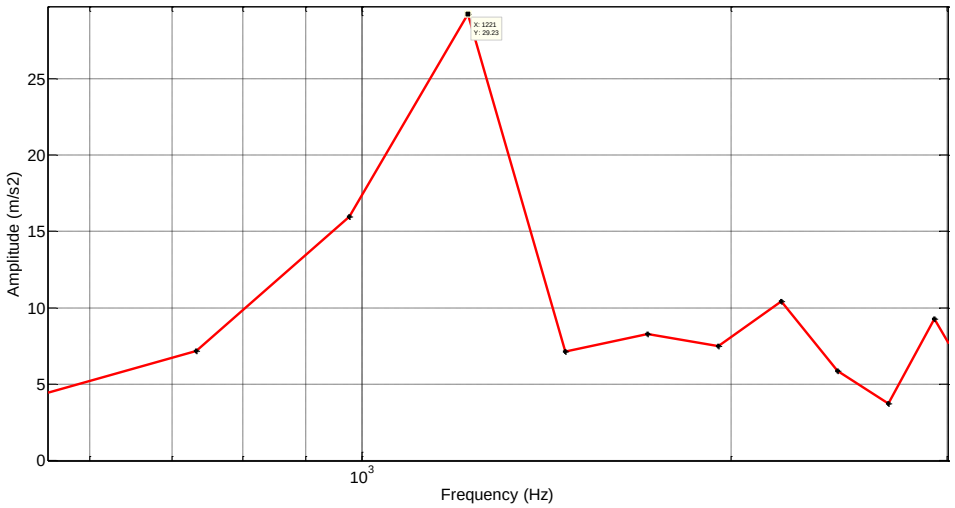

Figure G.9: Frequency Response of Hammer Impact on Steel Cylinder

G.3 Damping in LS-DYNA

The material models used in the LS-DYNA do not support any kind of material damping. Therefore the damping in the FE simulation needs to be externally defined. The FE model describes all kinds of material damping using Rayleigh damping. The Rayleigh damping defines the damping matrix C has

$$C = \alpha M + \beta K \tag{G.6}$$

where, α, β are mass and stiffness damping factor

M is the mass matrix

K is the stiffness matrix.

Therefore the damping matrix will be the linear combination of mass and stiffness matrices. While defining the damping matrix C, either M or K matrix can be used individually or a combination of both. Figure G.10 shows the relation between damping ratio and the frequency for Rayleigh damping. The Rayleigh damping equation can also be written in terms of damping ratio (ξ) as

$$\xi = \frac{\alpha}{2\omega} + \frac{\beta\omega}{2} \tag{G.7}$$

where, ω is the frequency.

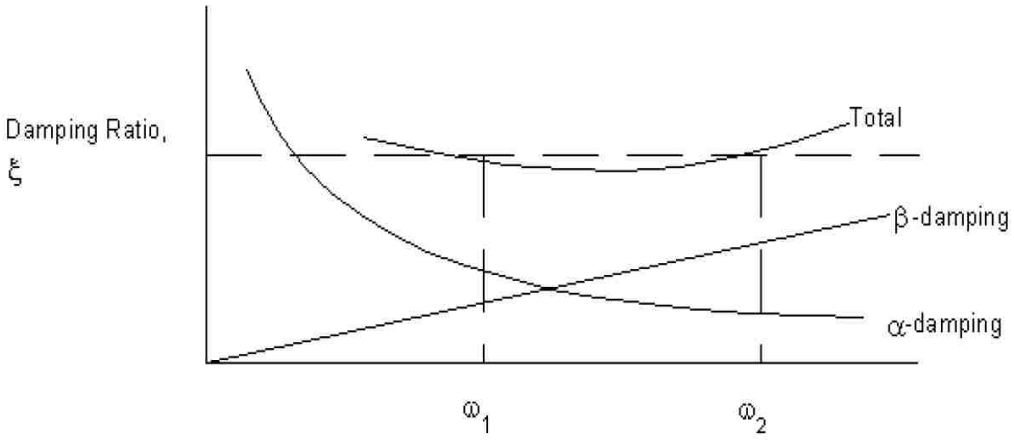

Figure G.10 Rayleigh Damping

Mass proportional damping will damp both the rigid body motion and the vibration in the lower frequency range. The mass proportional damping can be used for the whole structure or for a certain part of the structure. Also it is possible to choose different damping coefficient for different parts in a same structure. Stiffness proportional damping (SPD) is effective for damping high frequencies and is orthogonal to rigid body motion. The mass proportional damping and stiffness proportional damping can be found by solving two equations as shown below:

$$\xi = \frac{\alpha}{2\omega_1} + \frac{\beta\omega_1}{2} = \frac{\alpha}{2\omega_2} + \frac{\beta\omega_2}{2} \qquad \text{(G.8)}$$

By solving these equations, alpha (α) and beta (β) were found to be 289.23 s^{-1} and 7.23E-4 s.

G.4 Validation of Load cell Material Model and Damping Ratio

To validate the material model and damping ratio calculated from previous section, a drop weight experiment was conducted with steel cylinder from a height of 3mm. Acceleration and force signals are recorded using the oscilloscope. The experimental setup is shown in Figure G.11. Experimental parameters are listed in Table G.3. Typical unfiltered, filtered acceleration and force data are shown in Figure G.12 through G.18.

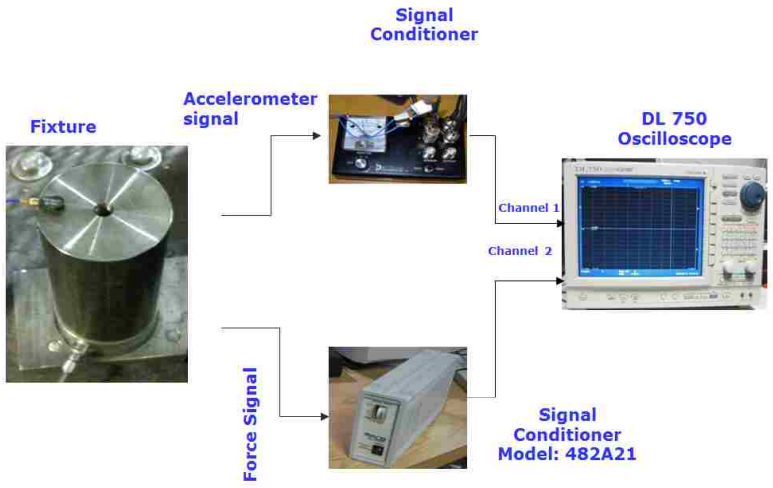

Figure G.11: Experimental Setup

Table G.3: Experimental Parameters

Parameter	Value
Drop Weight	4.5 Kg
Drop Height	3mm
Drop Velocity	0.233 m/s

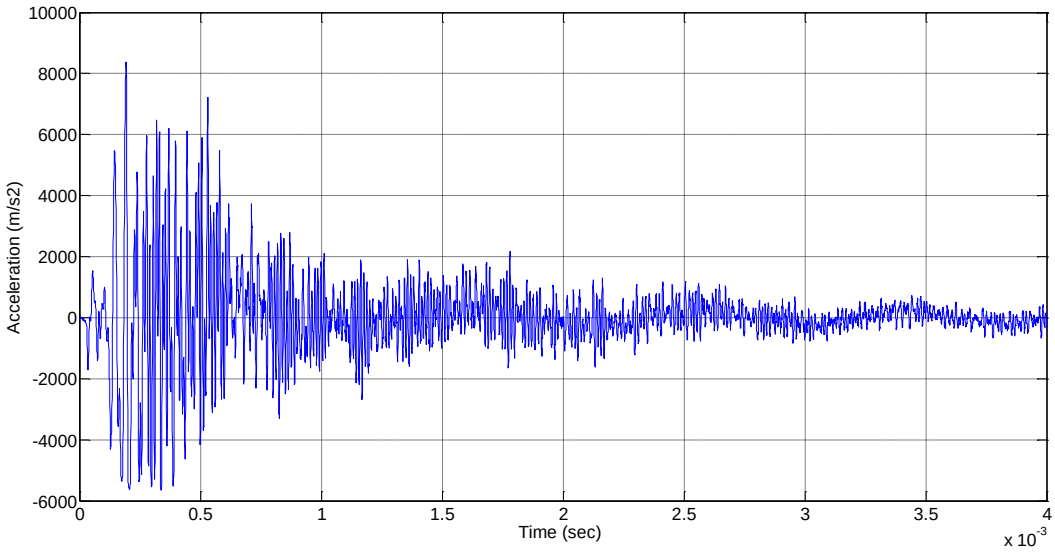

Figure G.12: Unfiltered Acceleration Data

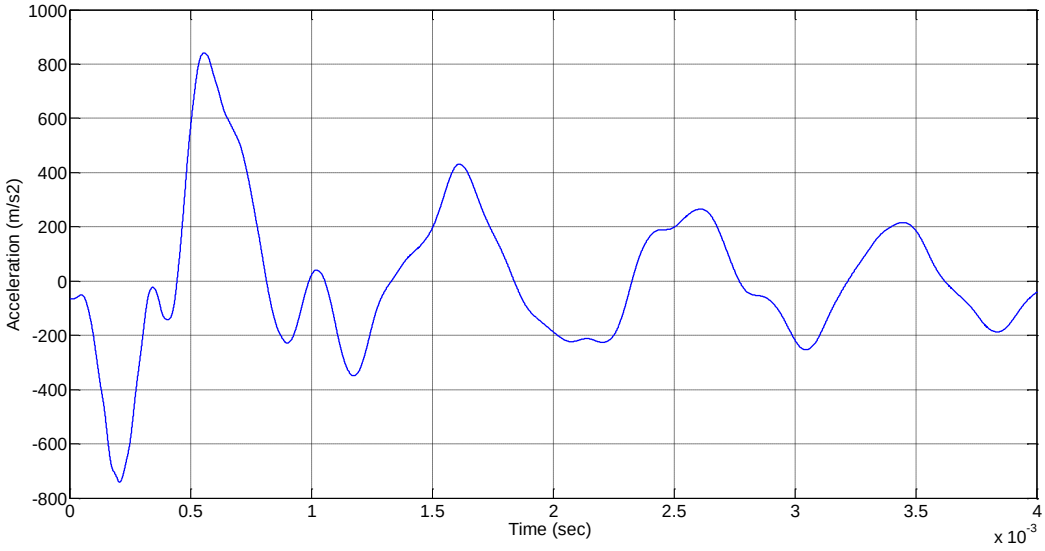

Figure G.13: Filtered Acceleration Data

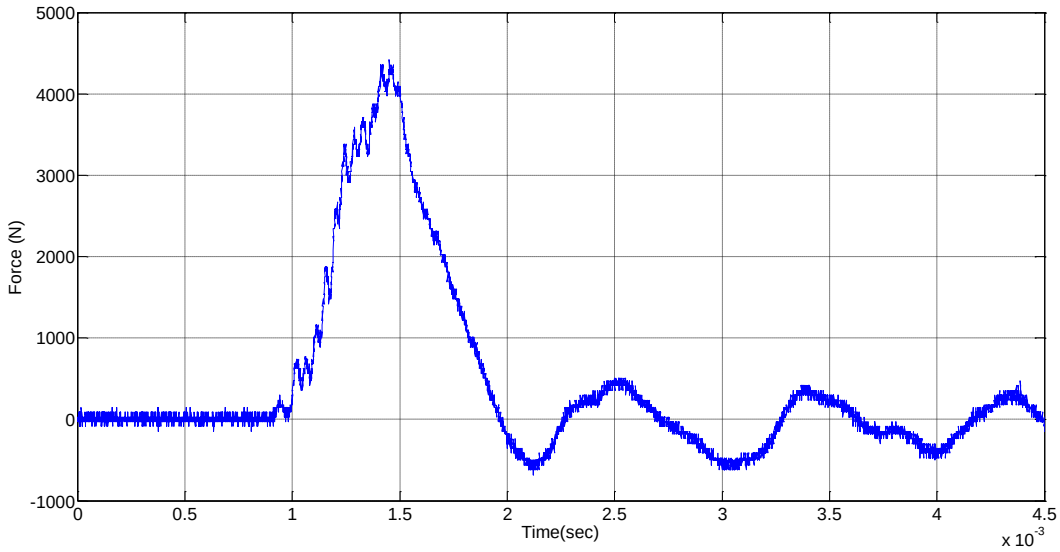

Figure G.14: Force Signal

The FEA model has three main components: drop weight mechanism, load cell and steel cylinder. The model was created in Solid Works as shown in Figure G.15. The Solid Works model was imported into ANSYS- WorkBench for meshing. The meshed model is shown in Figure G.16. An input file (.k) of the whole setup was created from ANSYS WorkBench.

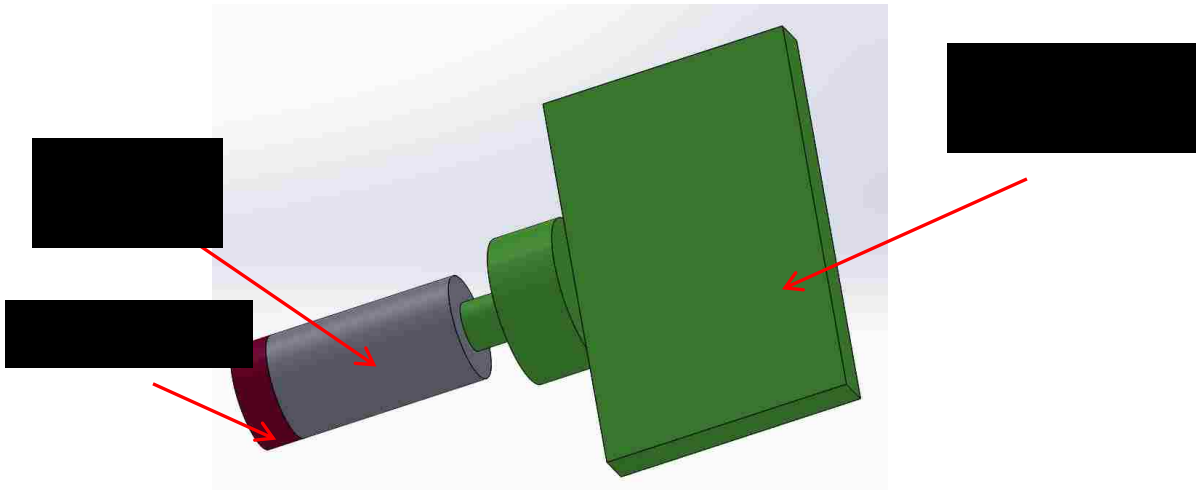

Figure G.15: Solid Works Model

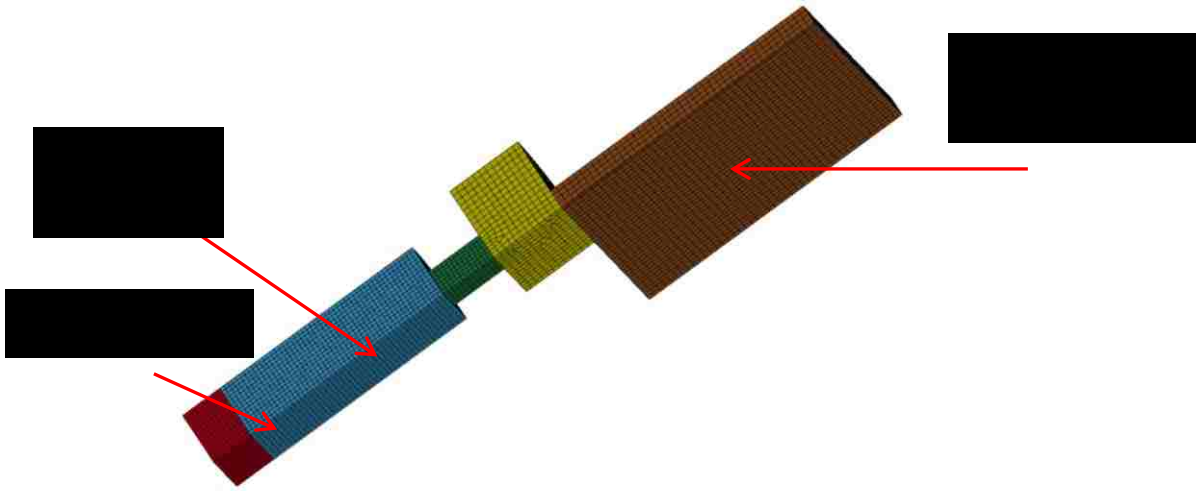

Figure G.16: Meshed Geometry of Fixture

The acceleration and force signals are outputted as explained in previous sections. An initial velocity of 0.233 m/s is applied to drop weight mechanism. Figure g.17 through G.19 shows the comparison of acceleration, force and FFT between experiment and simulation respectively.

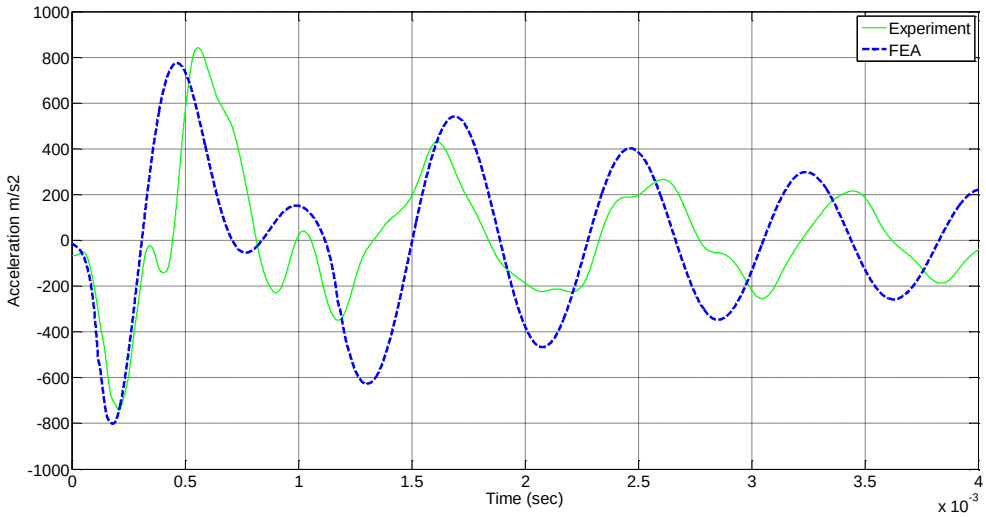

Figure G.17: Acceleration Comparison

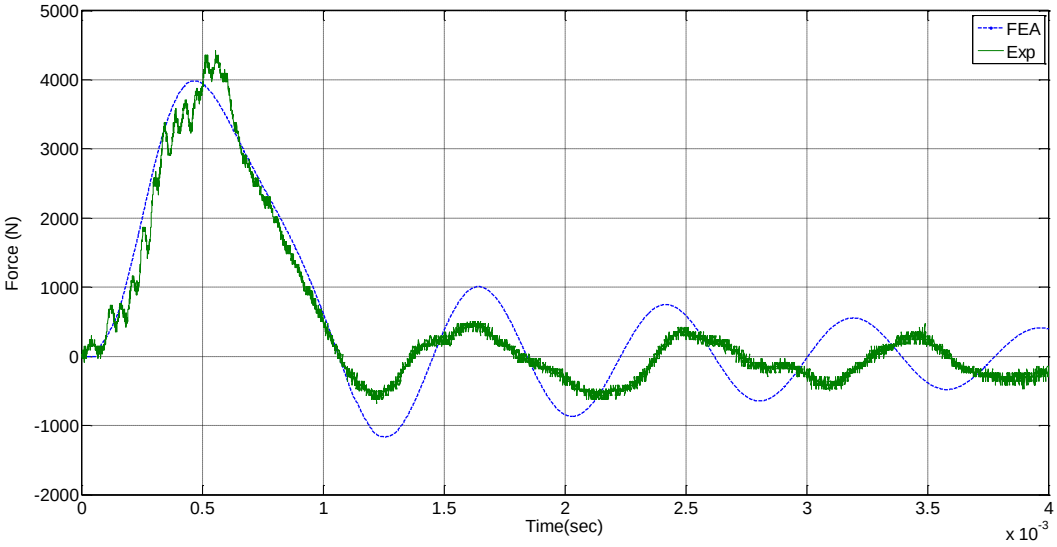

Figure G.18: Force Comparison

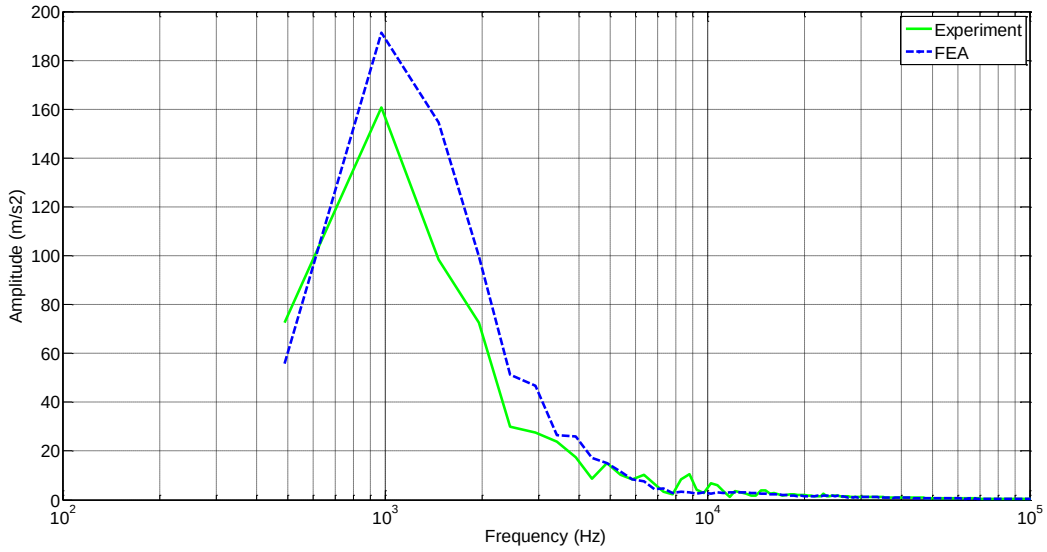

Figure G.19: FFT Comparison

Figure G.18 shows that the FEA is able to simulate the experiment; however the simulation starts to deviate after 1.0ms of impact. This can be attributed to the complexity of the drop tower itself. The force signal from 0 to 1ms is the impact force

and the rest of the force signal is from the impact wave being reflected from the base of the drop tower. The reflected wave would travel through complex structure and incur additional damping. So it would be safe to consider only 2ms of impact and neglect the rest of the signal.

REFERENCES

[1] M. R. Bahaari, A. N. Sherbourne, Structural Behavior of End-Plate Bolted Connections to Stiffened Columns, Journal of Structural Engineering, 122(1996), No 8, 926-935.

[2] S. H. Ju, C.Y. Fan, G.H. Wu, Three-Dimensional Finite Elements of Steel Bolted Connection, Engineering Structures, 26 (2004), 403-413.

[3] Y.I. Maggi, R. M. Goncalves, R.T. Leon and L. F. L. Ribeiro, Parametric Analysis of Steel Bolted End Plate Connections Using Finite Element Modeling, Journal of Constructional Steel Research, 61 (2005) 689-708.

[4] S. Mattern, K. Schweizerhof, Wave Propagation in Automotive Structures Induced by Impact Events, High Performance Computing in Science and Engineering ’06 (2007), 459-470.

[5] L. Gaul, J. Lenz, Nonlinear Dynamics Of Structures Assembled By Bolted Joints, Acta Mechanica, 125 (1997), 169-181.

[6] H. R. Kess, N. J. Rosnow, B. C. Sidle, Effects of Bearing Surfaces on Lap Joint Energy Dissipation, Proceedings of International Modal Analysis Conference (IMAC)-XX, Los Angeles, CA, United States (2002), 603-610.

[7] D. W. Lobitz, D. L. Gregory, D. O. Smallwood, Comparison of Finite Element Predictions to Measurements from the Sandia Microslip Experiment, Proceedings of International Modal Analysis Conference (IMAC)-XIX, Kissimmee, FL, United States, 2 (2001), 1388-1394.

[8] J. D. Reid, N. R. Hiser, Detailed Modeling of Bolted Joints with Slippage, Finite Elements in Analysis and Design, 41 (2005), 547-562.

[9] J. Kim, J. C. Yoon, B. S. Kang, Finite Element Analysis and Modeling of Structure with Bolted Joints, Applied Mathematical Modeling,31 (2007), 895–911.

[10] L. Gaul, R. Nitsche, The Role of Friction on Mechanical Joints, Applied Mechanics Reviews, 54 (2001), 93-106.

[11] A. Eskandarian, D. Marzougui, N. E. Bedewi, Impact finite-Element Analysis of Slip-Base Sign Support Mechanism, Journal of Transportation Engineering, 126 (2000), 143-153.

[12] H. Wentzel, M. Olsson, Mechanisms of Dissipation in Frictional Joints - Influence of Sharp Contact Edges and Plastic Deformation, Wear 26 (2008), 1814-1833

[13] S. U. Park, M. R. Koka, K. R. Thomson, J. L. Robbins, A FE Modeling and Validation of Vehicle Rubber Mount Preloading and Impact Response, 8th International LS-DYNA Users Conference, Crash/Safety, Dearborn, MI, USA, 5(2004), 23-32.

[14] K. Schiffner, C. Droste, Simulation of Prestressed Screw Joints in Complex Structures", Computers and Structures, 64 (1997), No 5/6, 995-1003.

[15] E. Esmailzadeh, M. Chorashi, A. R. Ohadi, Analysis of Preloaded Bolted Joints Under Exponentially Decaying Pressure, Journal of Pressure Vessel Technology, Transactions of the ASME, 118 (1996), 393-398.

[16] T. A. Duffey, B. B. Lewis, S. M. Bowers, Bolt Preload Selection for Pulse- Loaded Vessel Closures, Proceedings of the Joint ASME/JSME Pressure Vessels and Piping Conference, Honolulu, HI, United States, 301 (1995), 167-174.

[17] T. A. Duffey, Optimum Bolt Preload for Dynamic Loading International Journal of Mechanical Sciences, 35 (1993), No 3-4, 257-265.

[18] D. F. Pilkey, G. Park, D. J. Inman, Damping Matrix Identification and Experimental Verification, Proceedings of SPIE on Passive Damping and Isolation - The International Society for Optical Engineering, 3672 (1999), 350-357.

[19] B. O'Toole, K. K. Nakalswamy, M. Feghhi, Experimental and Finite Element Analysis of Preloaded Bolted Joints Under Impact Loading, Presented at 47th AIAA/ASME/ASCE/AHS/ASC Structures, Structural Dynamics, and Materials Conference, Newport, RI, United States, 3 (2006), 2024-2032.

[20] E. Kerekes, B. Szabo, B. Unger, Prestressed Bolt Joints Under Dynamical Load, Presented at 6th Mini Conference on Vehicle System Dynamics, Identification and Anomalies, Budapest, Hungary, (1998), 545-555.

[21] C. J. Hartwigsen, Y. Song, D. M. McFarland, L. A. Bergman, A. F. Vakakis, Experimental Study of Non-Linear Effects in a Typical Shear Lap joint Configuration, Journal of Sound and Vibration, 277 (2004), 327-351.

[22] Y. Songa, C. J. Hartwigsenb, D. M. McFarlanda, A. F. Vakakisb, L. A. Bergman, Simulation of Dynamics of Beam Structures with Bolted Joints Using Adjusted Iwan Beam Elements, Journal of Sound and Vibration, 273 (2004) 249–276.

[23] M. Feghhi, Experimental and Finite Element Studies of Shock Transmission through Bolted Joints, PhD. Dissertation, University of Nevada, Las Vegas, United States, 2007.

[24] K. K. Nakalswamy, Experimental and Numerical Analysis of Structures With Bolted Joints Subjected to Impact Load PhD. Dissertation, University of Nevada, Las Vegas, United States, 2010.

[25] W. H. Semke, G. D. Bibel, S. Jerath, S. B. Gurav, A. L. Webster, A Dynamic Investigation of Piping Systems with a Bolted Flange, Presented at Design and Analysis of Piping, Vessels and Components (2002 ASME Pressure Vessels and Piping Conference), Vancouver, BC, Canada, 440 (2002), 121-128.

[26] Y. D. Kwon, H. W. Kwon, J. H. Hwangbo, S. H. Jang, Finite Element Modeling for Static and Dynamic Analysis of Structures with Bolted Joint, Key Engineering Materials, 306 (2006), 547-552.

[27] H. G. Hopkins, H. Kolsky, Mechanics of Hypervelocity Impact of Solids, Proceedings of the 4th Hypervelocity Impact Symposium APGC-TR-60, 39 (1960).

[28] R.F. Rolsten, H. Hunt, Phenomena Resulting from Hypervelocity Impact, Journal of Spacecraft, 2 (1965), No 1, 38–43.

[29] C. J. Maiden, A. R. McMillan, An Investigation of the Protection Afforded a Spacecraft by a Thin Shield. AIAA Journal, 2 (1964), No 11, 1992–1998.

[30] J. S. Wilbeck, Impact Behavior of Low Strength Projectiles, No. AFML-TR-77-134. Air Force Materials Lab Wright-Patterson AFB OH, 1978.

[31] http://www.physicsapplications.com/

[32] M. J. Burchell, M. J. Cole, J. M. M McDonnel, J. C Zarnecki, Hypervelocity Impact Studies using the 2 MV Van de Graaff Accelerator and Two-Stage Light Gas Gun of

the University of Kent at Canterbury, Journal of Measurement Science and Technology, 10 (1999), 41-50.

[33] A.E. Seigel, Theory of High Speed Guns, No. AGARDOGRAPH-91. Advisory Group for Aerospace Research and Development Neuilly-Sur-Seine (France), 1965.

[34] R. E. Bergrren, R. M. Reynolds, The Light-Gas Gun Model Launcher, Ballistic Range Technologies, AGARDograph 138 (1970), 11-94

[35] L. A. Glenn, Shock waves in Condensed Matter – 1987, edited by S. C. Schmidt, N.C.Holmes, Elsevoir, (1988), 653.

[36] Dytran Intruments, Product Manual,http://www.dytran.com/img/products/3200B.pdf"

[37] Dytran, Product Manual, www.dytran.com

[38] Halloquist, J.O, LS-DYNA Version 970 Keyword user's Manual, Livermore Software Technology Corporation CA, 2007

[39] Halloquist, J.O, LS-DYNA Theoretical Manual, Livermore Software Technology Corporation CA, 2007

[40] C. Hayhurst, R. Clegg, Cylindrically Symmetric SPH Simulations of Hypervelocity Impacts on Thin Plates, International Journal of Impact Engineering; 20 (1997), No 1-5, 337-348

[41] L. E. Schwer, Aluminum Plate Perforation: A Comparative Study using Lagrange with Erosion, Multi-Material ALE, and Smooth Particle Hydrodynamics, 7th European LS-DYNA Conference, Stuttgart, Austria, 2009.

[42] M. Faraud, R. Destefanis, D. Palmieri, M. Marchetti, SPH Simulations of Debris Using Two Different Computer Codes, International Journal of Impact Engineering, 23 (1999), 249-260

[43] K. E. Jackson, Y. T. Fuchs, Comparison of ALE and SPH Simulations of Vertical Drop Tests of a Composite Fuselage Section into Water, 10th International LS-DYNA Users Conference, Michigan, USA, 2008

[44] J. A. Zukas, Some Common Problems in the Numerical Modeling of Impact Phenomena. Computing Systems in Engineering, 4 (1993), No 1, 43–58.

[45] G. R. Johnson, W. H. Cook, Fracture Characteristics of Three Metals Subjected to Various Strains, Strain Rates, Temperatures and Pressures. Engineering Fracture Mechanics, 21 (1985), No 1, 31–48.

[46] F. J. Zerilli, R. W. Armstrong, Dislocation-Mechanics-Based Constitutive Relations for Material Dynamics Calculations, Journal of Applied Physics, 61 (1987), 1816– 1825.

[47] D. J. Littlewood, Simulation of Dynamic Fracture using Peridynamics, Finite Element Modeling, and Contact, Proceedings of the ASME 2010 International Mechanical Engineering Congress and Exposition, Vancouver, Canada, 2010

[48] J. D. Seidt, A. Gilat, J. A. Klein, J. R. Leach, High Strain Rate, High Temperature Constitutive and Failure Models for EOD Impact Scenarios, Proceedings of the 2007 SEM Annual Conference and Exposition on Experimental and Applied Mechanics, Springfield, MA, June, 2007

[49] M. E. Backman, W. Goldsmith, The Mechanism of Penetration of Projectiles Into Target, International Journal of Engineering Science, 16 (1978), 1-99.

[50] D. J. Steinberg, Equation of State and Strength Properties of Selected Materials, Lawrence Livermore National Laboratory: Livermore, CA, 1996

[51] M. Lambert, J. Fery, X. Garaud, J. Dubois, E. Schneider, The Validation of Hydrocodes for Orbital Debris Impact Simulation, International Conference on Spacecraft Structures and Mechanical Testing, Noordwijk, 1991

[52] T. Elshenawy, Q. M. Li, Influences of Target Strength and Confinement on the Penetration Depth of an Oil Well Perforator, International Journal of Impact Engineering, 54 (2013),130-137.

[53] R. C. Juvinall, K. M. Marshek, Fundamentals of Machine Component Design, Third edition, John Wiley and sons, Inc.

[54] J. E. Shigley, L. D. Mitchel, Mechanical Engineering Design, Fourth Edition, McGraw-Hill Book Company

[55] T.Irvine, Shock Response Spectrum using Matlab "http://www.mathworks.com/matlabcentral/fileexchange/7398-shock-response-spectrum"

[56] Instron, Product Manual, "http://www.instron.us/wa/product/Impact-Testing-Systems.aspx"

[57] S. Lee, F. Barthelat, J. W. Hutchinson, H. D Espinosa, Dynamic Failure of Metallic Pyramidal Truss Core Materials–Experiments and Modeling, International Journal of Plasticity, 22(2006), No 11, 2118-2145.

[58] O. T.Strand, D. R. Goosman, C. Matinez and T. L. Withworth, Compact System of High-Speed Velocimetry using Heterodyne Techniques, Review of Science Instruments, 77 (2006),No 8, 083108-083108.

[59] D. C. Karnopp, D. L Margolis, R. C Rosenberg, System Dynamics: Modeling and Simulation of Mechatronic Systems, 3rd Ed., Wiley, 2000, Canada.

[60] M. J. Tucker, Waves in Ocean Engineering: Measurement, Analysis, and Interpretation, Ellis Horwood, London, 1991.

[61] C. E. Hammond, R. V. Doggett, Determination of Subcritical Damping by Moving-Block/Randomec Applications, Proc. National Aeronautics and Space Administration Symposium on Flutter Testing Techniques, , NASA CP-415, NASA, Washington, D.C., 59–76, 1975

[62] B. J. Lazan, Damping of Materials and Members in Structural Mechanics, Pergamon, Oxford, U.K, 1968.

VITA

Graduate College
University of Nevada, Las Vegas

Deepak Sankar Somasundaram

Degrees:

Bachelor of Engineering, Mechanical Engineering, 2003
Madras University, Chennai, India

Master of Science, Mechanical Engineering, 2008
University of Nevada, Las Vegas

Publications:

- Plastic Deformation of Steel Plates under High Impact Loading, Shock and Vibration Symposium, 2013, Atlanta, GA.
- Computational Simulation and Experimental Study of Plastic Deformation in A36 Steel during High Velocity Impact, ASME Verification and Validation Symposium, 2013, Las Vegas, NV
- Shock Mitigation for Electronic Boards within a Projectile, Int. J. Comp. Meth. & Exp. Meas., 2013, Approved
- Assessment of the Performance of an Armored Vehicle Joint Using a Two-Stage Gas Gun And Computational Analysis, 2012 ASME International Mechanical Engineering Congress and Exposition, Houston, Texas, November 2012 (abstract).
- Fuzzy-Controlled Hooke-Jeeves Optimization Search Algorithm, Engineering Optimization, 2011, 1043-1062
- Experimental Investigation of Shock Mitigation of Electronic Boards within Projectile, ASME Int. Mechanical Engineering Congress and Exposition Conference, 2008, Boston, Massachusetts

Dissertation Title: Analysis of Bolted Joints under Medium and High Impact Loading

Dissertation Examination Committee:

Co - Chairperson, Dr. Brendan J. O'Toole, Ph.D.
Co - Chairperson, Dr. Mohamed B.Trabia, Ph.D
Committee Member, Dr. Woosoon Yim, Ph.D.

Committee Member, Dr. Zhiyong Wang, Ph.D.
Committee Member, Dr. Yi-Yung Chen, Ph.D.
Graduate College Representative, Dr. Rama Venkat, Ph.D.